1969-3-Q = RL-2040

THE UNIVERSITY OF MICHIGAN

COLLEGE OF ENGINEERING
DEPARTMENT OF ELECTRICAL ENGINEERING
Radiation Laboratory

DOPPLER RADIATION STUDY

Interim Report No. 3

1 January - 1 April 1969

By C-M Chu, J. E. Ferris and W. E. Zimmerman

Contract N62269-68-C-0715

May 1969

Contract With: Naval Air Development Center
Johnsville, Warminster, Pennsylvania 18974

Administered through:
OFFICE OF RESEARCH ADMINISTRATION • ANN ARBOR

DOPPLER RADIATION STUDY

Interim Report No. 3

1969-3-Q

(1 January - 1 April 1969)

By

C-M Chu, J.E. Ferris and W.E. Zimmerman

Contract No. N62268-68-C-0715

Prepared For

U.S. Naval Air Development Center
Johnsville
Warminster, Pennsylvania 18974

FOREWORD

This report (1969-3-Q) was prepared by The University of Michigan, Radiation Laboratory, Department of Electrical Engineering. The report was written under Contract N62269-68-C-0715 "Doppler Radiation Study" and covers the period 1 January - 1 April 1969. The research was carried out under the direction of Professor Ralph E. Hiatt, Head of the Radiation Laboratory, and the Principal Investigator was Professor Chiao-Min Chu. The sponsor of this research is the U. S. Naval Air Development Center, Johnsville, Pennsylvania and the Technical Monitor was Mr. Edward Rickner.

ABSTRACT

This report presents a collection of experimental acquired bistatic scattering data. Results have been collected for flat and corrugated metallic surfaces and calm and agitated tap water surfaces. Most of the data is for a frequency of 13.0 GHz with some data at 15.0 GHz. A description of the test setup used is presented. Based on these results elementary calculations were made for a tactical situation and the results are reported. A description of the proposed fly-by test is presented.

TABLE OF CONTENTS

LIST OF ILLUSTRATIONS

List of Illustrations, Continued

List of Illustrations, Continued

List of Illustrations, Continued

List of Illustrations, Continued

I

INTRODUCTION

Investigation of the reflected radiation from a Doppler antenna by rough surfaces is continued. The theoretical formula for the scattering cross-section derived in the Interim Report No. 2 has been put into the computer programming and the results of the computation will be reported in the next report.

An experimental program to test the reflective characteristics of the rough surfaces such as the water and corrugated metallic surfaces was carried out in the laboratory. The test structure used is shown in Fig. 1-1. A detailed description of the experimental procedures and the results are given in Chapters II through VI. In Chapter VII a description of the planned fly-by tests is presented.

Based on the physical optics method, calculation has been carried out for the reflection from the corrugated metallic surfaces corresponding to the models used in the experiment and some preliminary computation checks fairly closely with the experimental results. This indicates that the physical optics method which we are presently employing for this project can be used for the calculation of the scattering cross-section of rough surfaces. To be sure that the method is a valid one for the estimation of polarization and aspect variation of the reflection, more computations are being carried out. This phase of the work will be summarized in a separate memo to be available shortly.

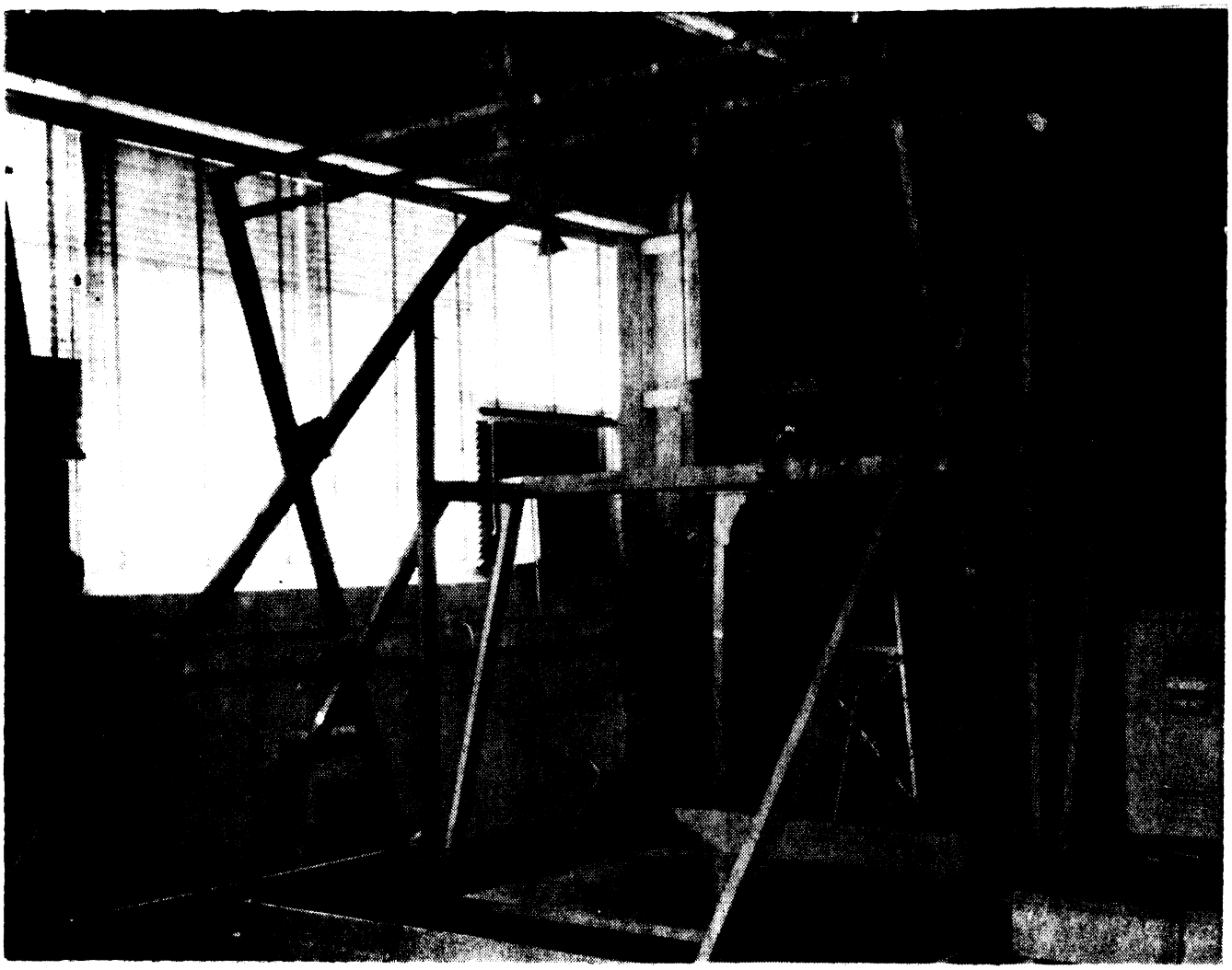

FIG. 1-1: SCATTERING TEST STRUCTURE.

II

FORWARD SCATTER TEST STRUCTURE

In Fig. 1-1 the antenna at the upper part of the picture is mounted on a swinging arm that can be continuously moved from $\theta = 0^{o}$ to near the horizon typically to $\theta = \sim 85^{o}$. In addition, holes are drilled in the board located on the side of the test structure at 5^{o} intervals such that it is possible to lock the swinging arm at any of these 5^{o} intervals by using a pinning mechanism. For most tests conducted, the swinging arm was moved continuously through the elevation angle employing the block and tackle visible in the upper part of Fig. 1-1. The transmitting antenna is a K_u-band gain standard horn of NRL design (NRL report 4433), which is the lower horn of Fig. 1-1 and is inclined 20^{o} from the local vertical at a height of 44 inches above the reflecting surface. The receiving antenna, located on the rotating arm, is a Microwave Associates model 628 having an aperture of 2-9/16 inch x 3-3/16 inch and is located 89 inches above the reflecting surface. The rotating arm is designed so that the axis of the major lobe of the receiving and transmitting horns are directed at a common point on the reflecting surface for all angles of elevation. Both the receiving and transmitting horns have a rotary joint as shown in Fig. 2-1 which allows one to easily change polarization. Note also that in Fig. 2-1, several directional couplers are employed to permit adequate monitoring of the transmitted signal for both power and frequency. The transmitting source is a Varian X-12 klystron which has a frequency range of 12.4 to 18 GHz. For the purposes of the present tests a frequency of 13.0 GHz has been employed with the exception of a few tests conducted at 15.0 GHz. The large rectangular tank of Fig. 1-1 was used making forward scattering measurements from an irregular reflecting surface such as water.

MISSING PAGE

III

REFLECTING SURFACES

Several reflecting surfaces have been used to gain a better understanding of the forward scattering of rf energy over water. The reference surface for all measurements has been a flat four foot square metallic plate so located that the axis of the main lobe of the transmitting antenna passed through its center. Two sinusoidal corrugated sheets having 'wavelengths' of 1-1/4 inch and 2-2/3 inches to simulate a ripply water surface were used. The peak-to-trough amplitude of the above corrugations were 1/4 inch and 1/2 inch respectively. The mid-point of the amplitude of each of these corrugations was adjusted to be at a height of the flat plate so that the antenna to reflecting-surface-dimensions remained unchanged. These reflecting surfaces were placed in the empty tank of Fig. 1-1. Positioning marks have been placed on the bottom of the tank to ensure the reflecting surfaces were always located in the same relative positions. Fig. 3-1 shows the 2-2/3 inch corrugated sheet inside the tank. When the tank was filled with water, the water level was adjusted to be at the same height as the reflecting surface of the flat metal plate.

MISSING PAGE

IV

DESCRIPTION OF THE SETUP

The test structure for the forward-scattering study is a compromise between electrical and mechanical properties. The transmitting horn, a K_u-band gain standard horn has a 5.98 inch by 4.91 inch aperture. This aperture at 13 GHz requires a distance of 6.55 feet to be in the far-field, i.e., fulfill the $2D^2/\lambda$ requirement for the Fraunhofer field. Placing the horn at a distance of 6.55 feet or greater above the reflecting surface causes the horn to illuminate a large area of the reflecting surface. If the receiving horn is at the Fraunhofer distance, this large scattering area requires a large and expensive test structure, i.e., a test structure with a 46 foot long swinging arm would be required for a 6.55 foot spacing between the transmitting horn and reflecting surface.

By placing the transmitting horn D^2/λ above the reflecting surface the illuminated area was reduced so that a structure of reasonable dimension could be constructed to measure the forward scattered field. The H-plane of the gain standard horn has a 3dB beamwidth of approximately 11^o. Four feet above the reflecting surface the transmitting horn illuminates a circular area approximately 9 inches in diameter. This scattering area requires a D^2/λ distance of 7.4 feet between the reflecting surface and receiving horn. For the forward scatter test structure the receiving horn aperture is 89 inches from the scattering surface. Although the D^2/λ distances from both the transmitting horn to scattering surface and the scattering surface to the receiving horn are not the desired $2D^2/\lambda$, the literature indicates satisfactory data may be acquired employing the D^2/λ criteria, (Silver, 1949) and (Beckmann, 1963).

The test structure was fabricated to position the illuminating horn aperture 44 inches above the reflecting surface such that the principal axis of the horn intersects the surface 20^o from vertical. The first sidelobe of the gain standard horn E-plane occurs at 22^o, intersecting the reflecting surface at approximately 1.6 feet from the

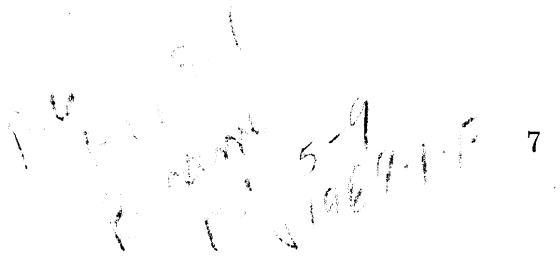

peak of the beam so that reflections from the tank sides are not considered to be significant. Continuous elevation angle information is provided by a gear located on the swinging arm that drives a syncro-generator to permit the use of a standard antenna pattern recorder.

The receiving horn was mounted on a 9 foot swinging arm that utilized indexed holes on the support frame to provide repeatable 5^{o} increments in elevation. The E and H-plane beamwidths of the receiving horn are 13^{o} and 16^{o} respectively to ensure the receiving horn will illuminate the currents induced on the reflecting surface. The 89 inch spacing between the securing horn and the scattering aperture places the scattering aperture in the far-field of the receiving horn.

Using the Friis transmission formula and the combined distance of the transmitting horn and the flat metal sheet to the receiving horn, one obtains a calculated free space loss of 22db. Experimental measurements indicated a 23.8dB loss. This difference of approximately 2dB is explained as being due to the beam broadening observed in the specular pattern measurements which may be due to phase errors as a result of employing the D^2/λ criteria. The test setup is shown in Fig. 1-1.

V

EXPERIMENTAL FORWARD SCATTERING PATTERNS

Because only a finite portion of the reflecting surface is employed, there is a question of the validity of the experimental results because of the edge effects associated with the reflecting surface and tank. Patterns were recorded with the metal plate in the tank and repeated with absorber lining the tank sides and at the receiving end of the metal plate. Fig. 5-1 is a forward scattering pattern for a flat plate employing parallel polarization and no absorber surrounding the plate or on the tank sides. Fig. 5-2 is a repeat of Fig. 5-1 except that absorber has been placed around the tank sides and at the end of the metal plate. It is felt these patterns repeat within the experimental accuracy of the setup. Figs. 5-3 and 5-4 show the effects with and without absorber for the 2-2/3 inch corrugated surface for parallel polarization.

From these measurements and similar ones for perpendicular polarization, it was concluded that the absorber was not necessary and that the reflections did not significantly change the patterns so that the remainder of the patterns were taken without the use of absorber. Two corrugated metal surfaces were studied as noted in Chapter III to give a basis for checking the theoretical calculations for periodic surfaces. By studying the data one will observe a trend that is established with these corrugated surfaces and may obtain a partial understanding of what will occur when energy is scattered from water waves.

To help the reader understand some of the general trends that are established, the data has been presented with the patterns for polarization parallel to the plane of incidence followed by data for the polarization perpendicular to the plane of incidence with the same reflecting surface geometry. The plane of incidence is defined to include the ray that radiates normal to the transmitting aperture and the normal to the reflecting surface.

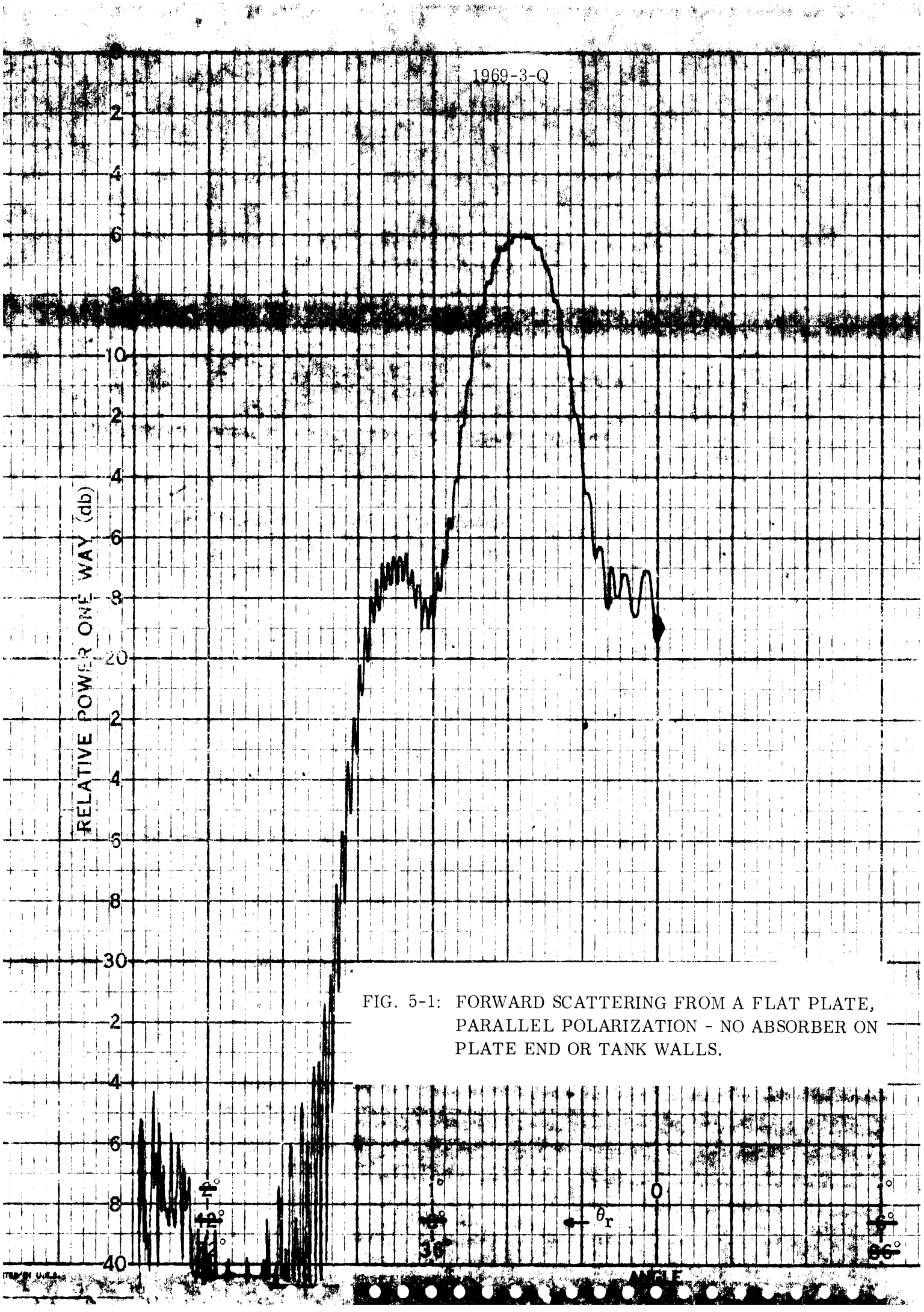

FIG. 5-1: FORWARD SCATTERING FROM A FLAT PLATE, PARALLEL POLARIZATION - NO ABSORBER ON PLATE END OR TANK WALLS.

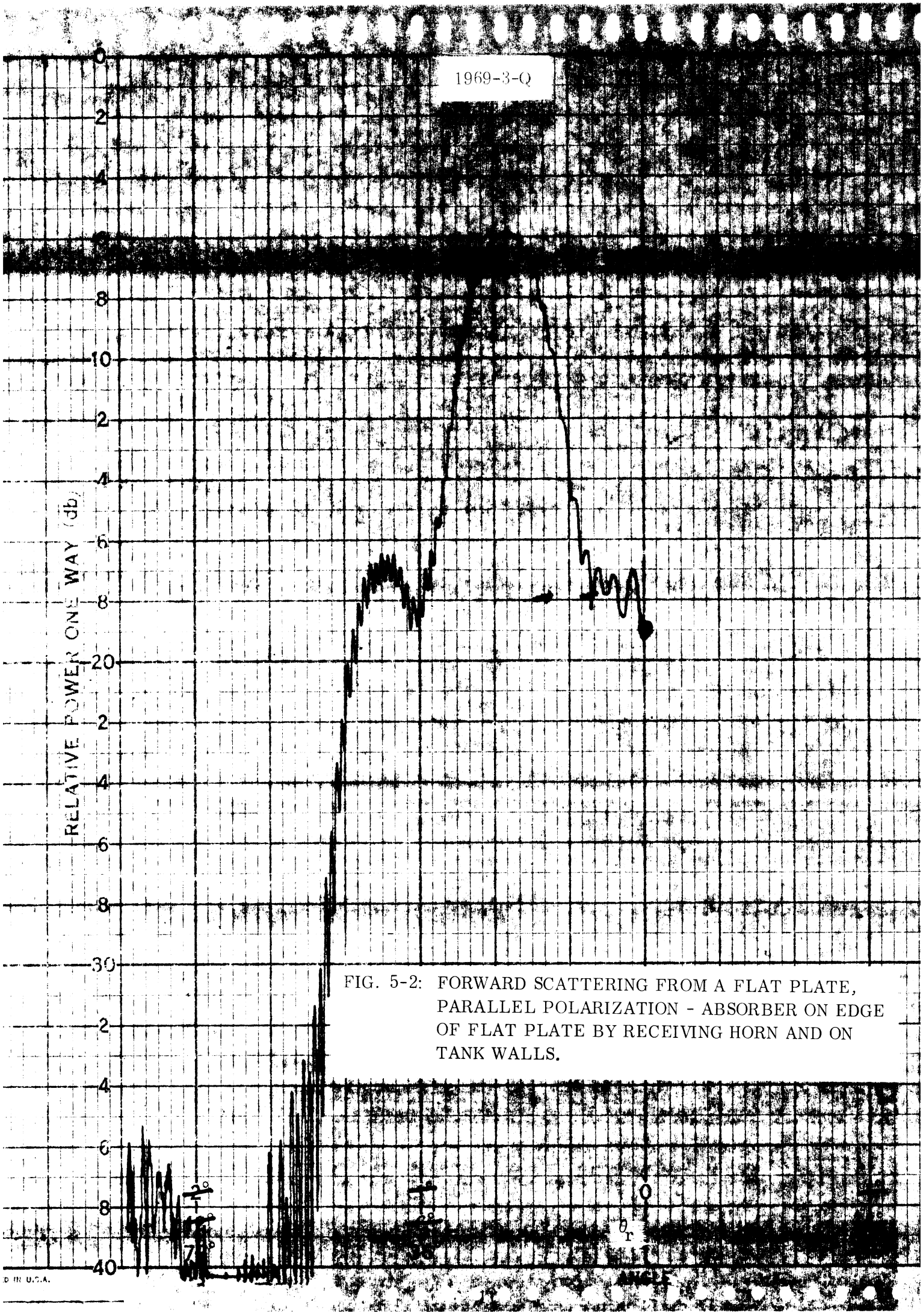

FIG. 5-2: FORWARD SCATTERING FROM A FLAT PLATE, PARALLEL POLARIZATION - ABSORBER ON EDGE OF FLAT PLATE BY RECEIVING HORN AND ON TANK WALLS.

FIG. 5-3: FORWARD SCATTERING FROM 2-2/3 INCH CORRUGATIONS, PARALLEL POLARIZATION, NO ABSORBER ON CORRUGATION ENDS OR TANK WALLS.

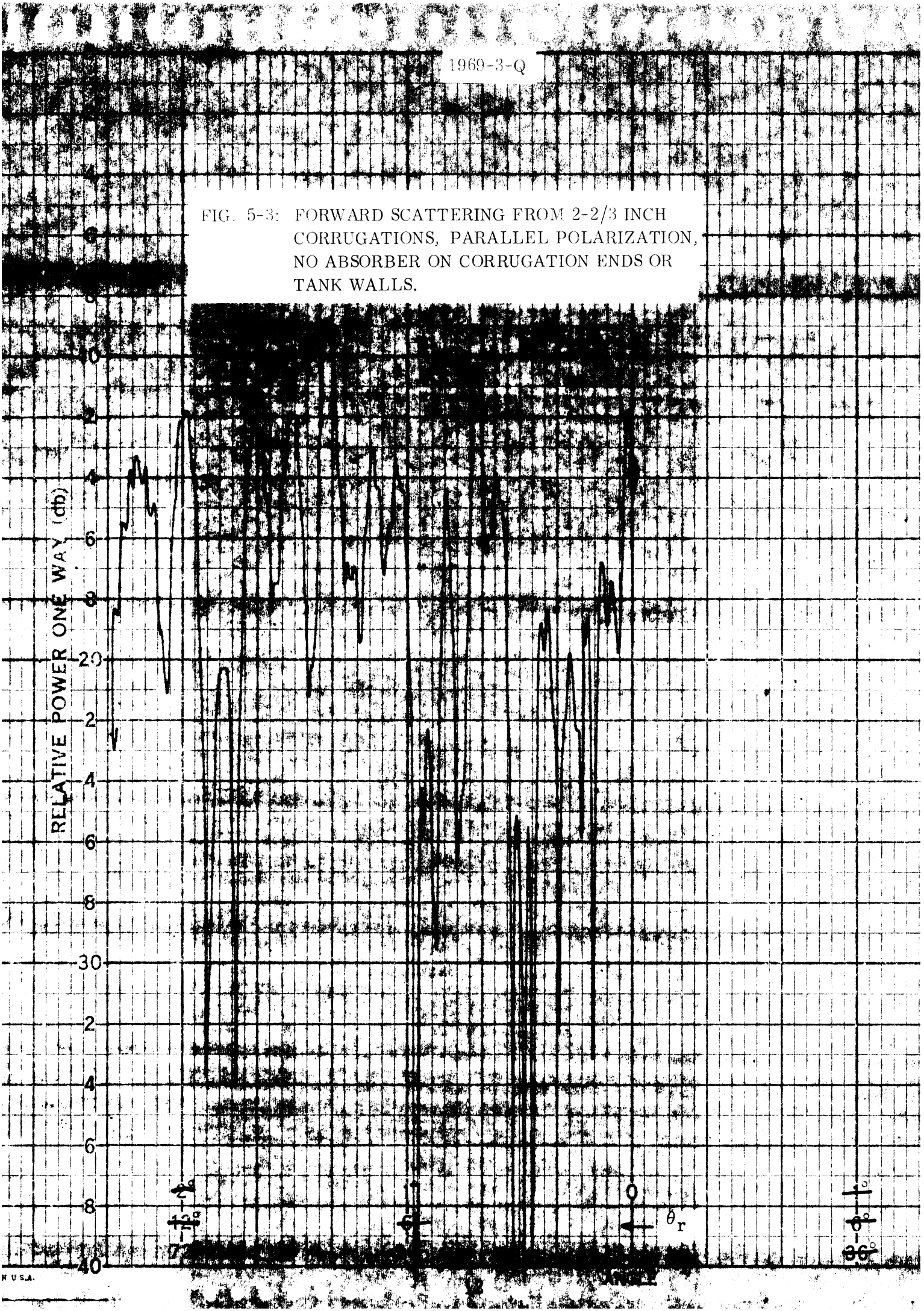

FIG. 5-4: FORWARD SCATTERING FROM 2-2/3 INCH CORRUGATED SURFACE, PARALLEL POLARIZATION, ABSORBER ON EDGE OF CORRUGATED SHEET BY RECEIVING HORN AND ON TANK WALLS.

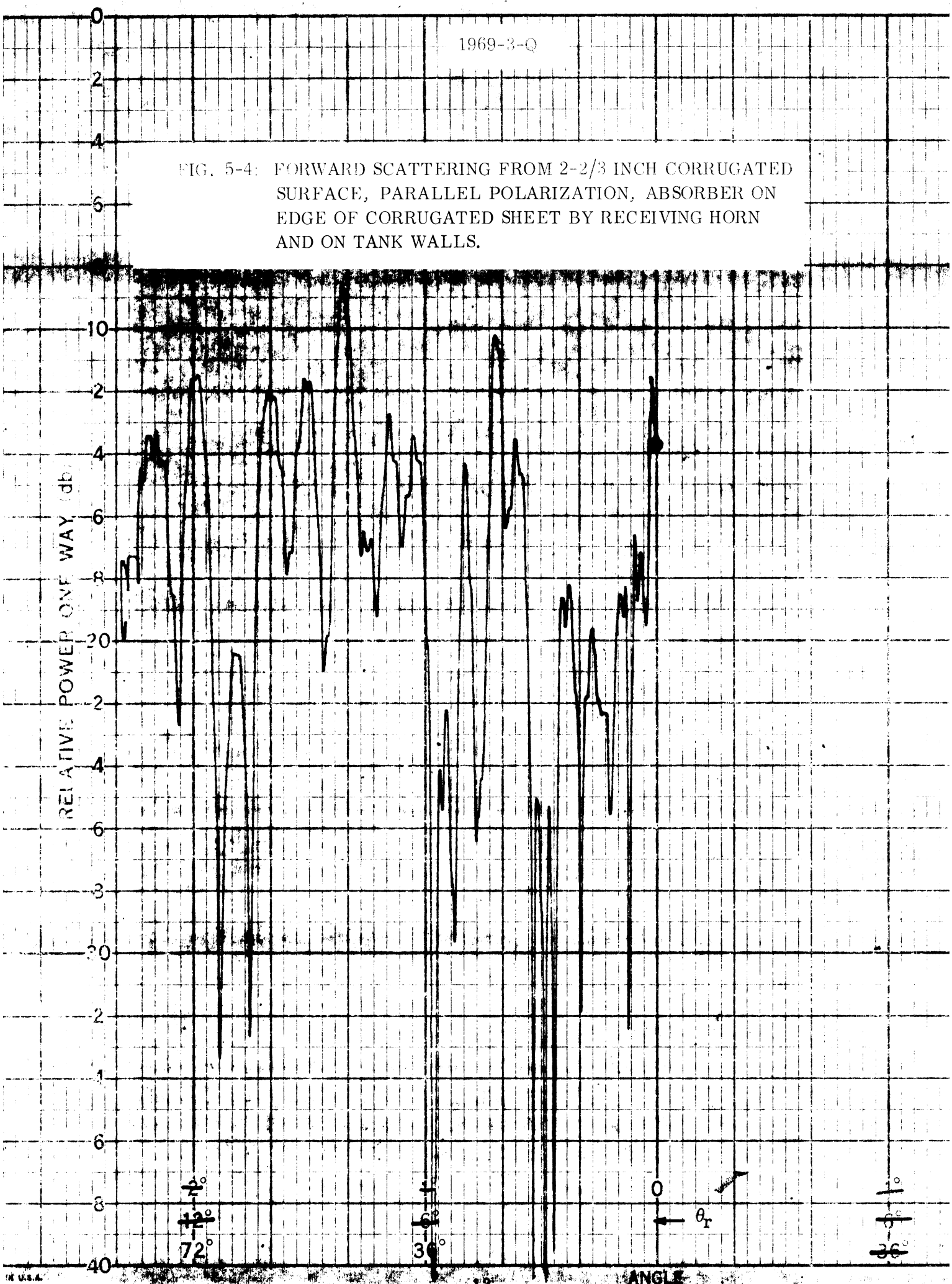

5.1 Metallic Scattering

The geometry of the scattering surface is shown in Fig. 5-5. Four conditions have been considered and are shown in Fig. 5-5 for both polarizations. For the first three conditions the transmitting antenna angle remained fixed (both θ_t and ϕ_t) with $\theta_t = 20^o$, and $\phi_t = 90^o$. For all conditions to be discussed the receiving angle θ_r was variable with $\phi_r = -90^o$. The first three conditions are associated with the scattering surface which was rotated in ϕ so that ϕ_{ss} was equal to 0^o, 45^o, and 90^o. The fourth condition was associated with the transmitting horn which was rotated in ϕ to a constant angle of $\phi_t = 70^o$ while keeping $\theta_t = 20^o$. Since most of the data is for the first three conditions, the azimuth angle ϕ_t in the scattering pattern data is 90^o unless specified otherwise in the figure caption.

Data for the first three conditions is shown in Figs. 5-7 through 5-35. Fig. 5-6 is further an illustration of the orientation of the plate in reference to the transmitting and receiving antenna as ϕ_{ss} is varied. Figures 5-36 through 5-47 are for the fourth condition. Figures 5-1 and 5-7 are calibration curves employing a flat metal plate and parallel and perpendicular polarization for 13.0 GHz.* The remaining data for parallel and perpendicular polarization may be referenced as the power level or receiver gain were not changed after these patterns were recorded.

Figures 5-8 through 5-13 are for 1-1/4 inch corrugated surfaces with ϕ_{ss} equal to 0^o, -45^o, and -90^o. Figures 5-8 and 5-9, for $\phi_{ss} = 0^o$, suggest that parallel polarization is more greatly affected than the perpendicular polarization because of the more pronounced nulls and peaks. Further, there is a greater amount of energy available at the horizon, e.g., there is approximately 6dB more energy near the horizon for the parallel polarized data, than for the perpendicular polarization. In Figs. 5-10 and 5-11 ($\phi_{ss} = -45^o$), the two forward scatter patterns for the two polarizations are similar with sharper amplitude variations for parallel polarization.

---

*unless otherwise noted in the caption, the frequency for all patterns is 13.0 GHz.

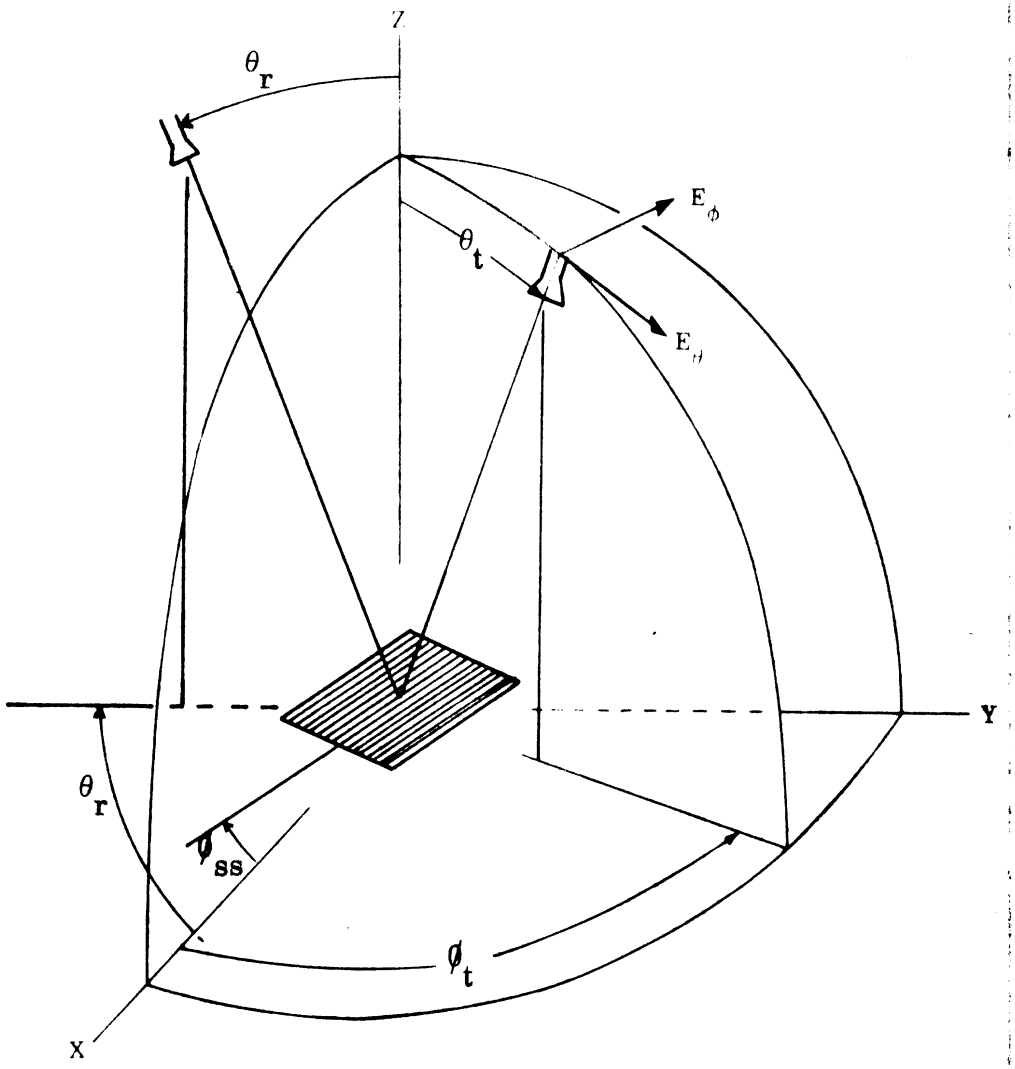

FIG. 5-5: COORDINATE SYSTEM USED FOR THE FOUR TYPES OF SCATTERING GEOMETRY.

1) Transmitting Horn $\theta_t = 20^o$, $\phi_t = 90^o$
Receiving Horn θ_r = var., $\phi_r = -90^o$
Corrugated Surface in X-Y plane $\phi_{ss} = 0^o$

2) Transmitting Horn $\theta_t = 20^o$ $\phi_t = 90^o$
Receiving Horn θ_r = var., $\phi_r = -90^o$
$\phi_{ss} = -45^o$

3) Transmitting Horn $\theta_t = 20^o$, $\phi_t = 90^o$
Receiving Horn θ_r = var., $\phi_r = -90^o$
$\phi_{ss} = -90^o$

4) Transmitting Horn $\theta_t = 20^o$, $\phi_t = 70^o$
Receiving Horn θ_r = var., $\phi_r = -90^o$
$\phi_{ss} = 0^o$, -45^o, -90^o, as in above 3 types.

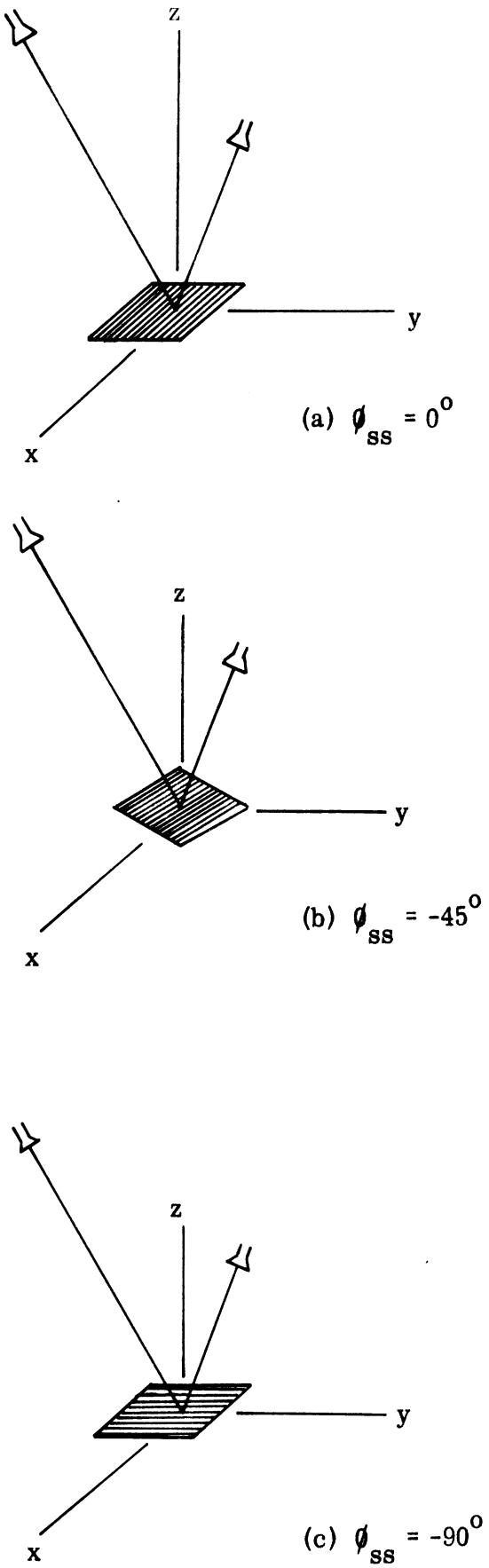

FIG. 5-6: THREE ORIENTATIONS OF THE CORRUGATED SURFACES.

Patterns 5-12 and 5-13 for $\phi_{ss} = -90^{o}$ suggest that the parallel polarization tends to scatter more energy forward (approximately 8dB) than perpendicular polarization; and more closely resembles the forward scattered data from a flat plate illuminated with the same polarization.

Patterns 5-14 through 5-19 were obtained for both polarizations employing $\phi_{ss} = 0^{o}$, -45^{o}, and -90^{o} for the 2-2/3 inch corrugated plate. From patterns 5-14 and 5-15 it is apparent that the parallel polarization is again more greatly affected by the corrugations because of the more pronounced nulls and larger amount of energy near the horizon (approximately 4dB) as compared to the data for perpendicular polarization. It appears from Fig. 5-15 (perpendicular polarization) that a major portion of the forward scattered energy occurs at elevation angles below the specular point ($\theta_r = 20^{o}$). This data also has an average energy level of approximately 4dB below that of the specular reflection and the 3dB beamwidth is increased to 26^{o}. The remainder of the elevation energy levels are higher but not equal to that of parallel polarized data. In Fig. 5-14 the energy has an overall level of approximately 6dB below the specular reflection, but a much more random distribution as a function of the elevation angle. As with the 1-1/4 inch corrugations, Figs. 5-16 and 5-17 for $\phi_{ss} = -45^{o}$ show the similarity between the forward scattered patterns for perpendicular and parallel polarization. Note, however, that in this case again that rapid energy variations (peak to null variations) are experienced with the parallel polarization. For $\phi_{ss} = -90^{o}$, the patterns show some similarity with the 1-1/4 inch corrugations with the peak forward scattering level being approximately the same for both polarizations.

Figures 5-20 through 5-33 are for the same two corrugated sheets at a frequency of 15 GHz. The frequency change shows that the scattered energy at the lower elevation angle (i.e., near the horizon) from the corrugated surface was not a resonant effect of the periodic structure (occurring for narrow frequency

bands) such that it would not be observed at other frequencies. In general, the scattering effects noted for 13 GHz were also observed in data collected at 15 GHz. The behavior with respect to surface orientation and the response with respect to polarization for the two frequencies are quite similar. Because of this it is felt that further comment on these patterns is unnecessary.

When the transmitting and receiving horns are cross-polarized, there is no measurable forward scatter at any elevation angle for the corrugated surfaces for $\phi_{ss} = 0^{o}$, and -90^{o}. However, when the corrugated sheet is rotated so that $\phi_{ss} = -45^{o}$, some cross polarization does occur at the higher elevation angle. The 1-1/4 inch corrugation shows the greater affect with the peak of the forward scattering being only about 9dB below that of scattered waves in the specular elevation ($\theta_r = 20^{o}$).

Figures 5-36 through 5-47 are for the fourth type of data, i.e., with the transmitting horn offset in ϕ (ϕ_t is equal to 70^{o}). This data confirms the trends that were set for both corrugations that have been discussed earlier, except that the overall level of the forward scatter is reduced. It is interesting to note that the forward scatter of the two polarizations become more similar as the angle defined by the plane of observation and the plane of incidence increases.

5.2 Water Scattering

The value of the dielectric constant, ϵ_r, of sea water as given in the open literature is approximately 81 with a conductivity of 4 to 5 mhos per meter. For fresh water the dielectric constant is given as 80 with a conductivity of 10^{-2} to the 10^{-3} mhos per meter (Von Hippel, 1954) which is dependent upon the level of mineral content in the water. Most references fail to report that the dielectric constant and loss tangent (which is related to the conductivity) vary significantly as the rf frequency is changed. There appears to be very little data for the dielectric constant and loss tangent of fresh water or sea water at frequencies above 10 GHz.

One source (Von Hippel, 1954) quotes limited high frequency characteristics of aqueous sodium chloride and water, however, the dielectric constant and loss tangent are for a temperature of 25°C which is a higher temperature than found in the ocean. Von Hippel's data is used for lack of any other at this frequency. The data for fresh water has a temperature dependence with the loss tangent being lower for a lower temperature. However, the use of the 25° C data does not significantly change the following calculated values. The data for the aqueous sodium chloride solution is presented in terms of molar solutions and range from 1/10 molal to 7/10 molal in steps of 2/10 of a molal. The concentration of salt in the sea water is 30 to 35 parts per thousand (NAVEPS) which would be approximately 1/10 molal solution. For a 1/10 molal solution of sodium chloride at 10 GHz the dielectric constant and loss tangent are given as 54 and 0.56 respectively by Von Hippel. For water at 25°C the value given for dielectric constant and loss tangent respectively is 55 and 0.54 by Von Hippel. The loss tangent can be converted to conductivity by equation (5.1) as follows.

$$\sigma = \frac{1}{\rho} \frac{f(\epsilon'/\epsilon_0) \tan \delta}{1.8 \times 10^{12}} \quad \text{mho-cm} \quad \text{(f in cps)} \tag{5.1}$$

where

$$\epsilon^* = \epsilon' - j\,\epsilon''$$

This expression gives a conductivity of 21.4 mhos per meter for fresh water at 13 GHz and a conductivity of 21.0 mhos per meter for 1/10 molal salt solution according to the data available. The skin depth calculated from equation (5.2) is determined in terms of the rf frequency, the dielectric constant, and the loss tangent. Skin depth for fresh water at 25°C is .074 inches and for a 1/10 molal solution it is 0.072 inches.

$$\frac{1}{\alpha} = \frac{\lambda_0}{2\pi} \left(\frac{2}{k' \left(\sqrt{1 + \tan^2 \delta} - 1 \right)} \right)^{1/2} \quad m \qquad (5.2)$$

where

$$k' = \epsilon'/\epsilon_0$$

From this it is apparent there would be very little difference in the fresh water and sea water for forward scattering measurements. For this reason tap water, which is assumed to be equivalent to fresh water, was used in the measurements reported here.

Figure 5-46 is for forward scattering from a flat plate for a frequency of 13 GHz and perpendicular polarization. This is the calibration curve taken for the forward scattered data from water. Figure 5-49 is the forward scattering of calm water, i.e., no waves. There appears to be 2.4dB loss associated with the water data as compared to the flat plate data and the major lobe has broadened slightly. Figures 5-50 and 5-51 are for water with waves that were made by using a board in the tank and employing a hand sloshing action. This is preliminary data and gives at least an indication of the forward scattering pattern to be expected from water.

Reflections of the waves from the sides of the tank and the lack of periodicity produced a wave somewhat spherical as compared to ocean waves. In Fig. 5-50 the waves had a greater distance between the peaks with deeper peak to null depth. For Fig. 5-51 the waves were closer together and shallower. The water waves scatter a significant amount of energy toward the horizon as did the corrugated surfaces. However, this data is somewhat limited and further measurements should be made to more accurately characterize the behavior of the scattered energy near the horizon as a function of the parameters of interest.

To collect data near the horizon $\theta_r = 80^\circ, -87^\circ$ it has been necessary to enlarge the tank so the receiving horn will fit inside the tank. The new setup is shown in

Fig. 5-52. This allows the horn to be lowered closer to the surface of the water to obtain more meaningful data near the horizon. Figures 5-53 and 5-54 show some values for scattering from metallic corrugations and a rough water surface. It is to be emphasized these are approximations and are presented to show there exists some similarity between the data obtained from metal corrugations and the water surface with waves. It is to be kept in mind that the wave height and periodicity may not be identical to the metal corrugations. While the agreement at higher elevation angles is not good, the pattern shape near the horizon displays similar characteristics. In Fig. 5-53 for the larger surface variations (both the metal corrugations and the water waves) display a similar null and peak pattern. Observing the range $\theta_r = 30^o - 80^o$, the angular position of the peaks and nulls are surprisingly good in agreement when one considers the randomness of the water wave generation. In Fig. 5-54 there is similar null and peak patterns near the horizon, but these are not as clearly defined, possibly due to the difficulty in making shallow waves with a periodicity similar to the 1-1/4 inch corrugations.

These pattern comparisons are presented to show a similarity between the corrugations and a wavy water surface. This indicates there may be sea conditions which would give scattering levels near the horizon as large as those shown for the metal corrugations of section 5.1.

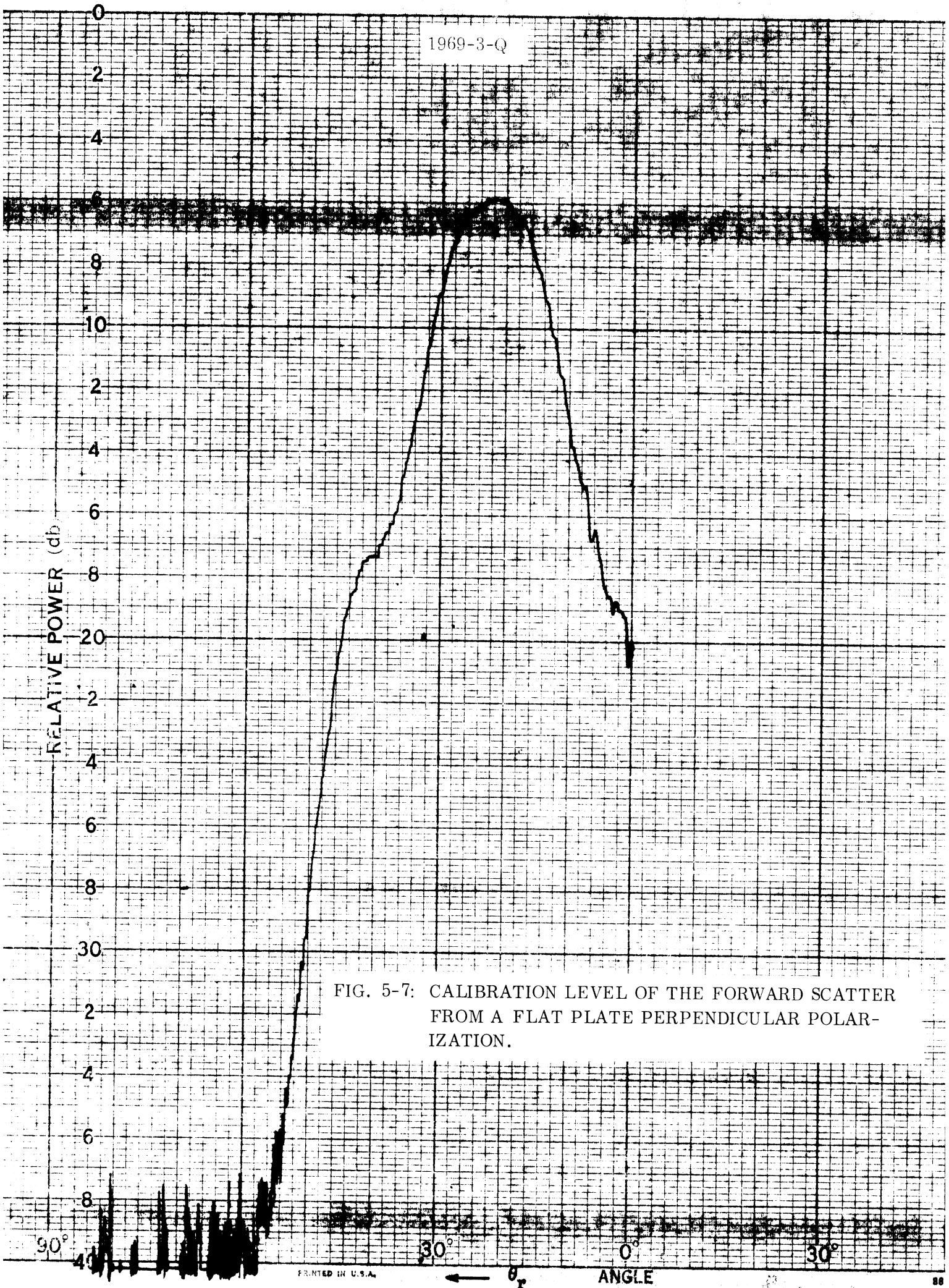

FIG. 5-7: CALIBRATION LEVEL OF THE FORWARD SCATTER FROM A FLAT PLATE PERPENDICULAR POLARIZATION.

FIG. 5-8: FORWARD SCATTER FROM 1-1/4" CORRUGATION, $\phi_{ss} = 0^{o}$, PARALLEL POLARIZATION.

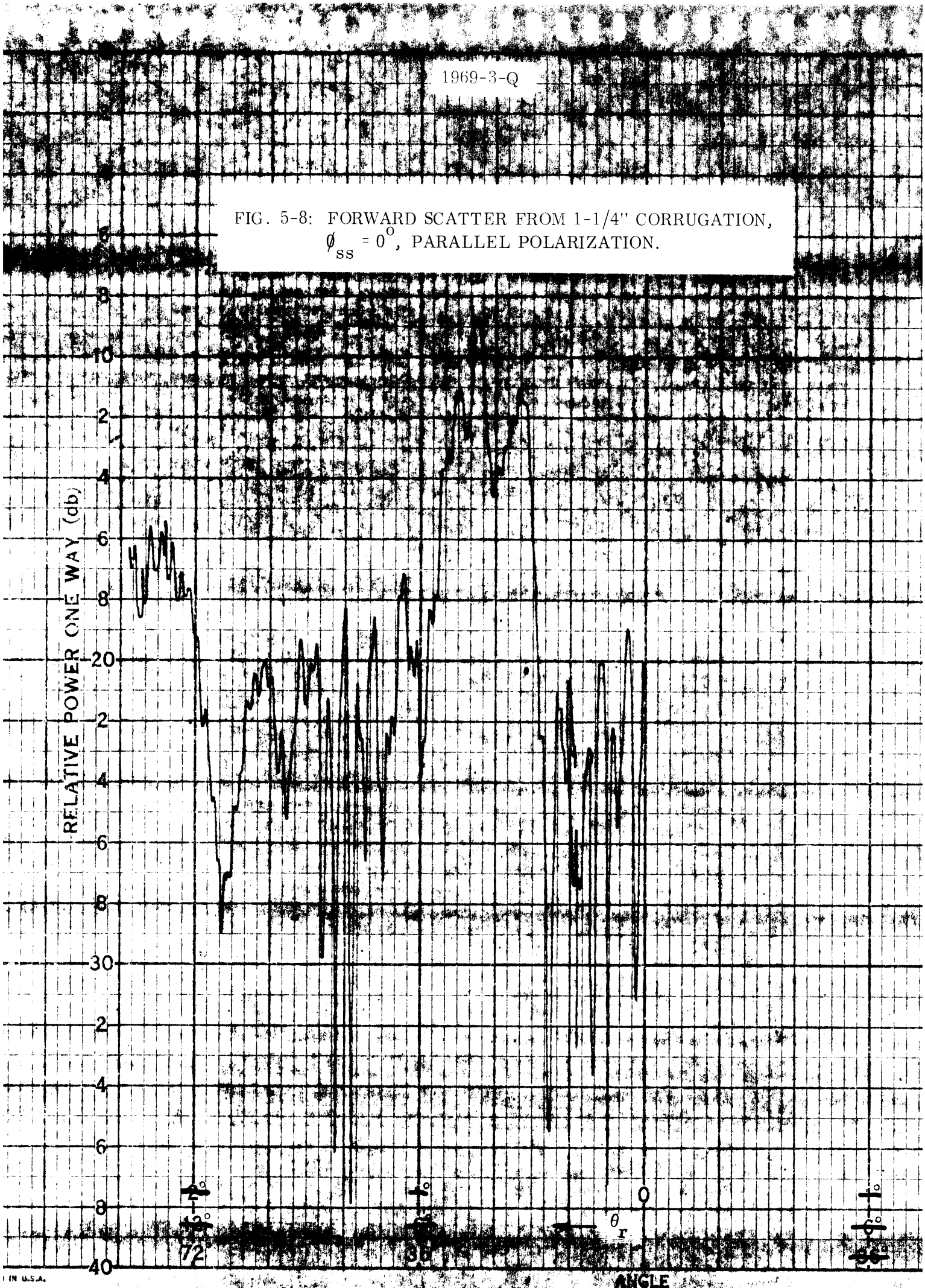

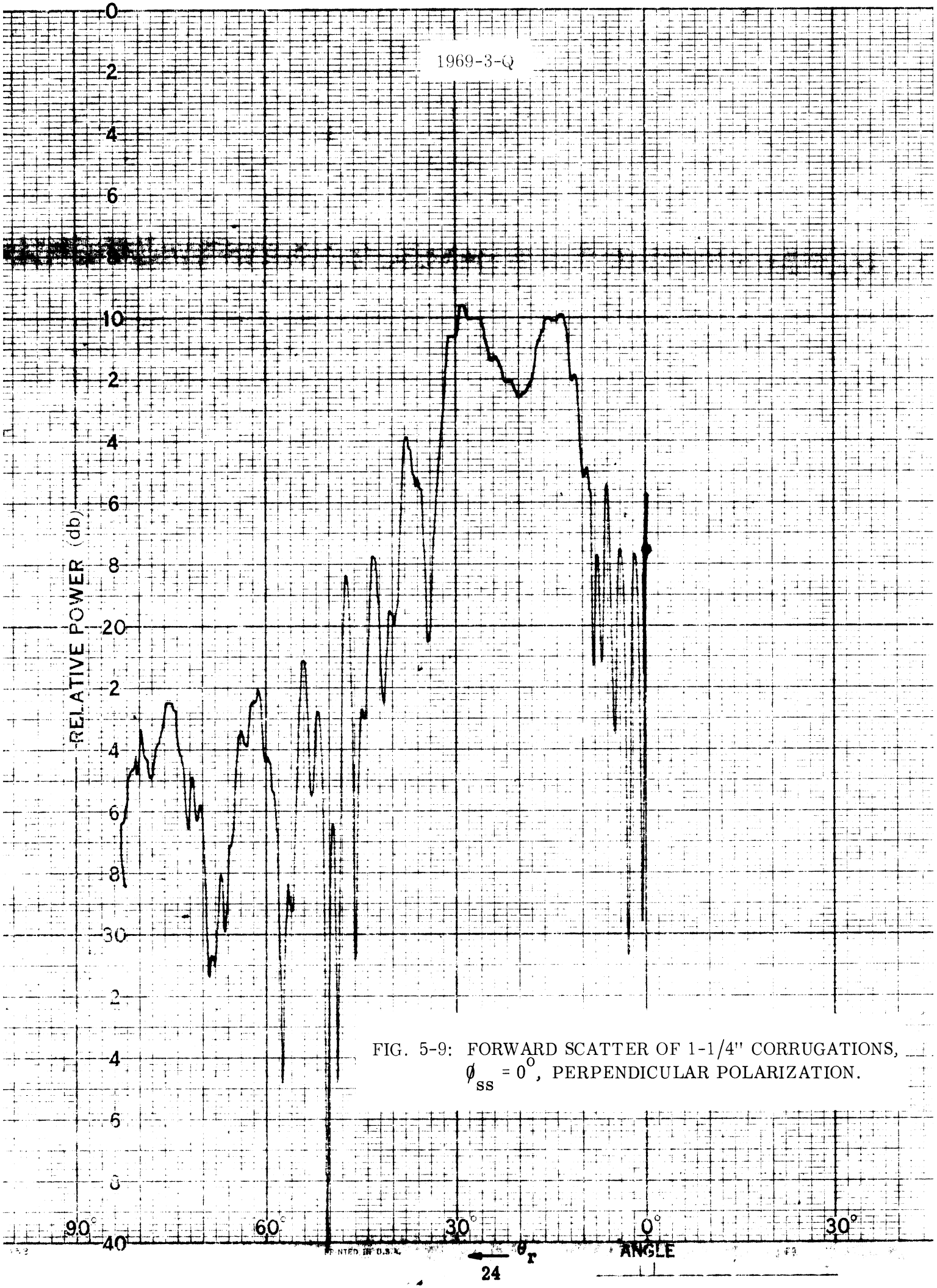

FIG. 5-9: FORWARD SCATTER OF 1-1/4" CORRUGATIONS, $\phi_{ss} = 0^{\circ}$, PERPENDICULAR POLARIZATION.

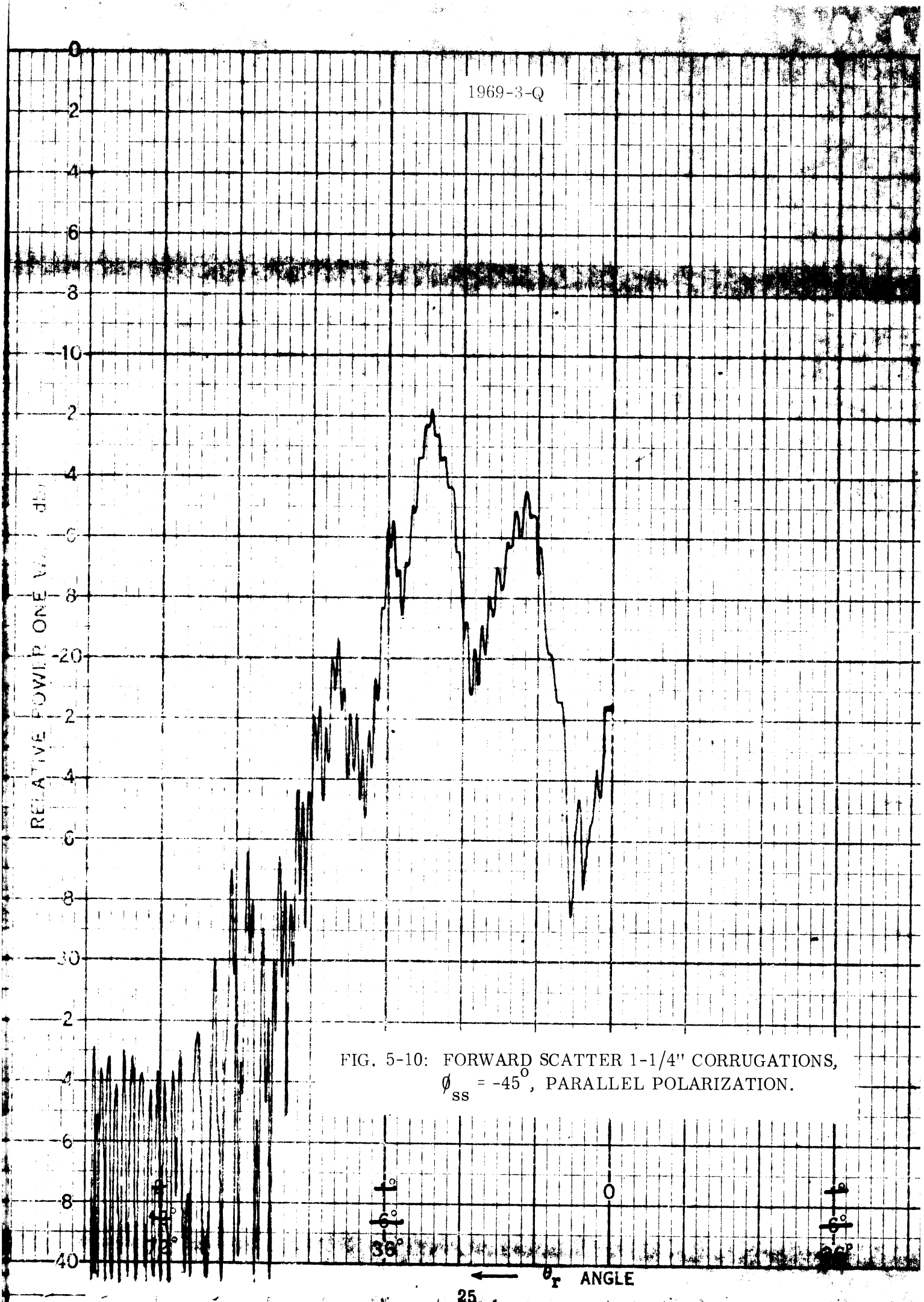

FIG. 5-10: FORWARD SCATTER 1-1/4" CORRUGATIONS, $\phi_{ss} = -45^{o}$, PARALLEL POLARIZATION.

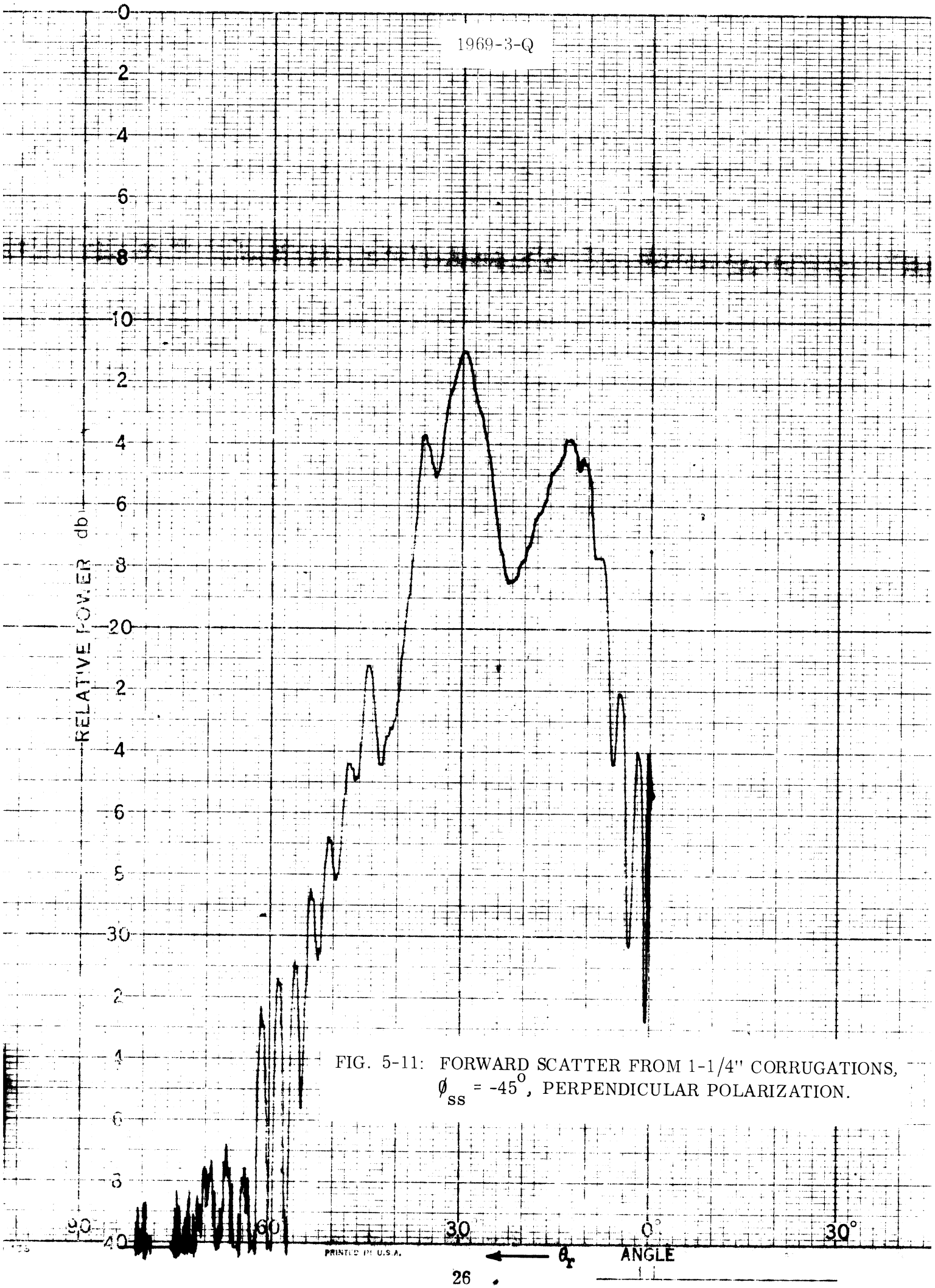

FIG. 5-11: FORWARD SCATTER FROM 1-1/4" CORRUGATIONS, $\phi_{ss} = -45^{o}$, PERPENDICULAR POLARIZATION.

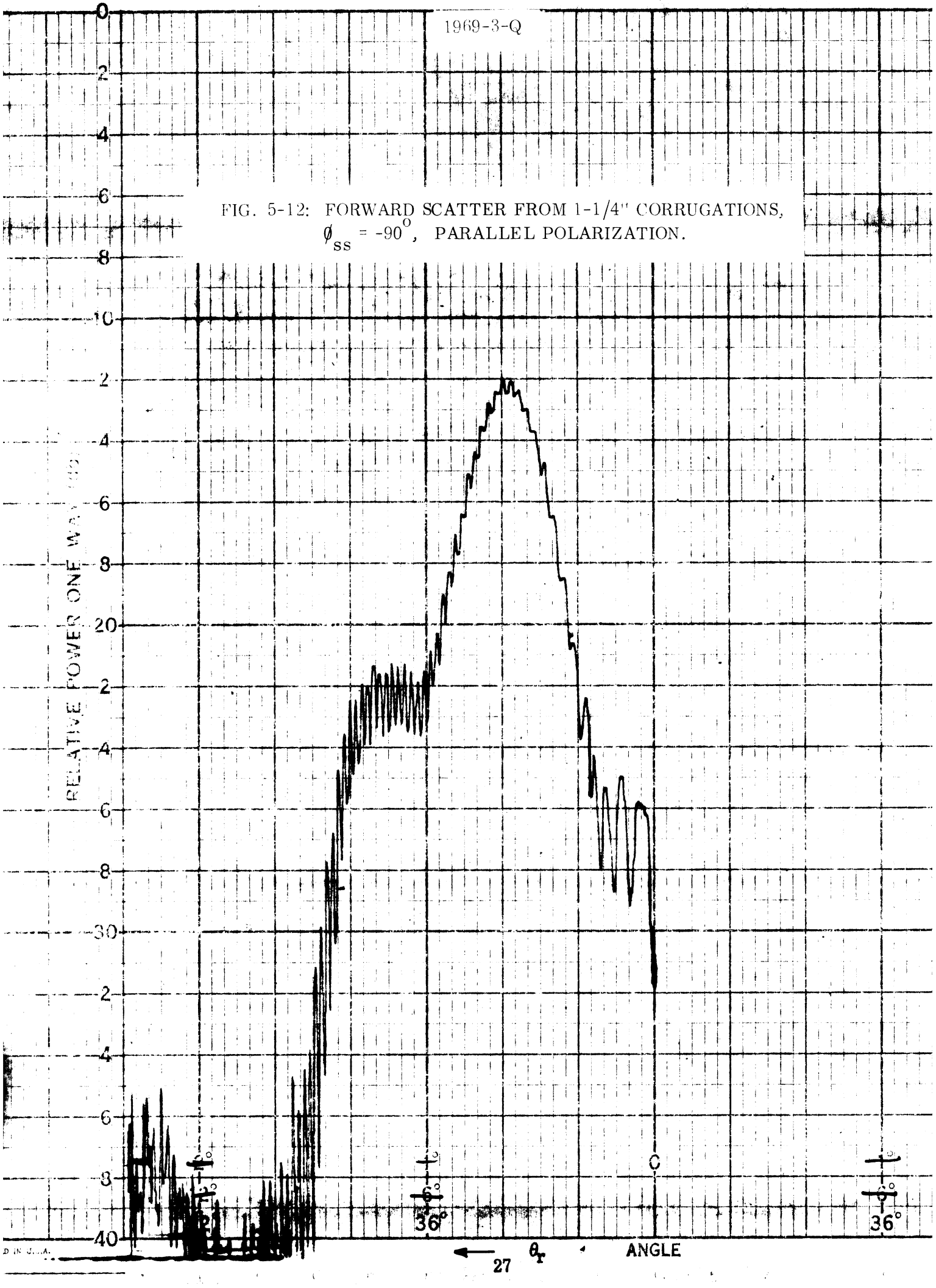

FIG. 5-12: FORWARD SCATTER FROM 1-1/4" CORRUGATIONS, $\phi_{ss} = -90^{o}$, PARALLEL POLARIZATION.

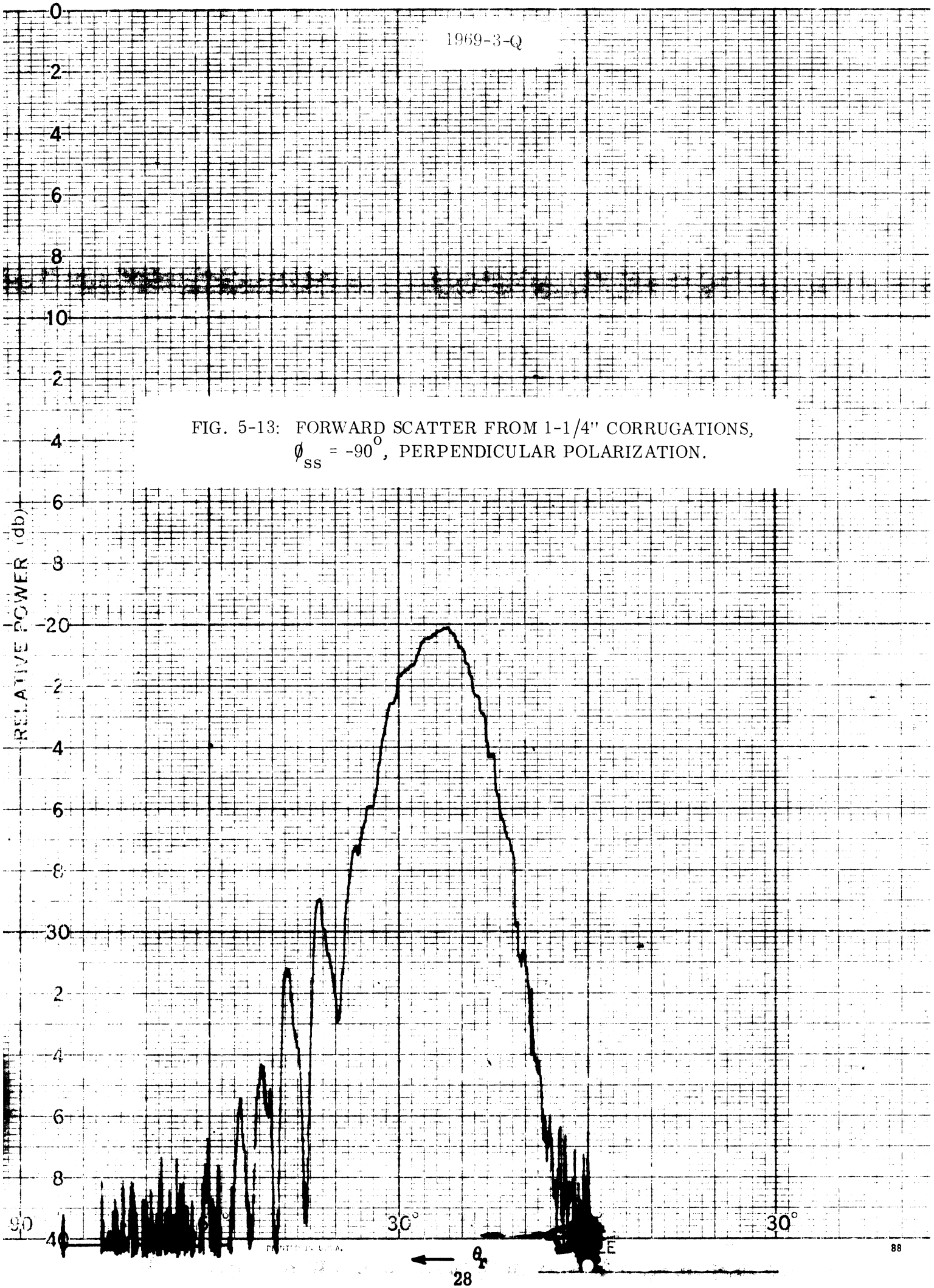

FIG. 5-13: FORWARD SCATTER FROM 1-1/4" CORRUGATIONS, $\phi_{ss} = -90^{o}$, PERPENDICULAR POLARIZATION.

FIG. 5-14: FORWARD SCATTER FROM 2-2/3" CORRUGATIONS, $\phi_{ss} = 0^{o}$, PARALLEL POLARIZATION.

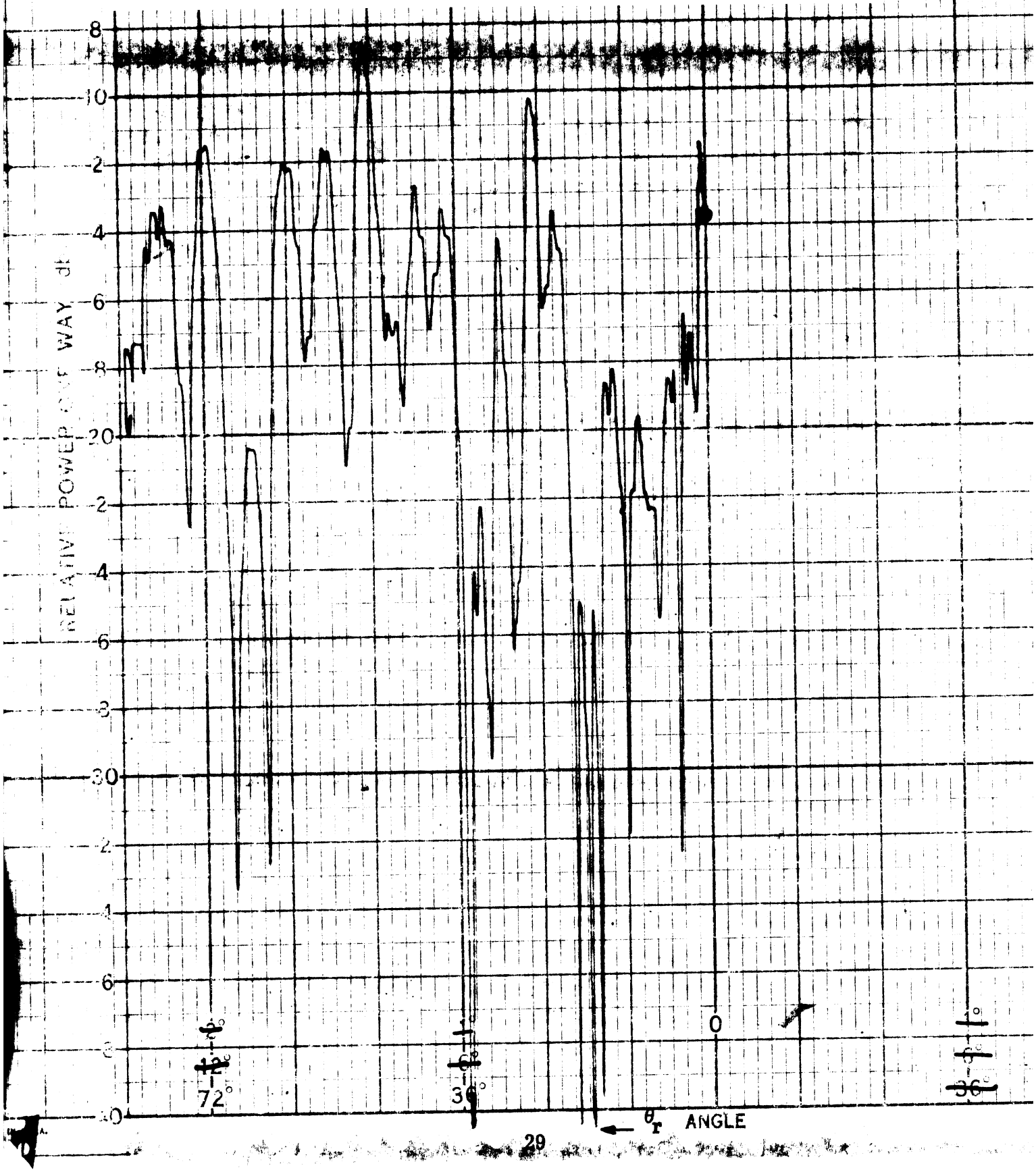

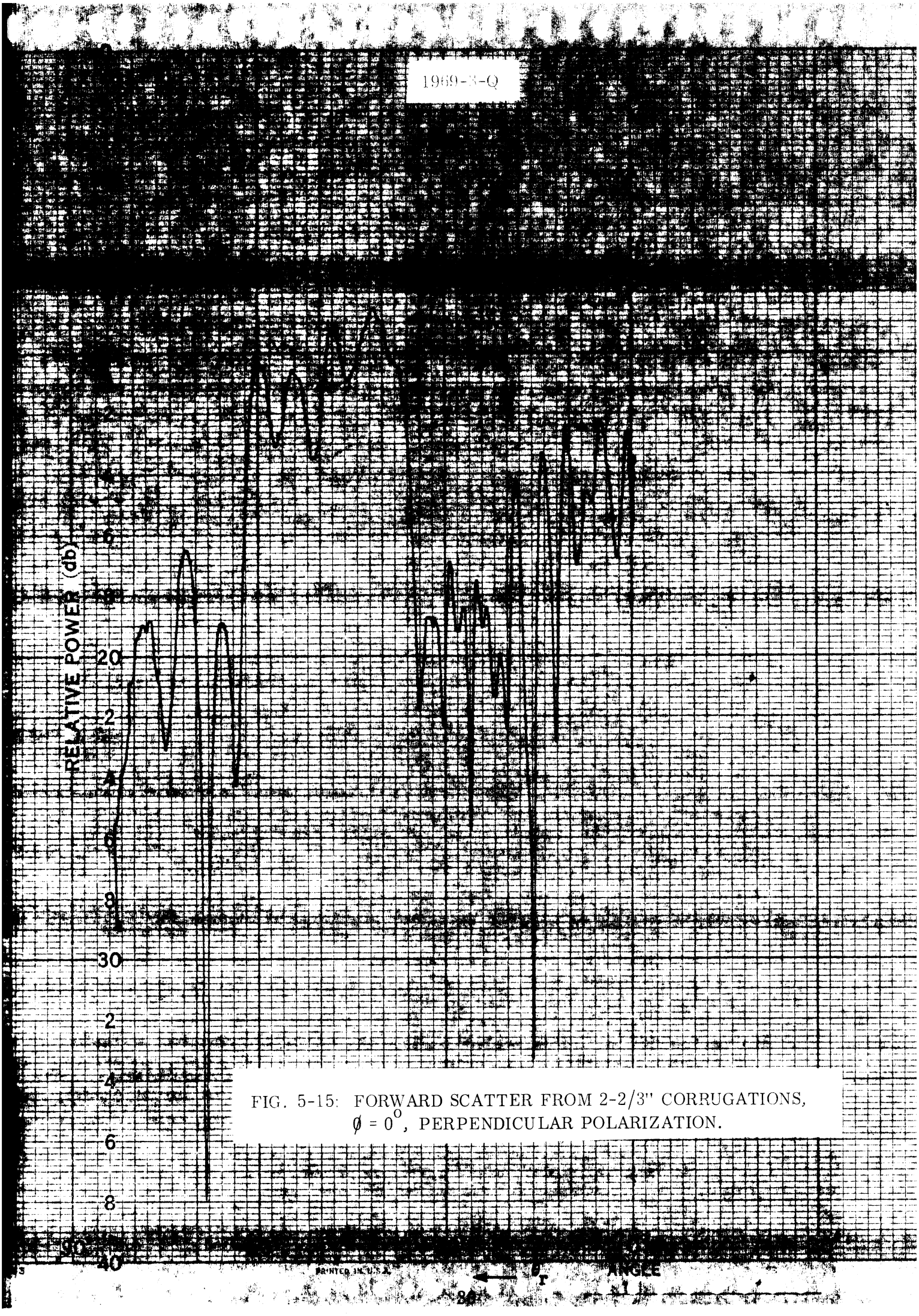

FIG. 5-15: FORWARD SCATTER FROM 2-2/3" CORRUGATIONS, $\phi = 0^{o}$, PERPENDICULAR POLARIZATION.

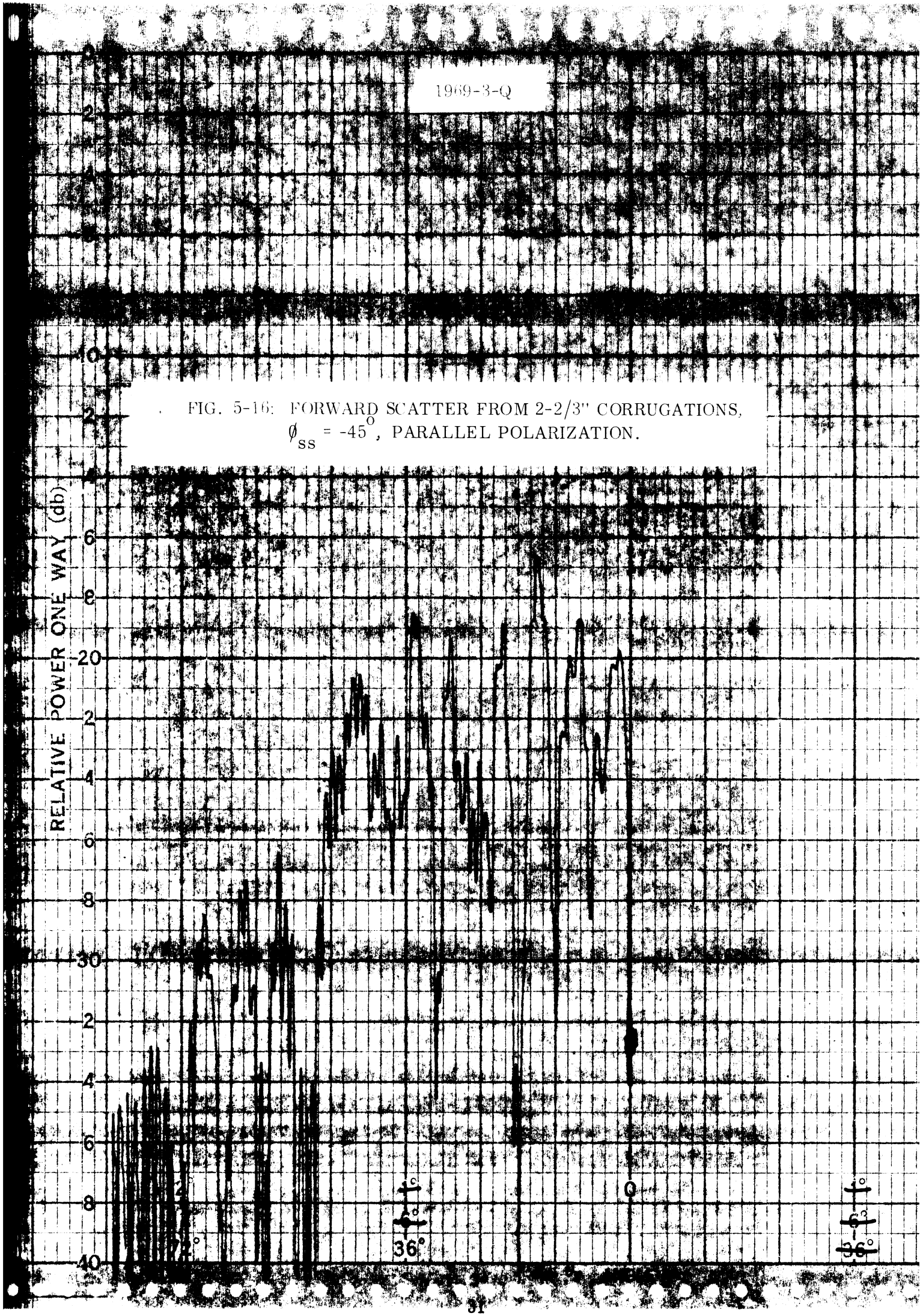

FIG. 5-16: FORWARD SCATTER FROM 2-2/3" CORRUGATIONS, $\phi_{ss} = -45^{o}$, PARALLEL POLARIZATION.

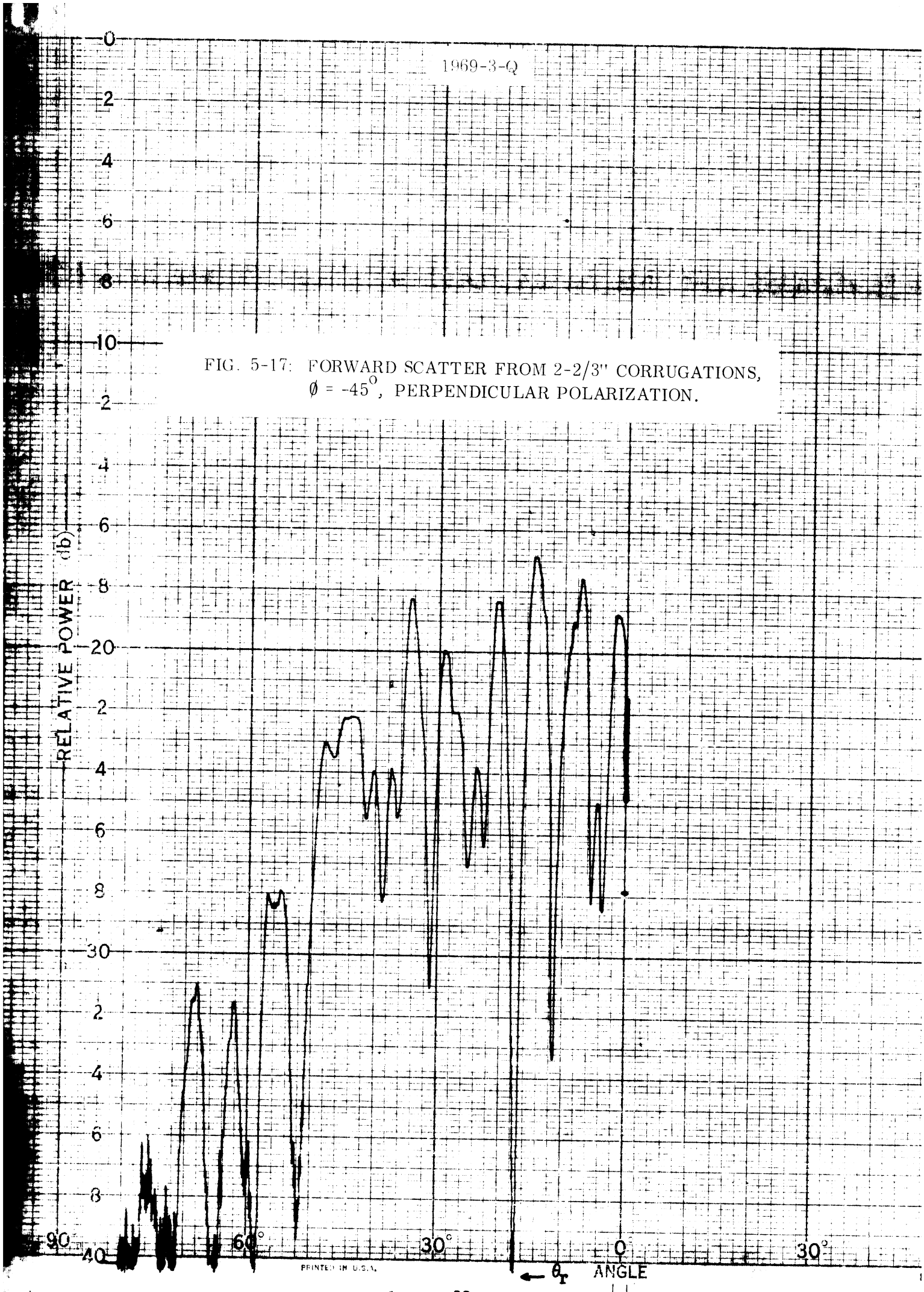

FIG. 5-17: FORWARD SCATTER FROM 2-2/3" CORRUGATIONS, $\phi = -45^{\circ}$, PERPENDICULAR POLARIZATION.

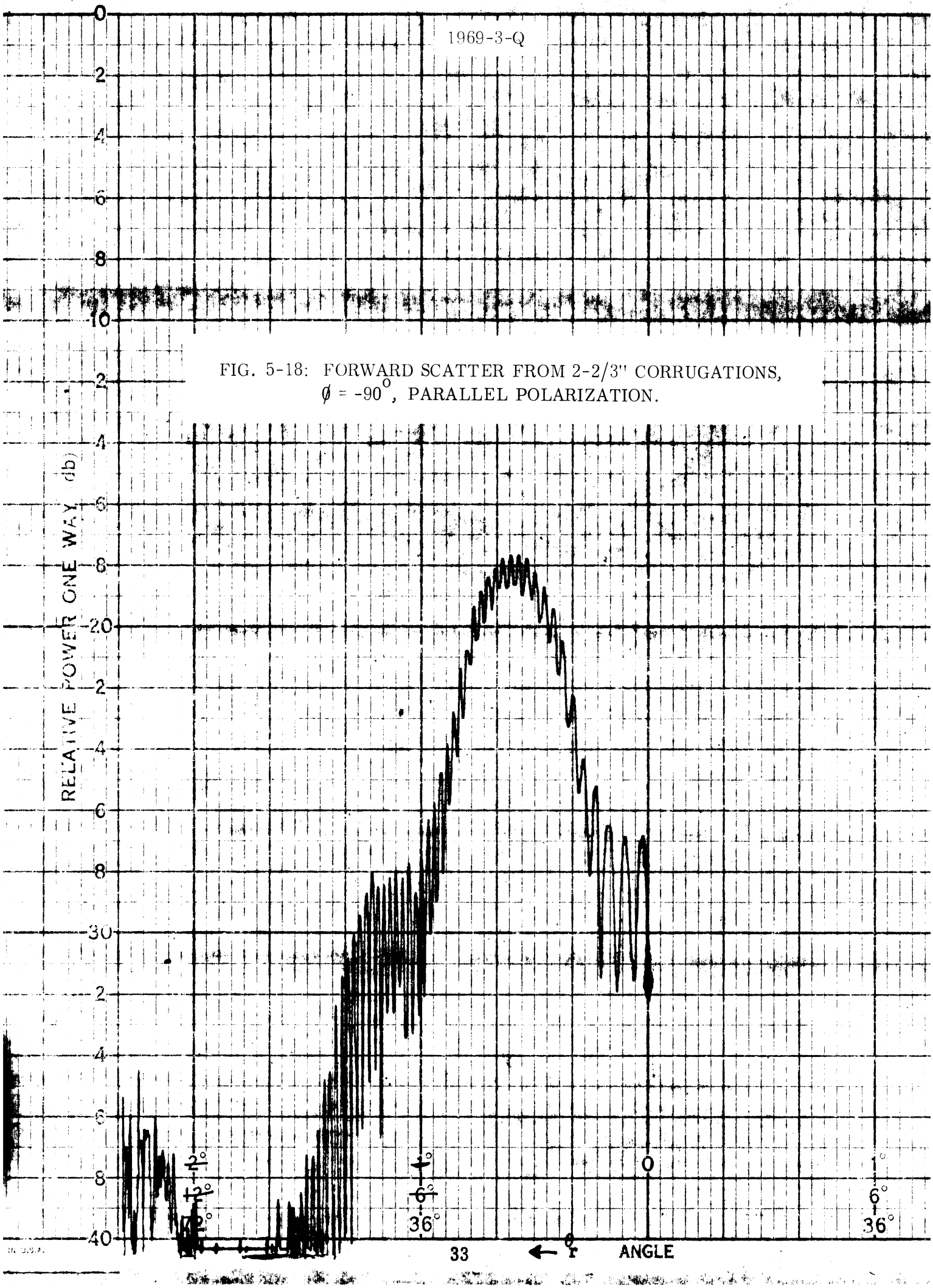

FIG. 5-18: FORWARD SCATTER FROM 2-2/3" CORRUGATIONS, $\phi = -90^{\circ}$, PARALLEL POLARIZATION.

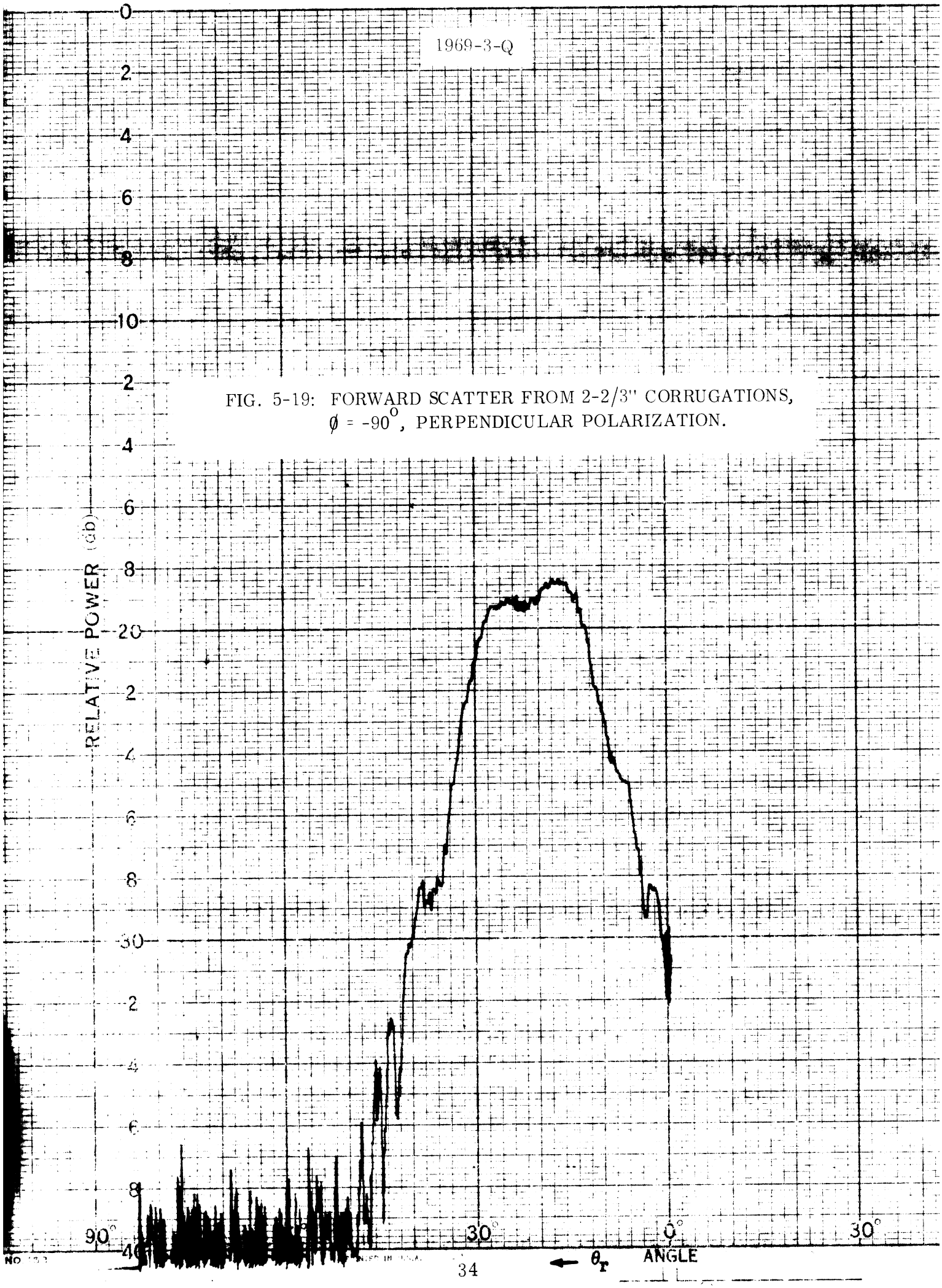

FIG. 5-19: FORWARD SCATTER FROM 2-2/3" CORRUGATIONS, $\phi = -90^{\circ}$, PERPENDICULAR POLARIZATION.

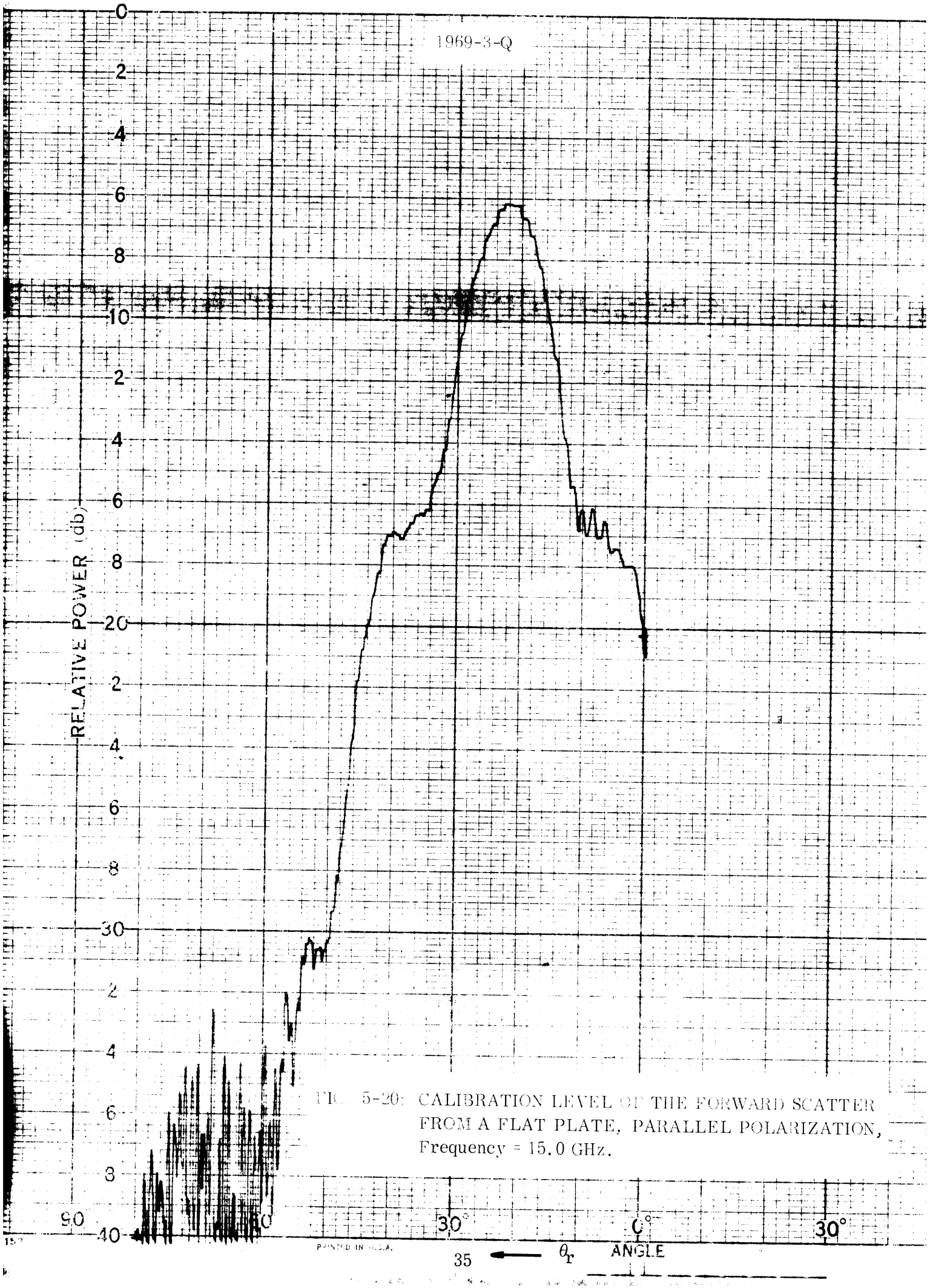

FIG. 5-20: CALIBRATION LEVEL OF THE FORWARD SCATTER FROM A FLAT PLATE, PARALLEL POLARIZATION, Frequency = 15.0 GHz.

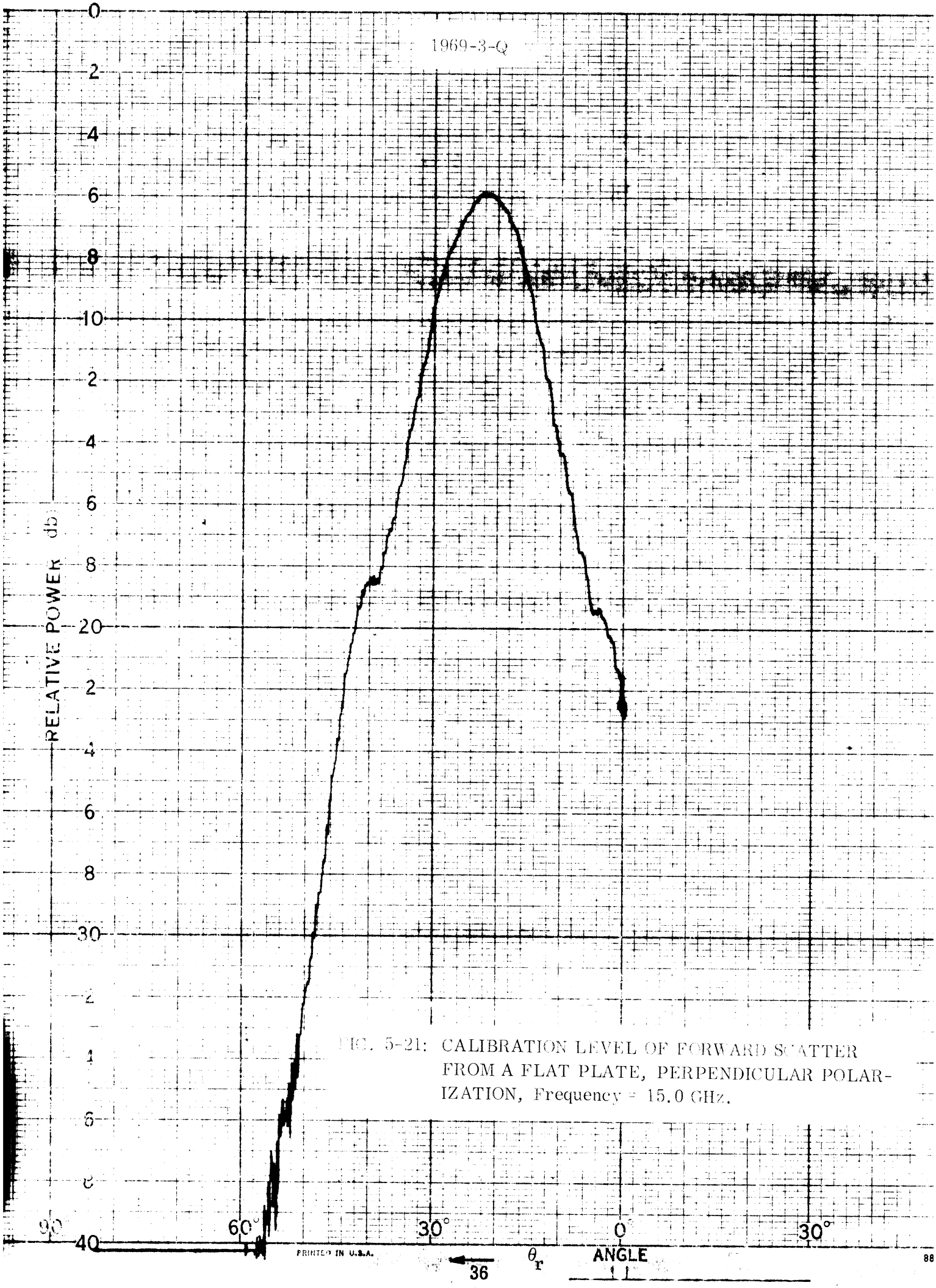

FIG. 5-21: CALIBRATION LEVEL OF FORWARD SCATTER FROM A FLAT PLATE, PERPENDICULAR POLARIZATION, Frequency = 15.0 GHz.

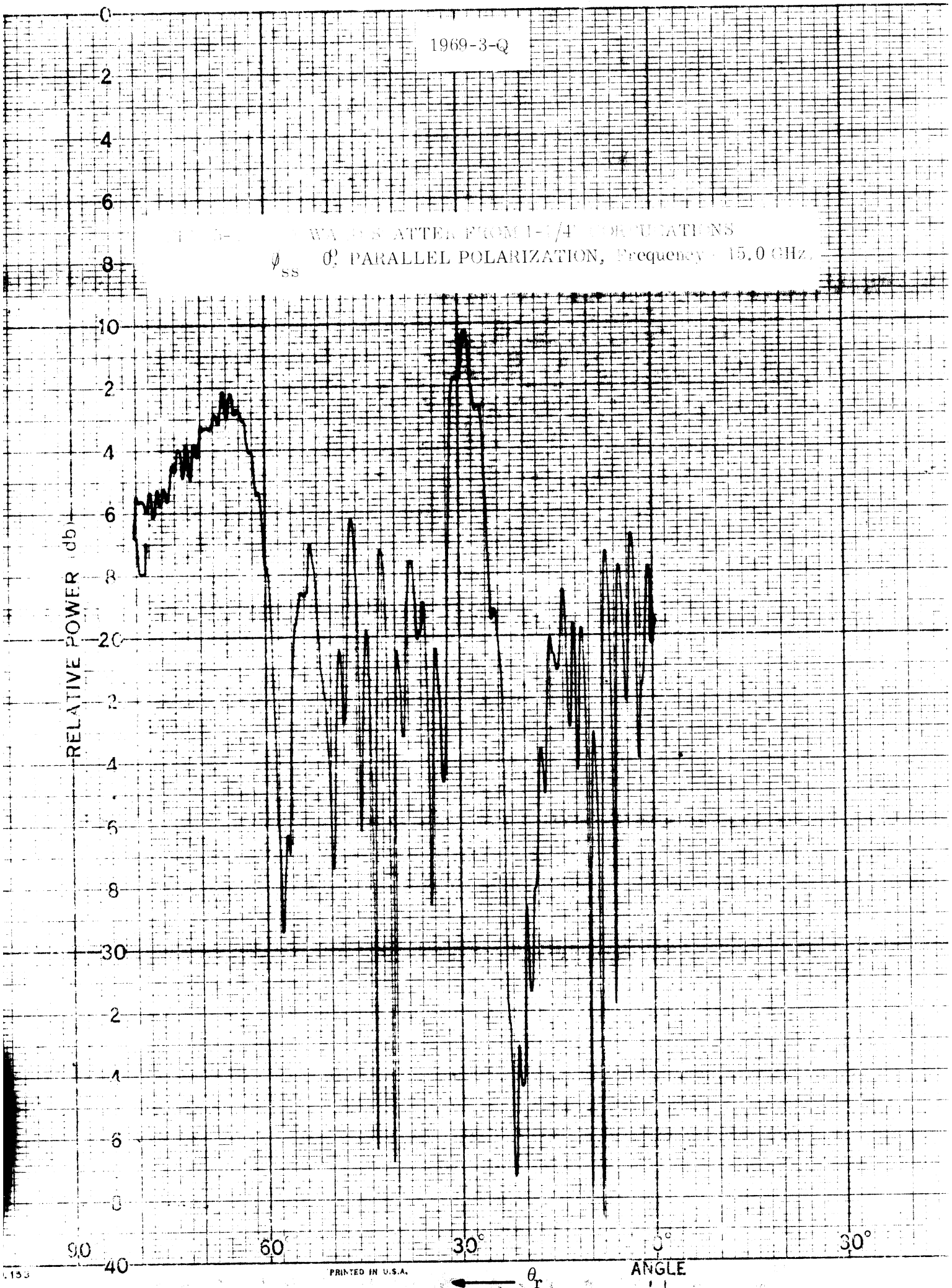

PRINTED IN U.S.A.

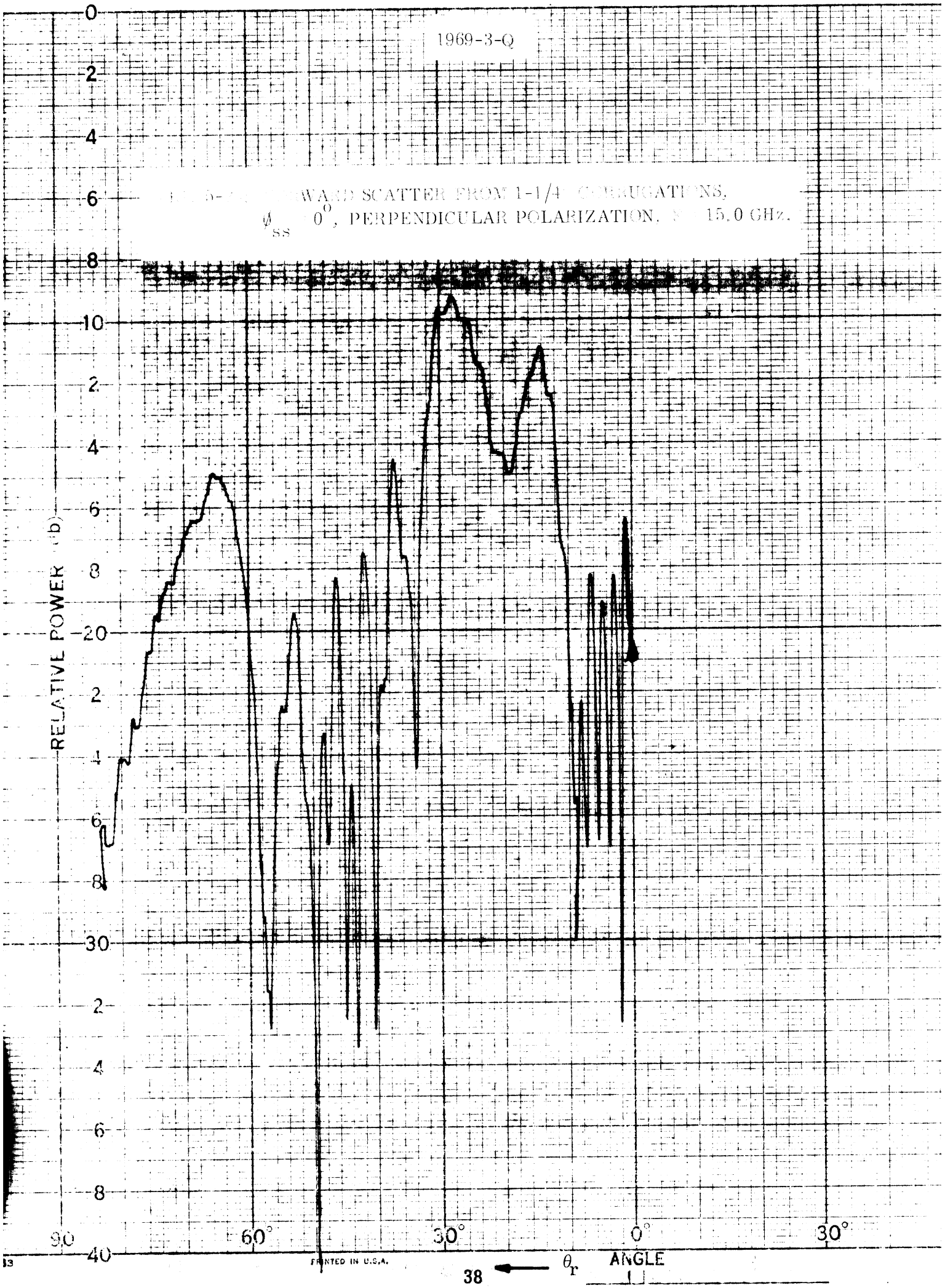
1969-3-Q
FORWARD SCATTER FROM 1-1/4 CORRUGATIONS,
$\phi_{ss} = 0^{\circ}$, PERPENDICULAR POLARIZATION, f = 15.0 GHz.
RELATIVE POWER (db)
0
2
4
6
8
10
2
4
6
8
20
2
4
6
8
30
2
4
6
8
40
90°
60°
30°
0°
30°
θ_r ANGLE

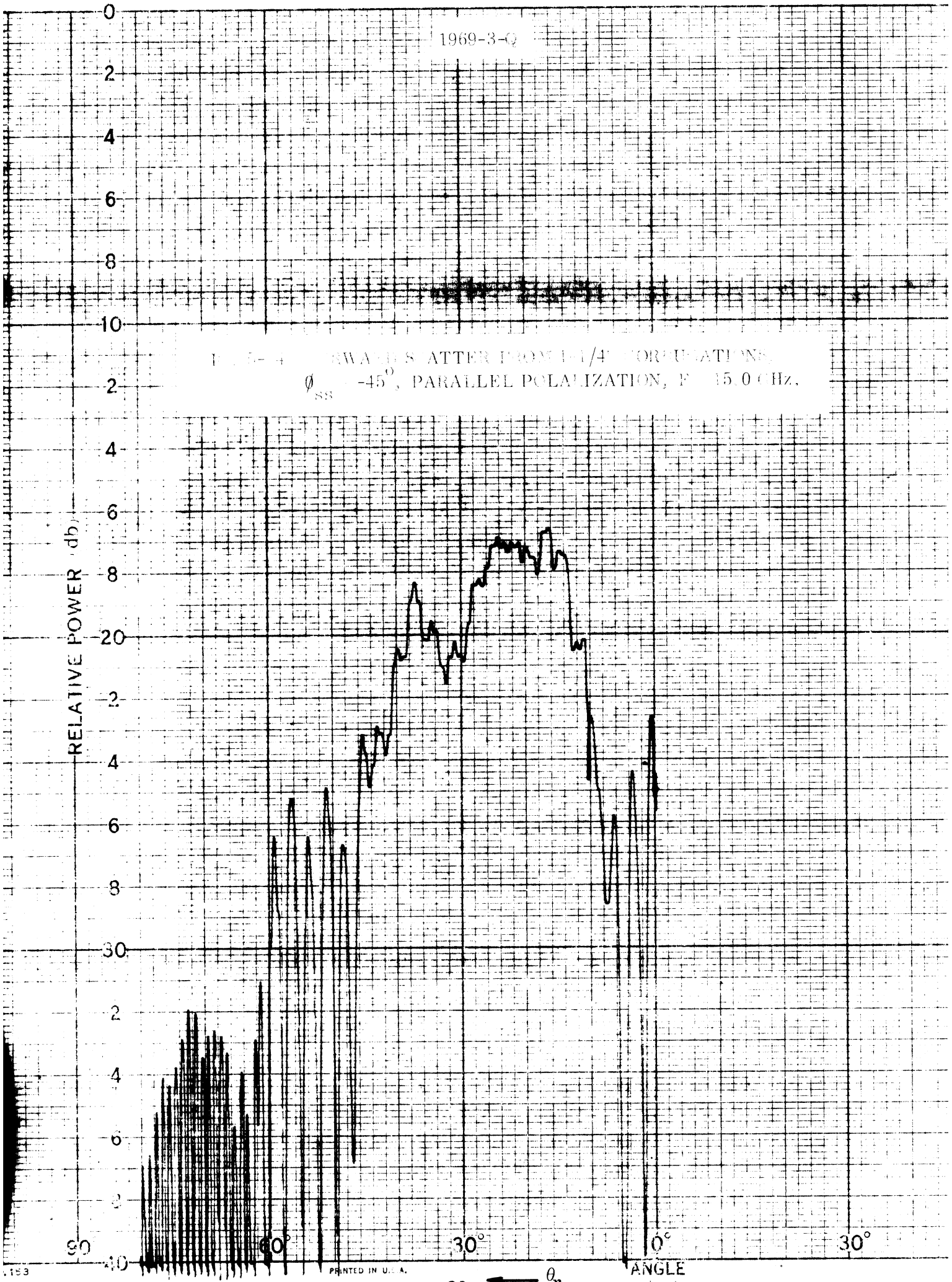

FIG. 3-4 ... SCATTERED FROM 1/4" CORRUGATIONS, $\phi_{SB} = -45^{\circ}$, PARALLEL POLARIZATION, F = 15.0 GHz.

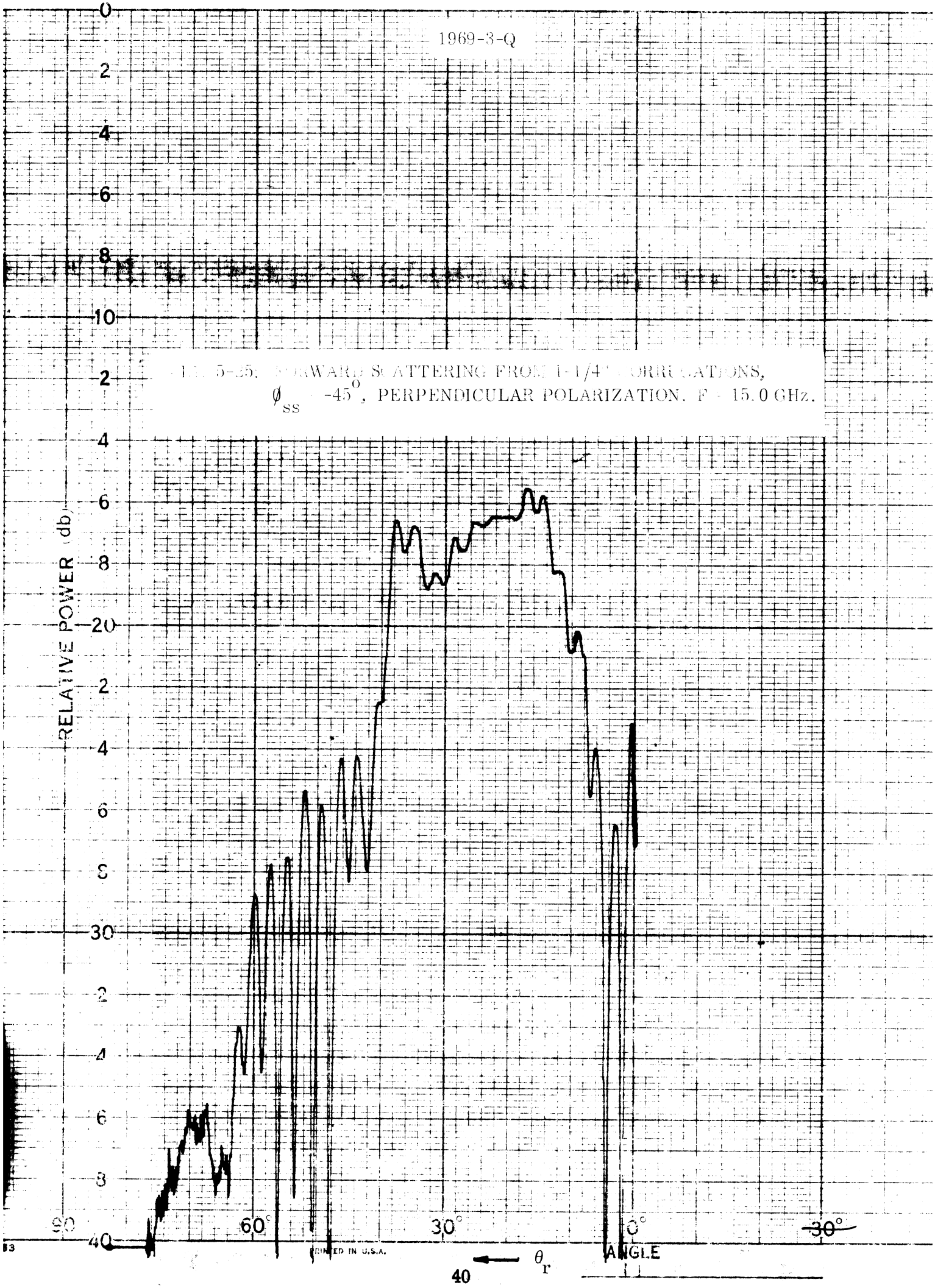

FIG. 5-25. FORWARD SCATTERING FROM 1-1/4" CORRUGATIONS, $\phi_{ss} = -45^{\circ}$, PERPENDICULAR POLARIZATION, F = 15.0 GHz.

1969-3-Q

FIG. 5-26: FORWARD SCATTER FROM 1-1/4" CORRUGATIONS, $\phi_{ss} = -90^{o}$, PARALLEL POLARIZATION, F = 15.0 GHz.

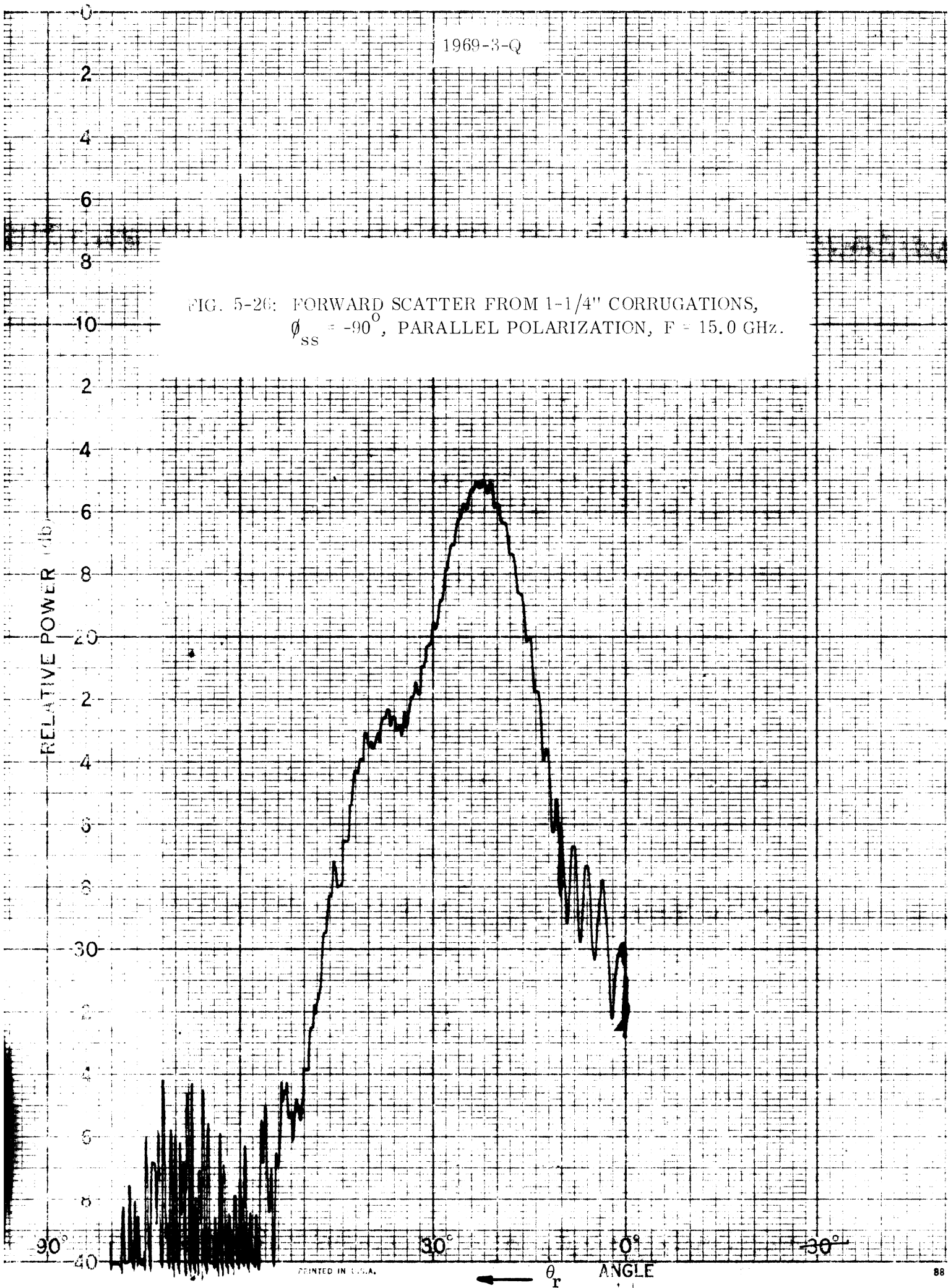

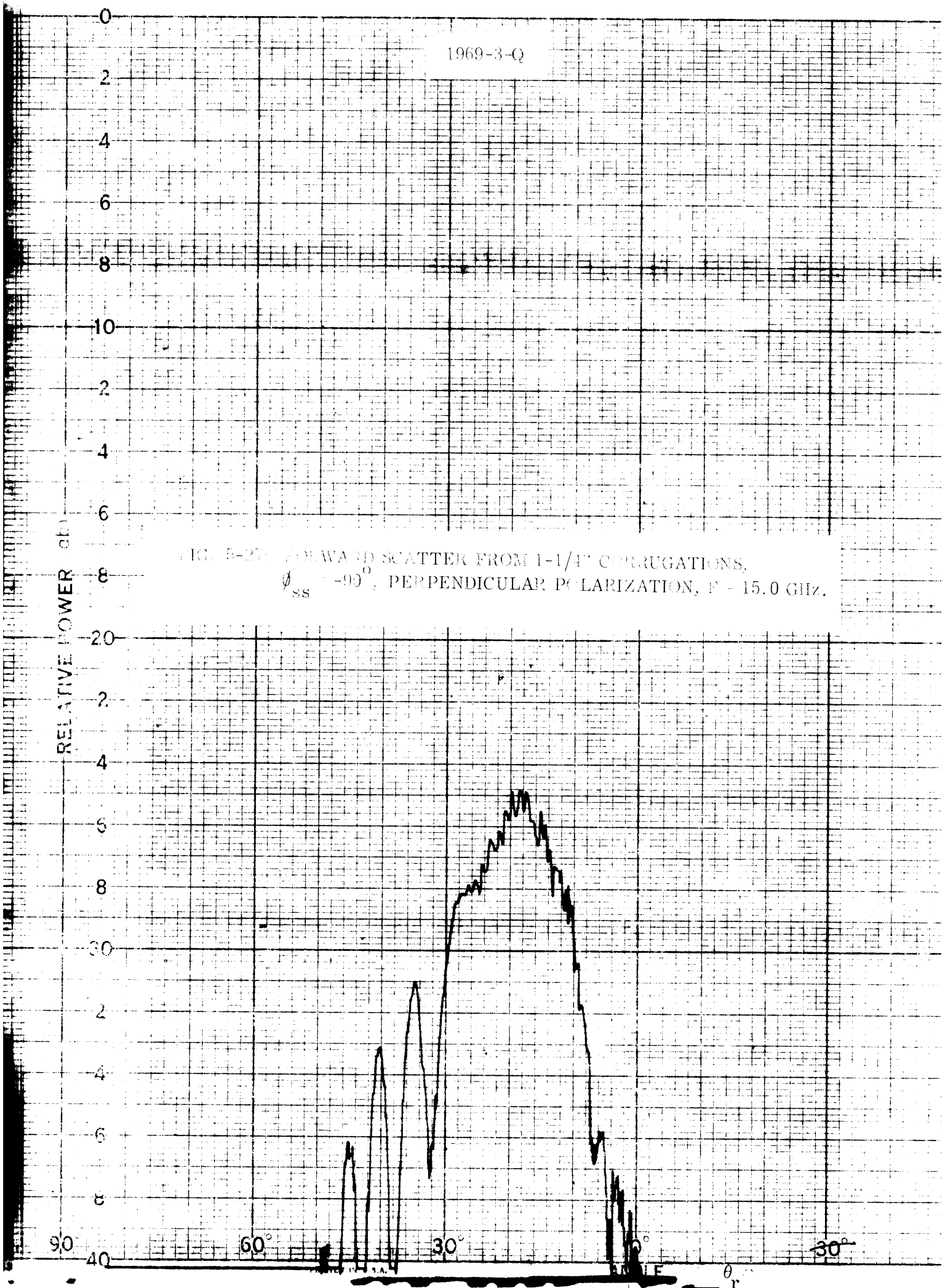

FIG. 5-27. FORWARD SCATTER FROM 1-1/4" CORRUGATIONS, $\phi_{ss} = -90^{\circ}$, PERPENDICULAR POLARIZATION, F = 15.0 GHz.

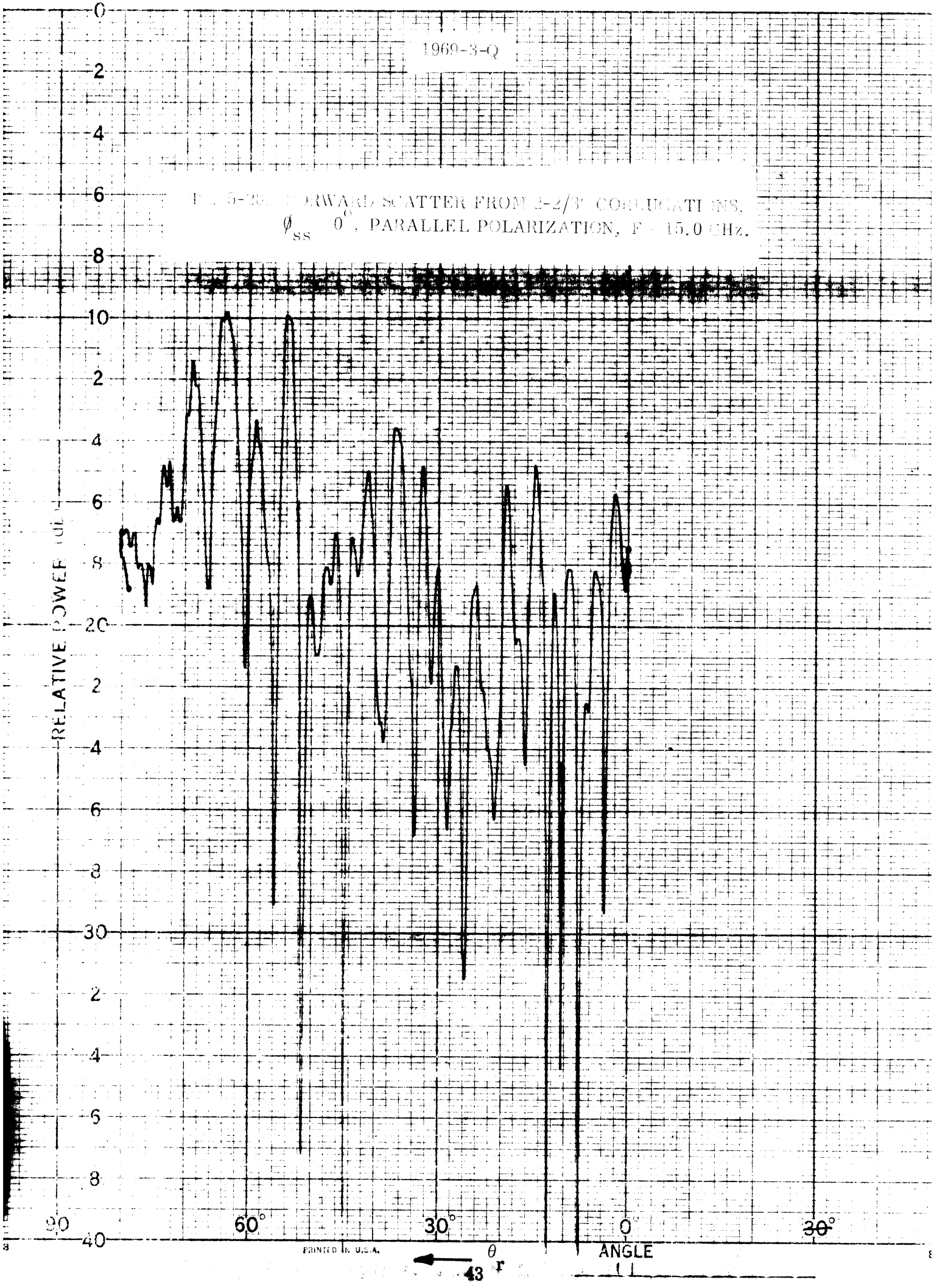
1969-3-Q
FIG. 5-28. FORWARD SCATTER FROM 2-2/3" CORRUGATIONS,
ϕ_{SS} 0°, PARALLEL POLARIZATION, F = 15.0 GHz.
RELATIVE POWER (dB)
0
2
4
6
8
10
2
4
6
8
20
2
4
6
8
30
2
4
6
8
40
90°
60°
30°
0°
30°
ANGLE
θr

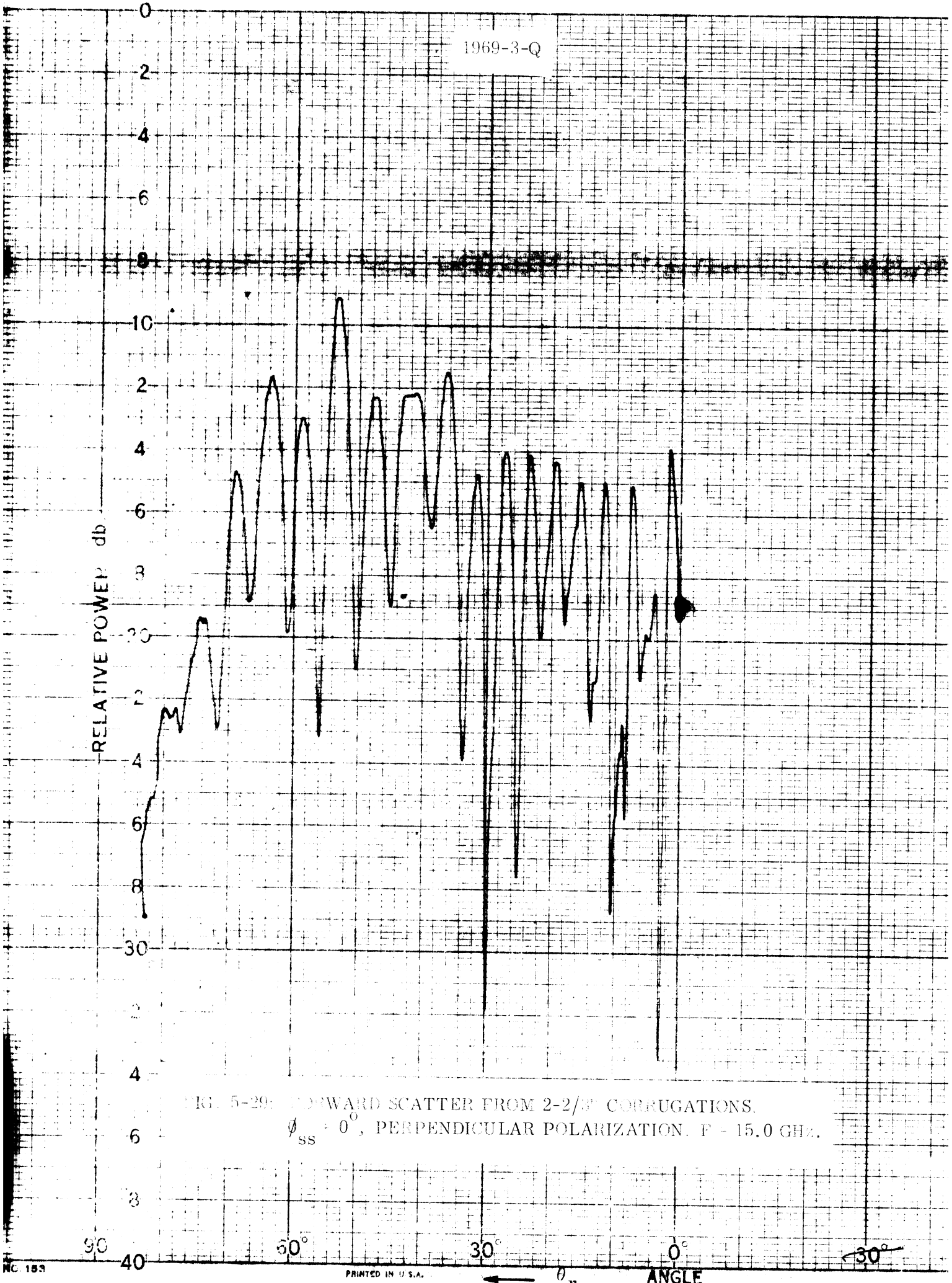

FIG. 5-29. FORWARD SCATTER FROM 2-2/3" CORRUGATIONS. $\phi_{ss} = 0^{\circ}$, PERPENDICULAR POLARIZATION. F = 15.0 GHz.

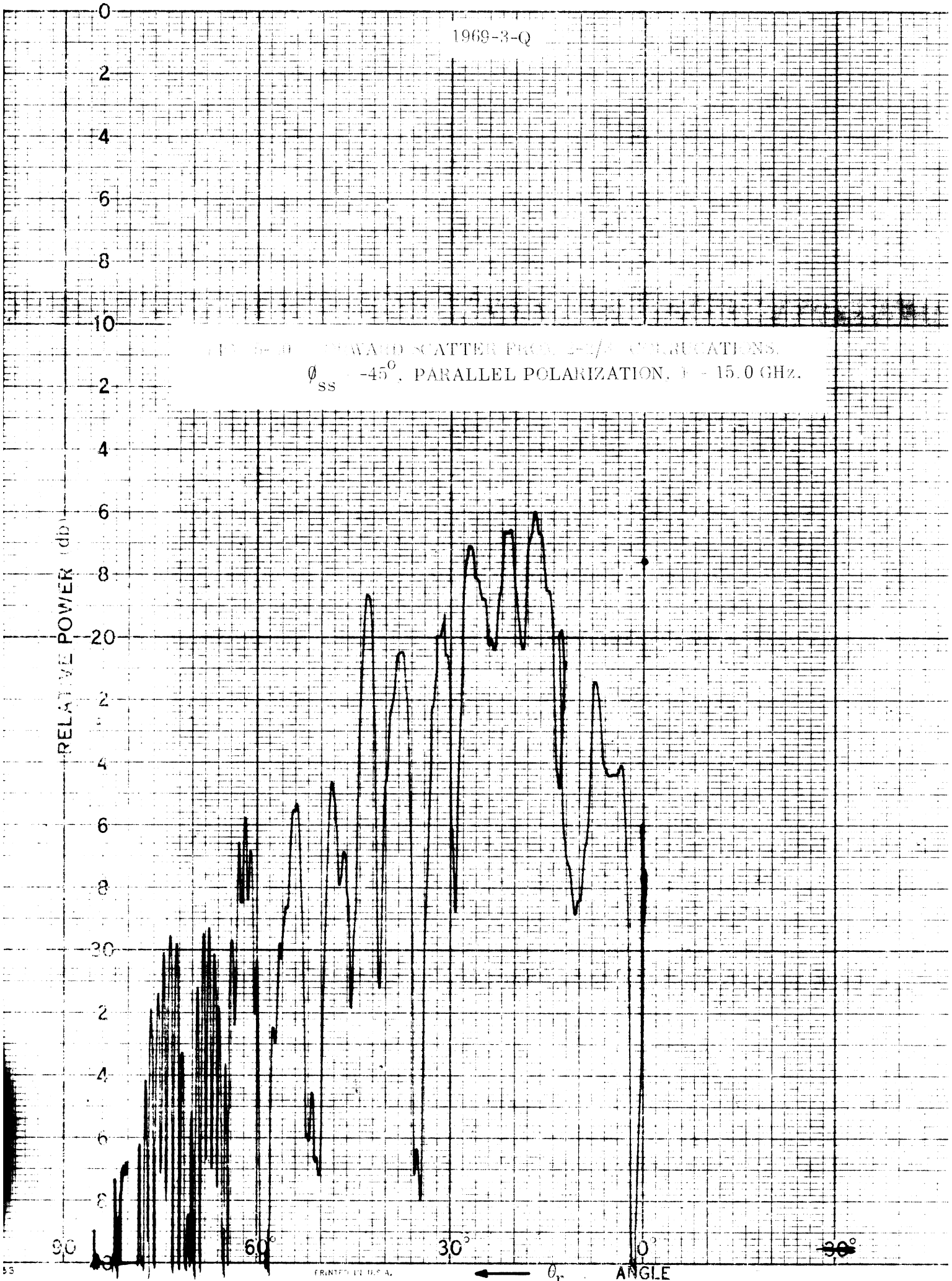
1969-3-Q
ϕ_{ss} -45°, PARALLEL POLARIZATION, f = 15.0 GHz.
RELATIVE POWER (db)
0
2
4
6
8
10
2
4
6
8
20
2
4
6
8
30
2
4
6
8
90°
60°
30°
0°
-30°
θ_r ANGLE

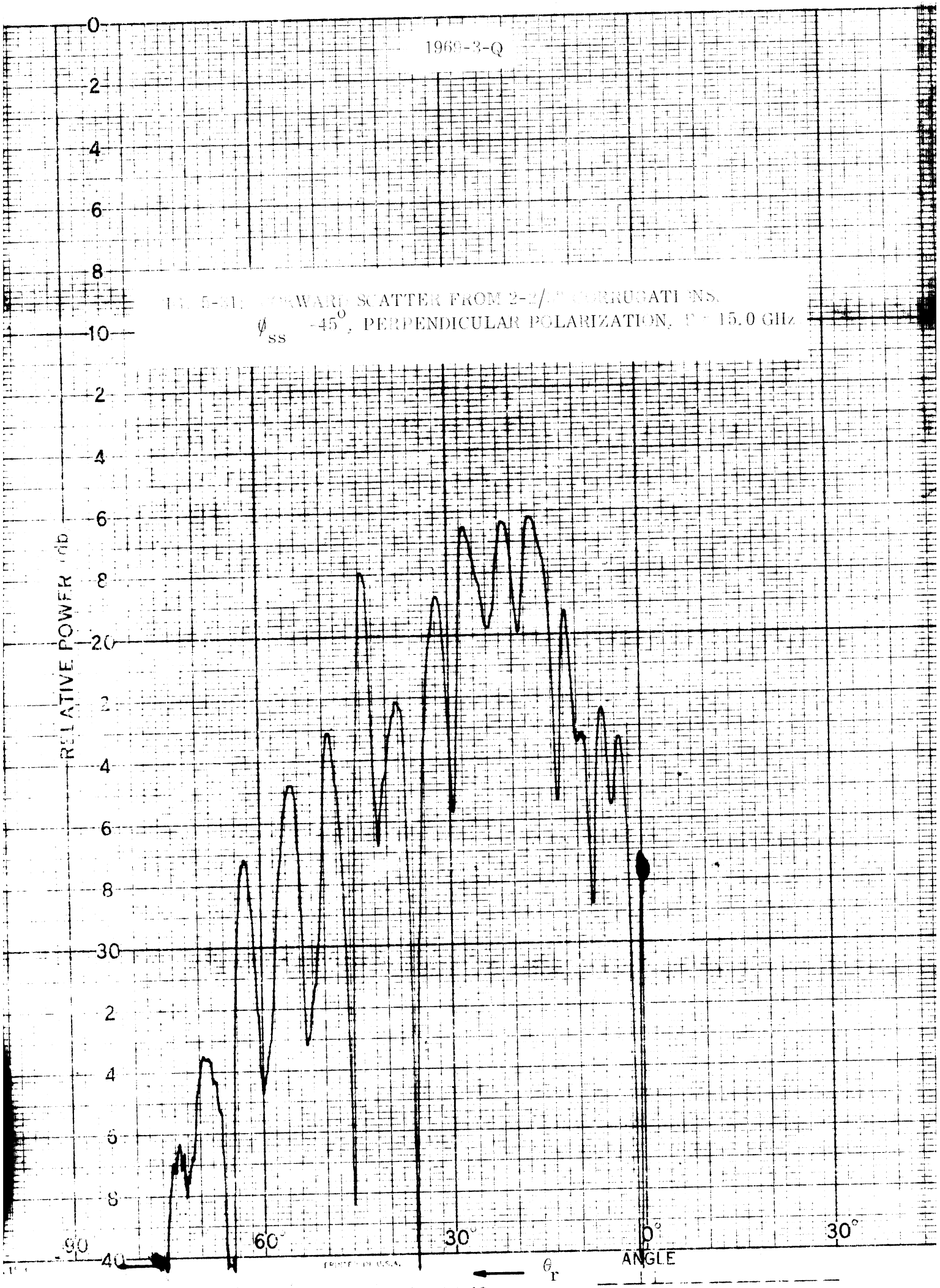
1969-3-Q
ψ_{ss} -45°, PERPENDICULAR POLARIZATION, f = 15.0 GHz
RELATIVE POWER, db
0
2
4
6
8
10
20
30
40
90
60
30
0
30
ANGLE
θ_r

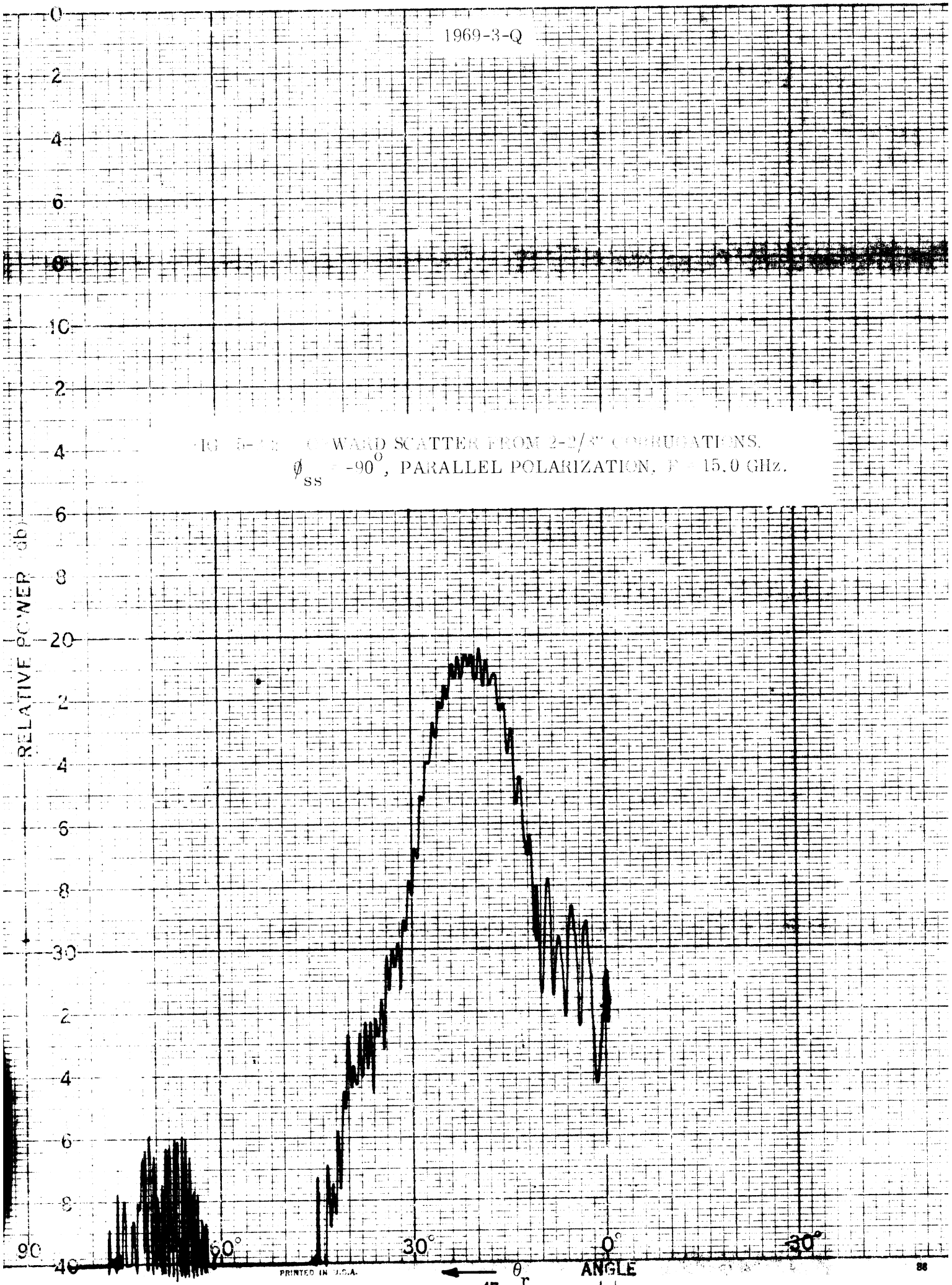

FIG. 5-12 FORWARD SCATTER FROM 2-2/3" CORRUGATIONS.
$\phi_{ss} = -90^{\circ}$, PARALLEL POLARIZATION, F = 15.0 GHz.

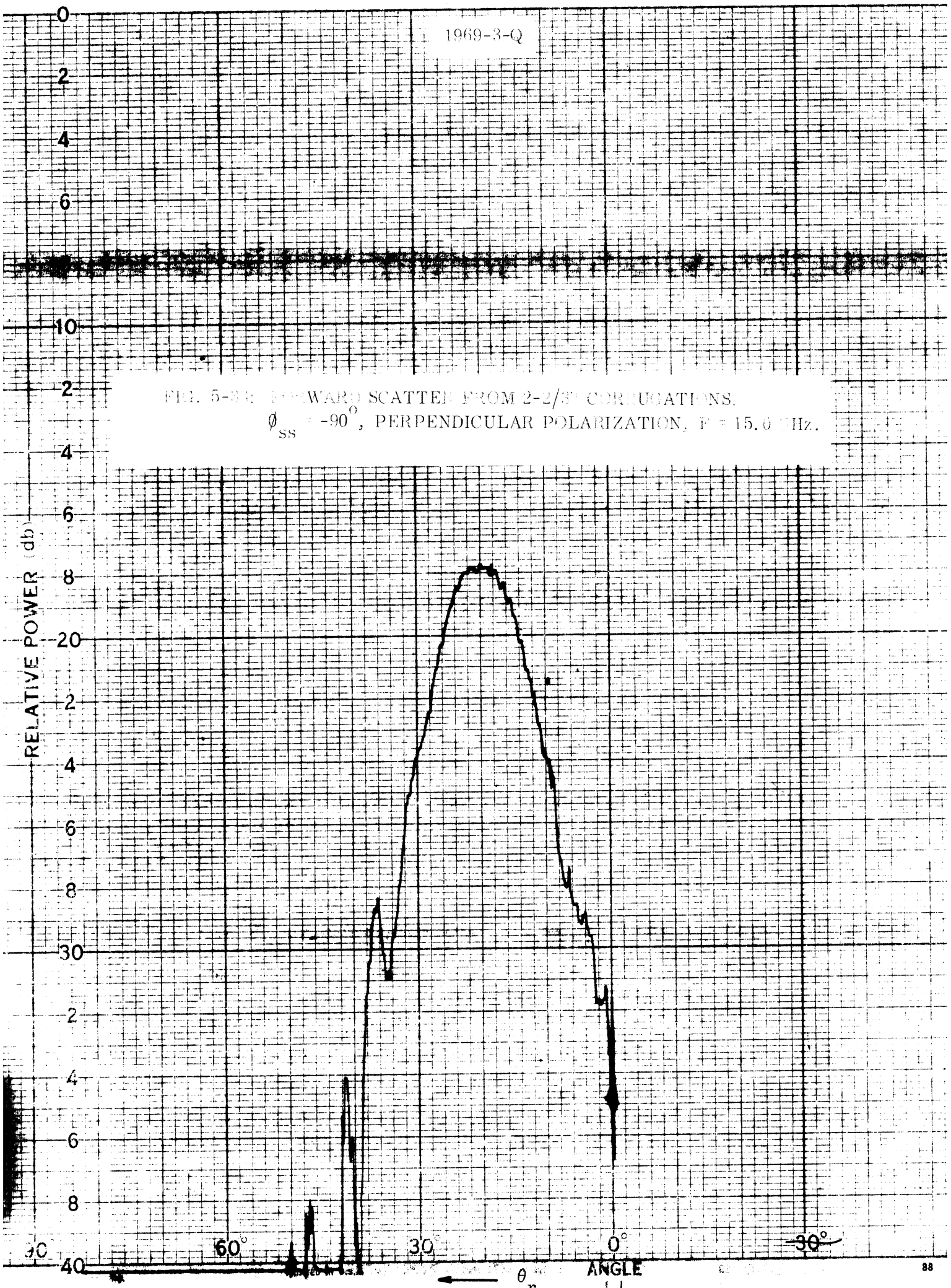

FIG. 5-33 FORWARD SCATTER FROM 2-2/3" CORRUGATIONS.
$\phi_{ss} = -90^{\circ}$, PERPENDICULAR POLARIZATION, F = 15.0 GHz.

1969-3-Q

FIG. 5-64 FORWARD SCATTER OF CROSS-POLARIZED ENERGY FROM 1-1/4" CORRUGATIONS, $\phi_{ss} = -45^{\circ}$, TRANSMIT PARALLEL POLARIZATION, RECEIVE PERPENDICULAR POLARIZATION.

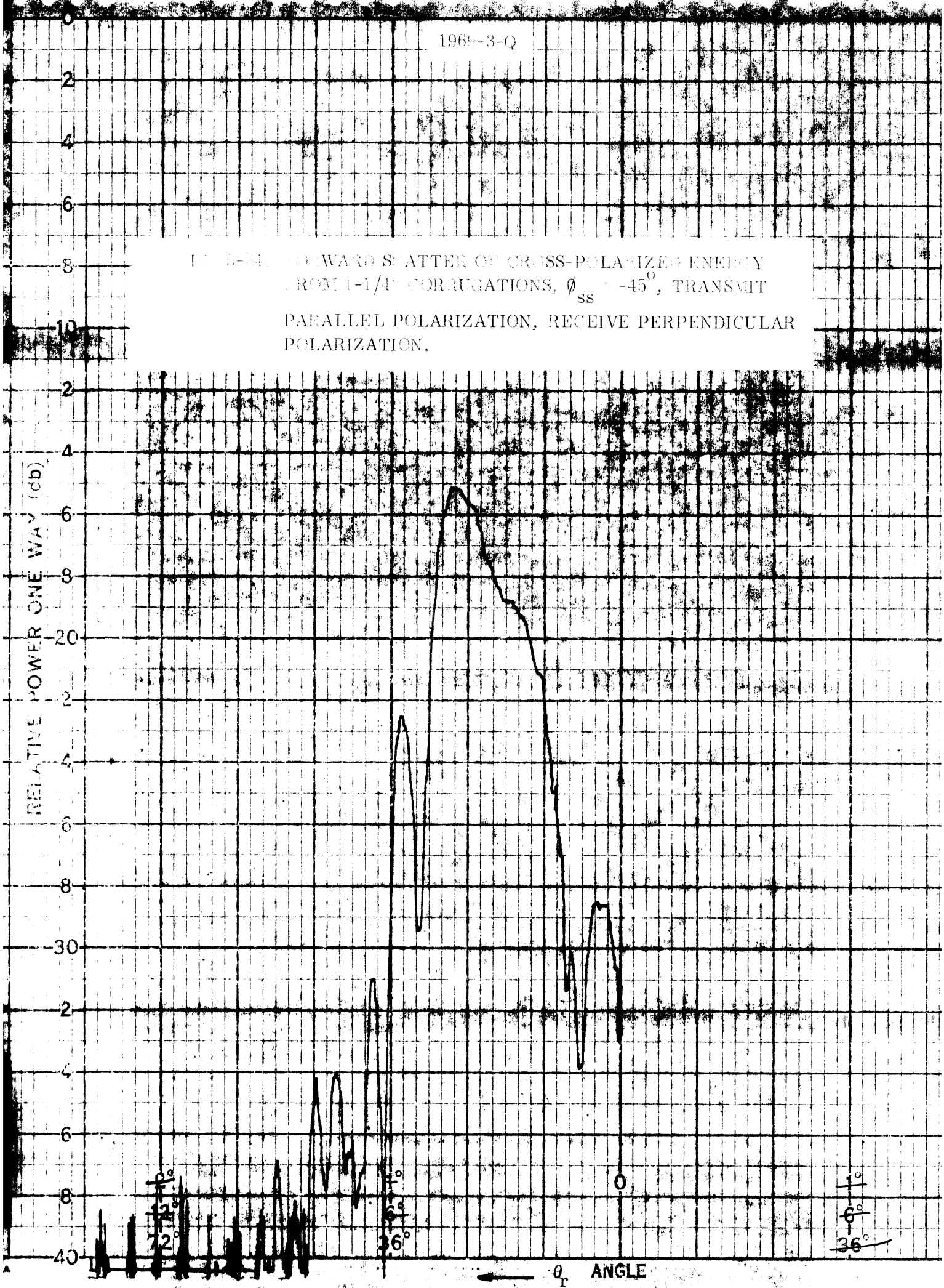

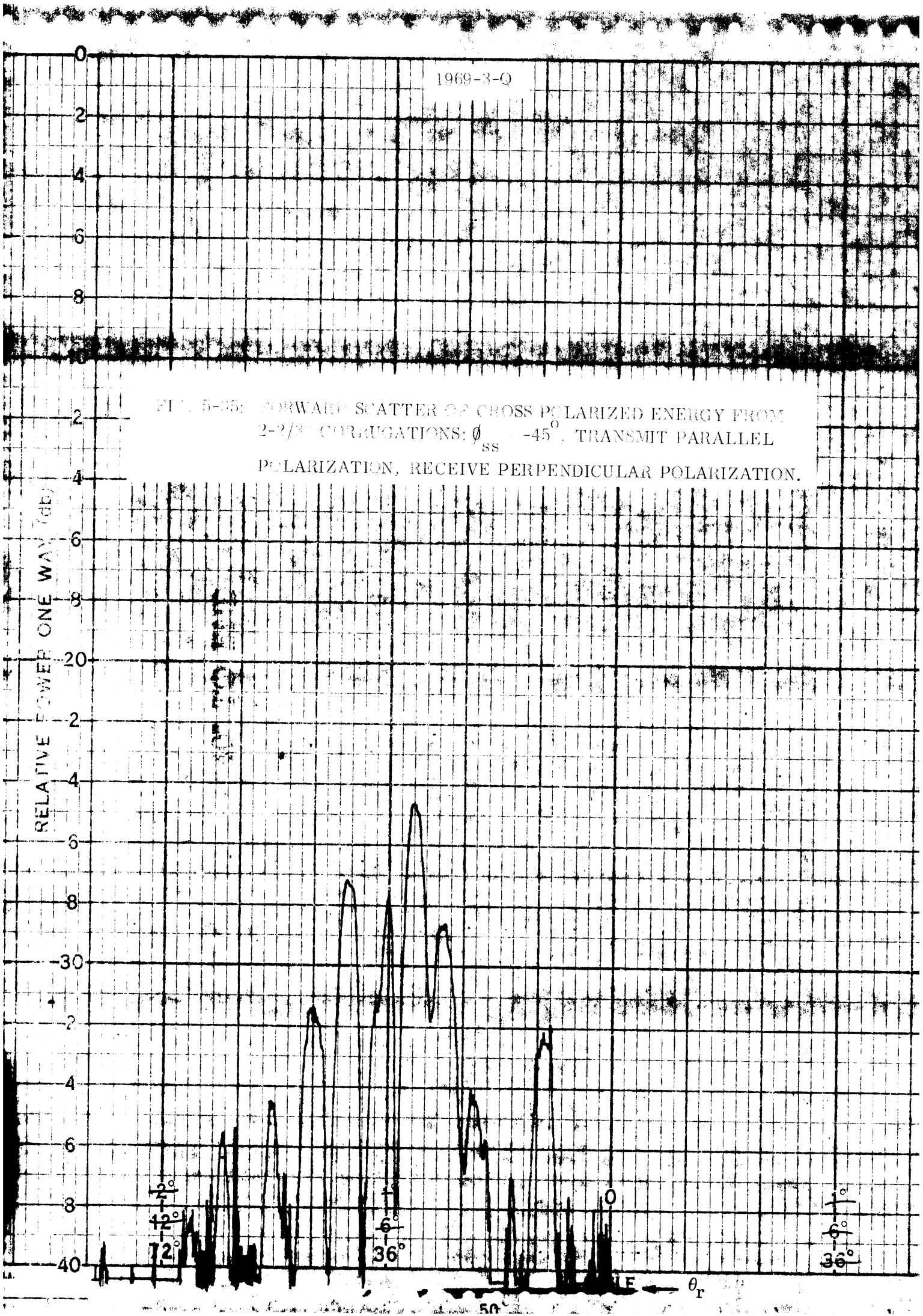

FIG. 5-35: FORWARD SCATTER OF CROSS POLARIZED ENERGY FROM 2-2/3" CORRUGATIONS: $\phi_{ss} = -45^{o}$, TRANSMIT PARALLEL POLARIZATION, RECEIVE PERPENDICULAR POLARIZATION.

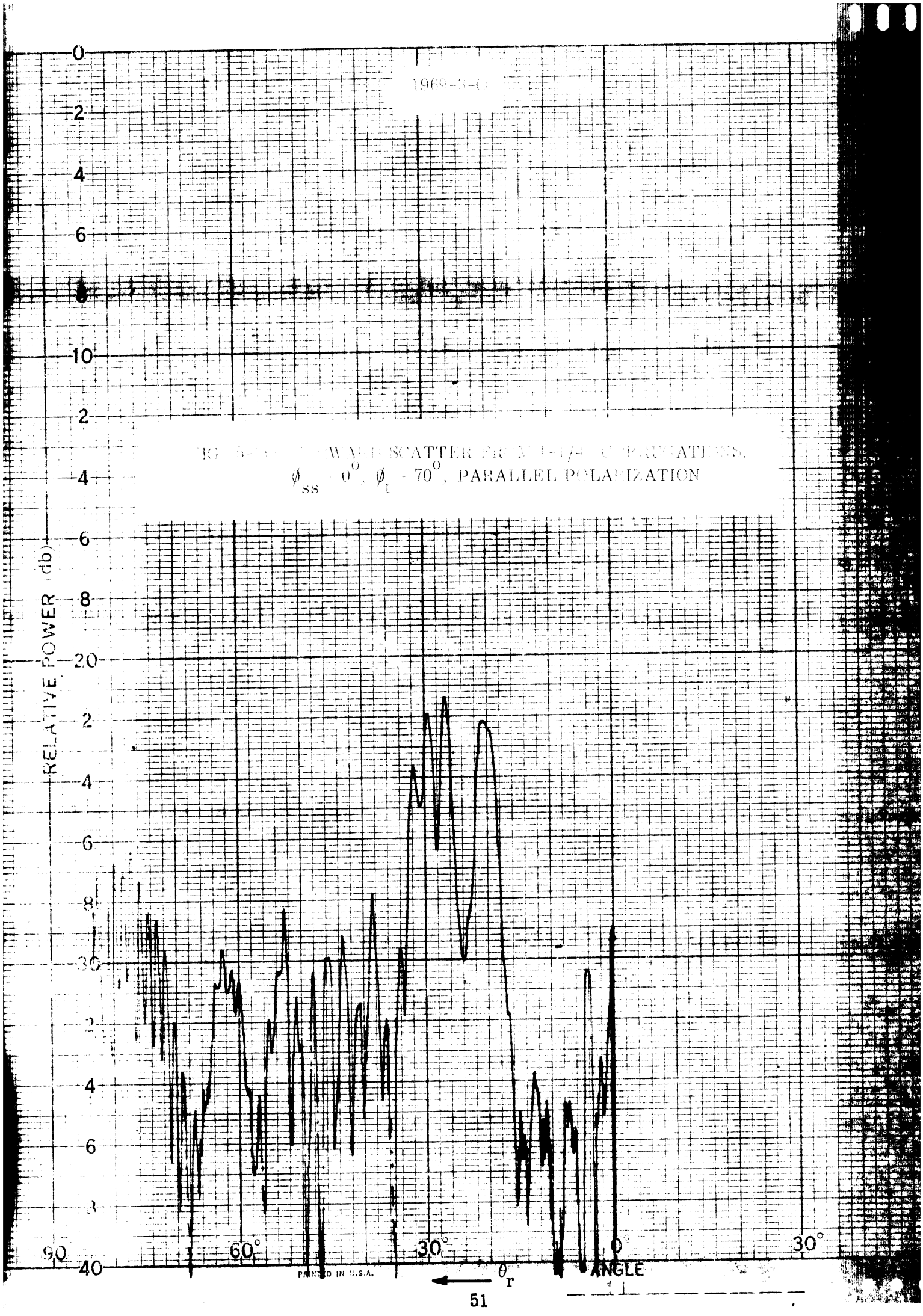

$\phi_{ss} = 0^{o}$, $\phi_t = 70^{o}$, PARALLEL POLARIZATION

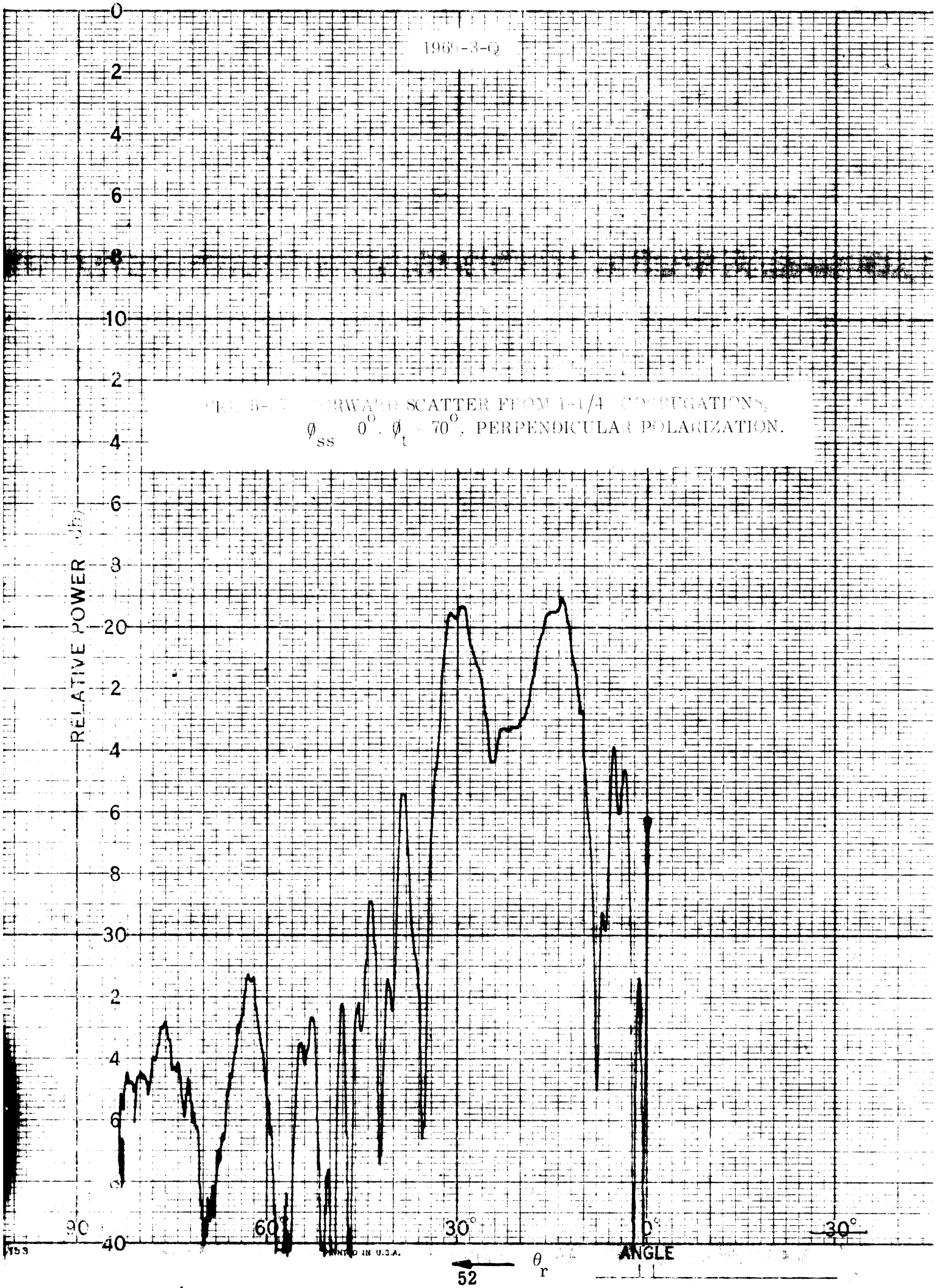

FIG. 3-7. FORWARD SCATTER FROM 1-1/4" CORRUGATIONS, ϕ_{ss} 0°, ϕ_t = 70°, PERPENDICULAR POLARIZATION.

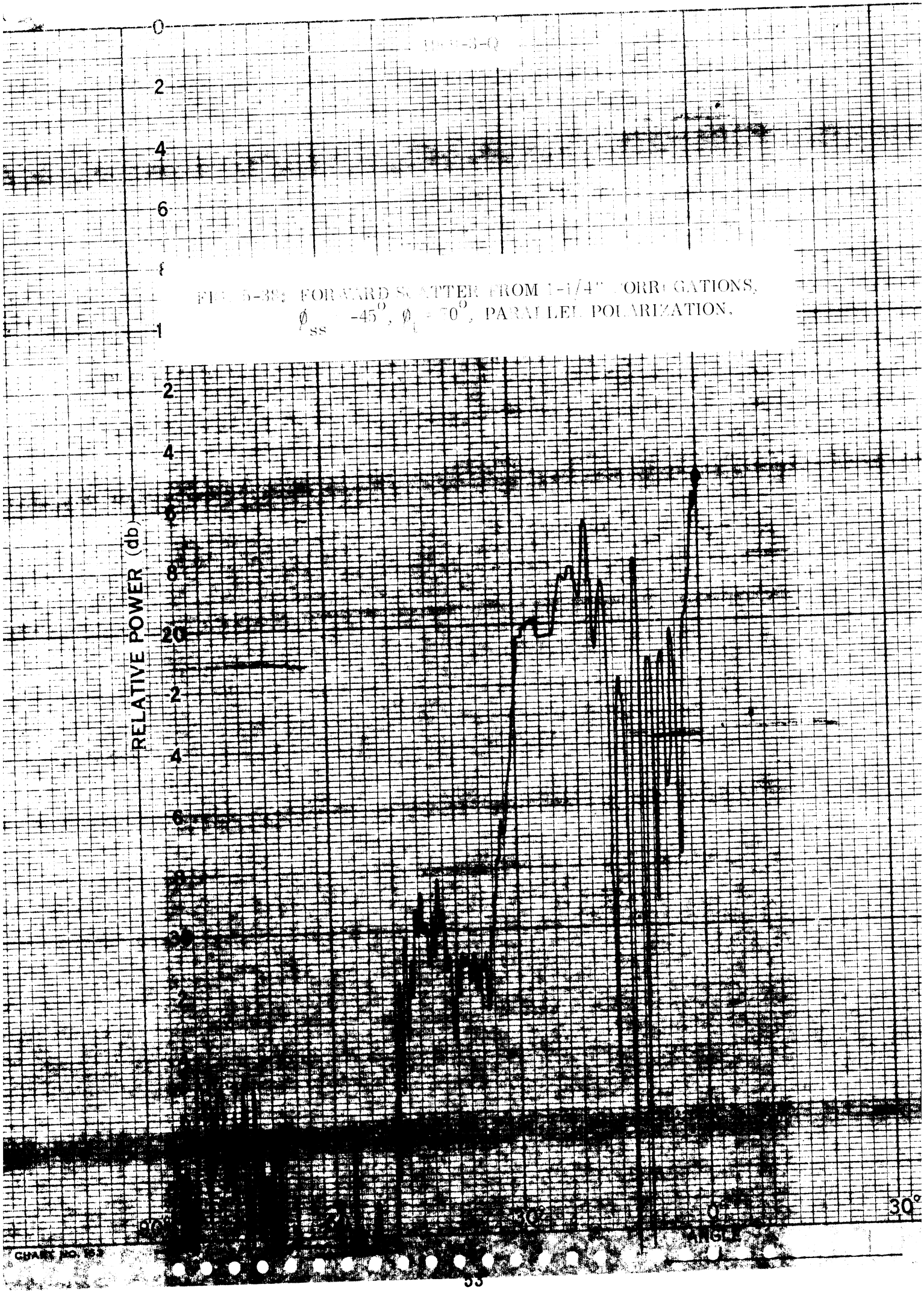

FIG. 5-38: FORWARD SCATTER FROM 1-1/4" CORRUGATIONS, $\phi_{ss} = -45^{\circ}$, $\phi_i = 0^{\circ}$, PARALLEL POLARIZATION.

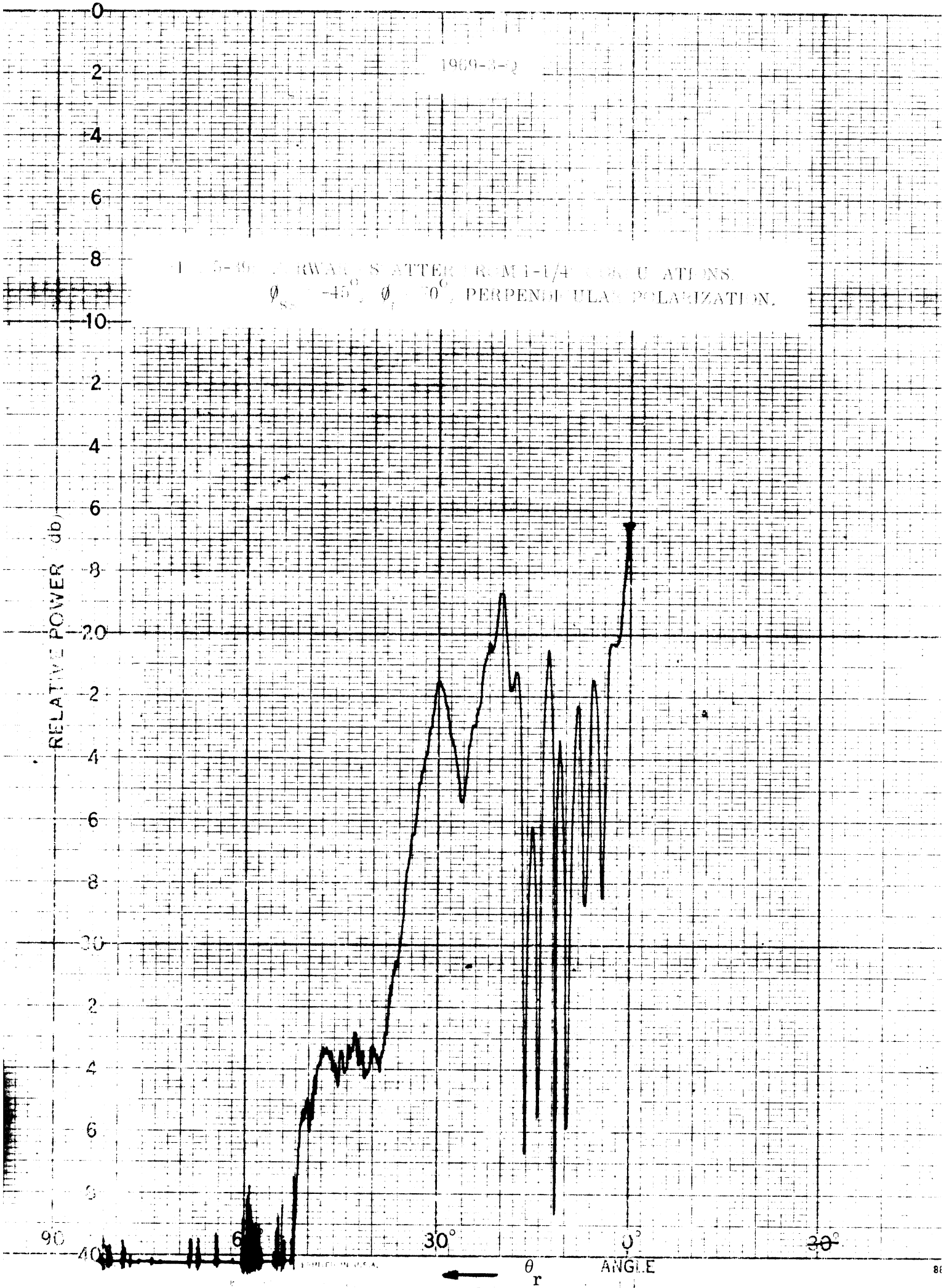
1969-1-2
RELATIVE POWER (db)
0
2
4
6
8
10
2
4
6
8
20
2
4
6
8
20
2
4
6
8
90
60°
30°
0°
20°
ANGLE
θr

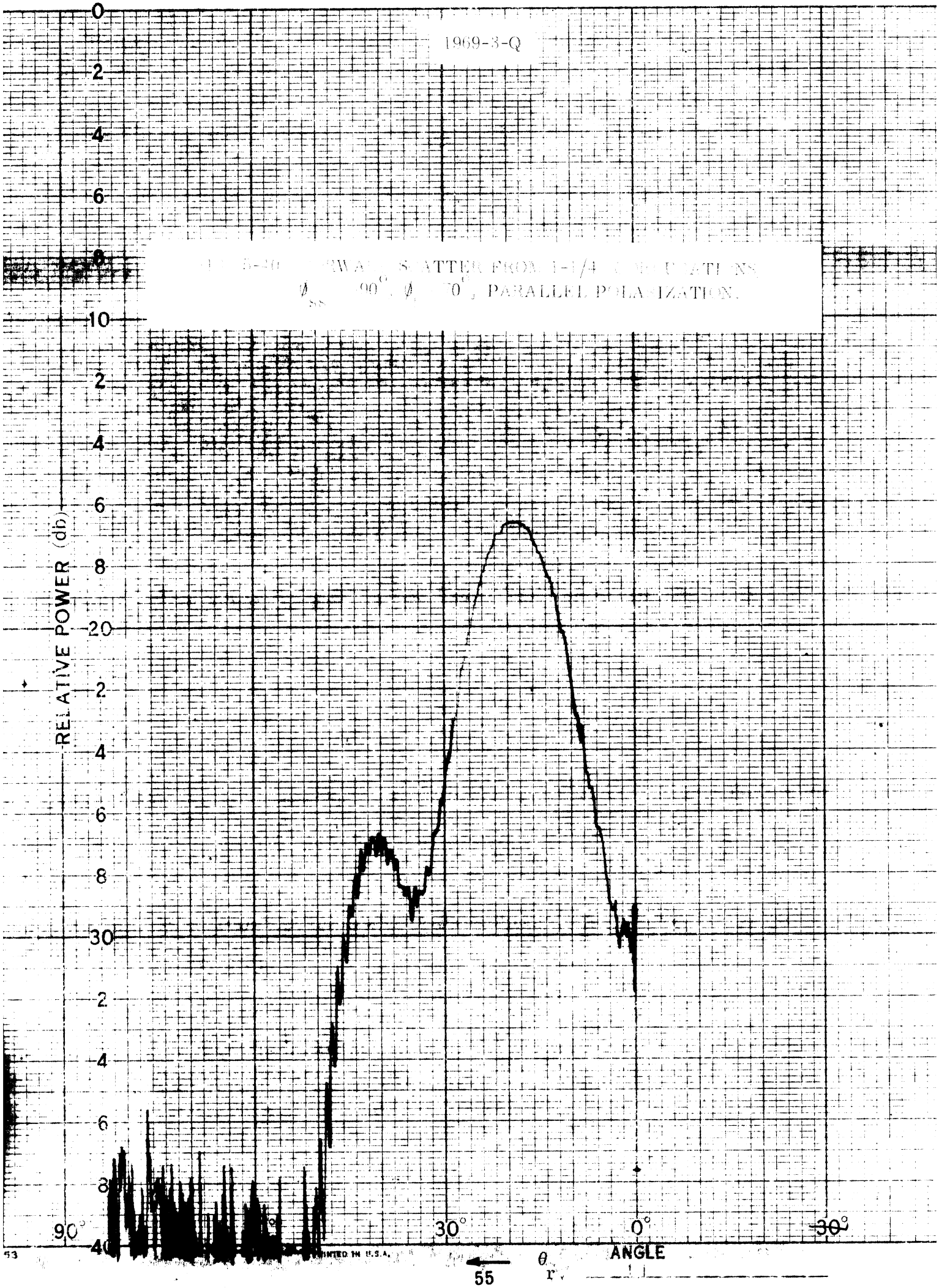
1969-3-Q
RELATIVE POWER (db)
0
2
4
6
8
10
2
4
6
8
20
2
4
6
8
30
2
4
6
8
40
90°
30°
0°
30°
ANGLE
θr

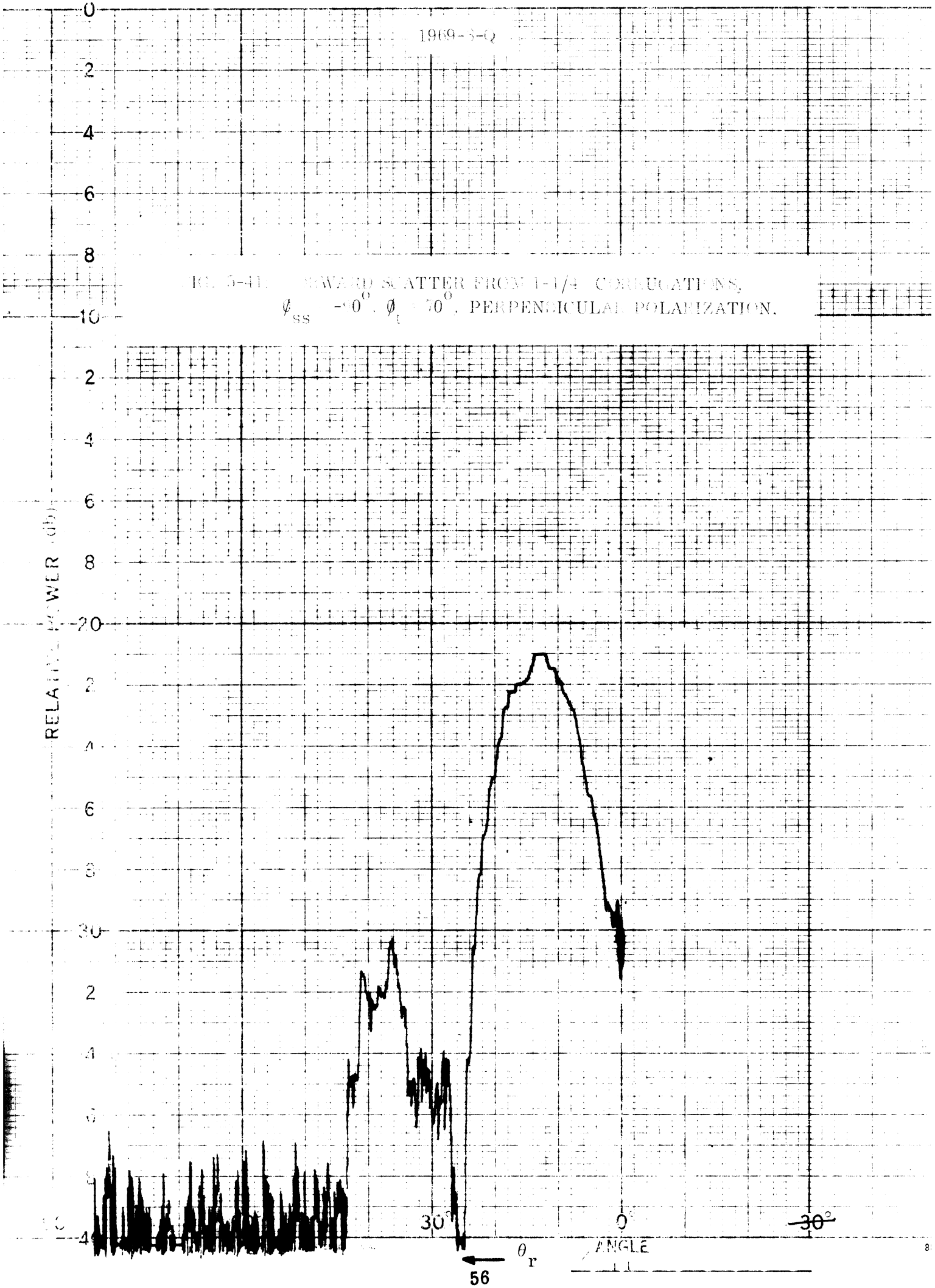
1969-3-Q
FORWARD SCATTER FROM 1-1/4 CORRUGATIONS,
ψ_{ss} = 0°, ϕ_i = 30°, PERPENDICULAR POLARIZATION.
RELATIVE POWER (db)
0
2
4
6
8
10
2
4
6
8
20
2
4
6
8
30
2
4
30°
0
30°
θ_r
ANGLE

1969-3-Q

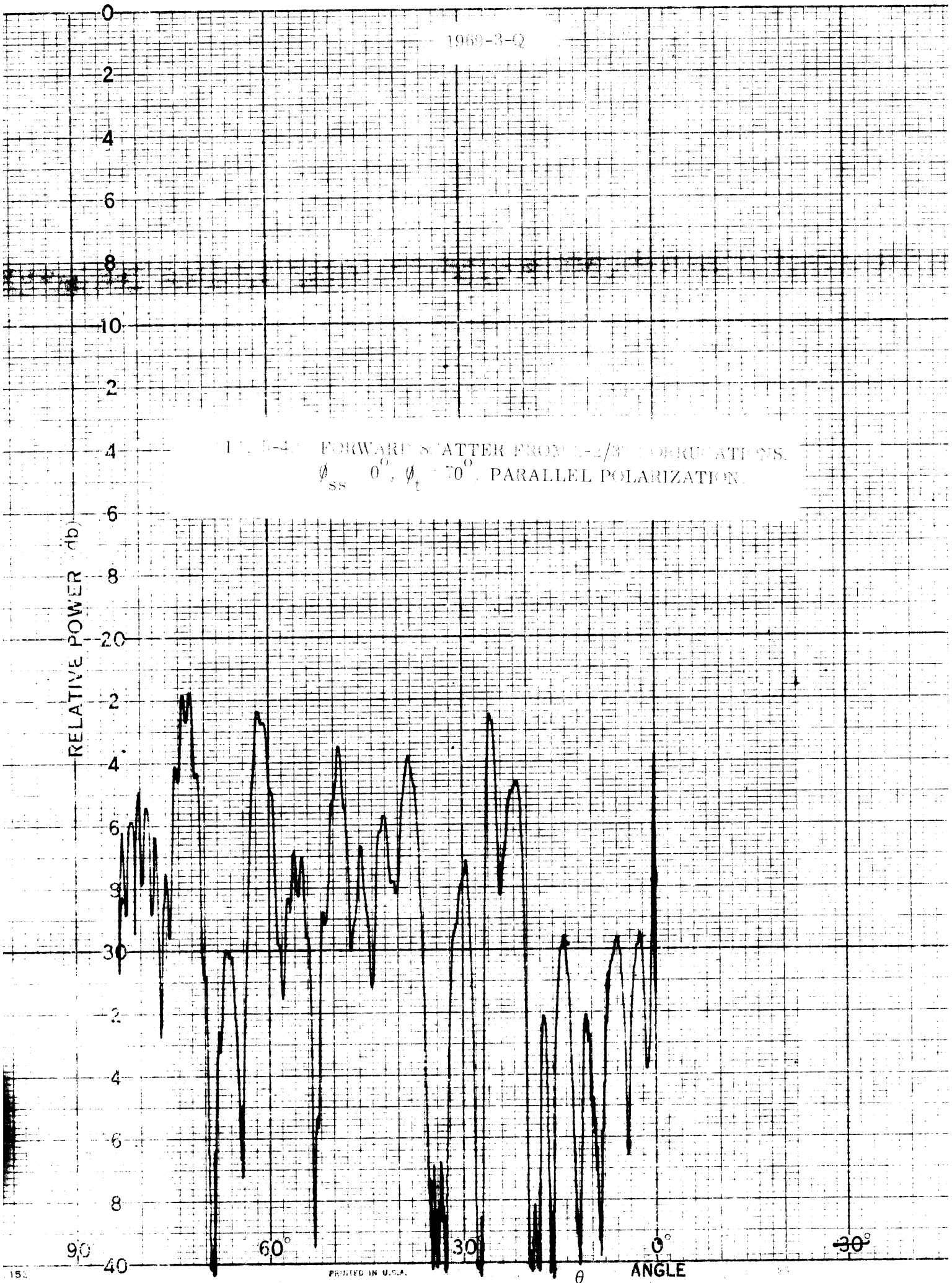

FIG. 3-4. FORWARD SCATTER FROM 2-2/3 λ CORRUGATIONS.
ϕ_{ss} 0°, ϕ_t 70°, PARALLEL POLARIZATION.

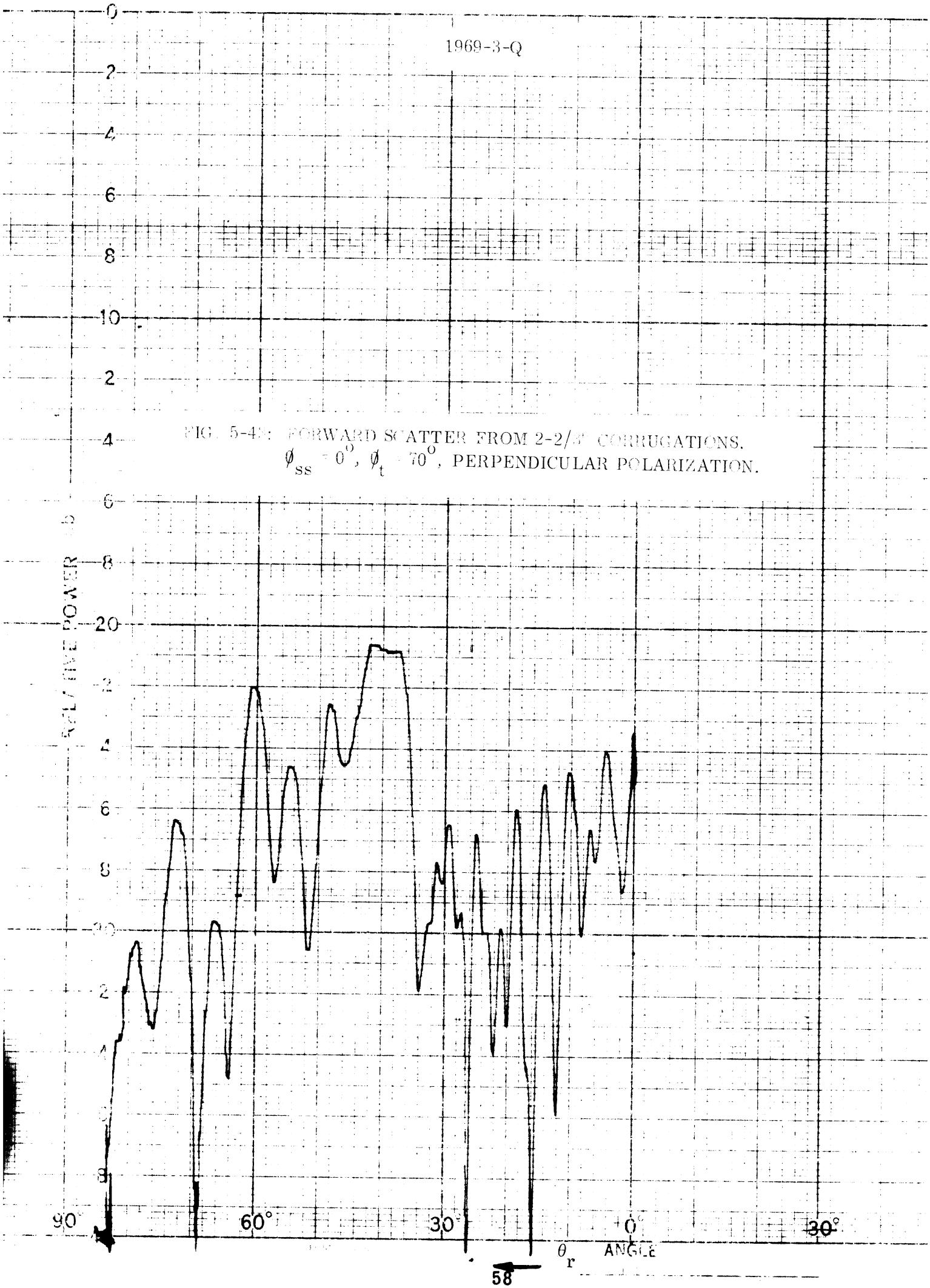

FIG. 5-43: FORWARD SCATTER FROM 2-2/3" CORRUGATIONS. $\phi_{ss} = 0^{o}$, $\phi_t = 70^{o}$, PERPENDICULAR POLARIZATION.

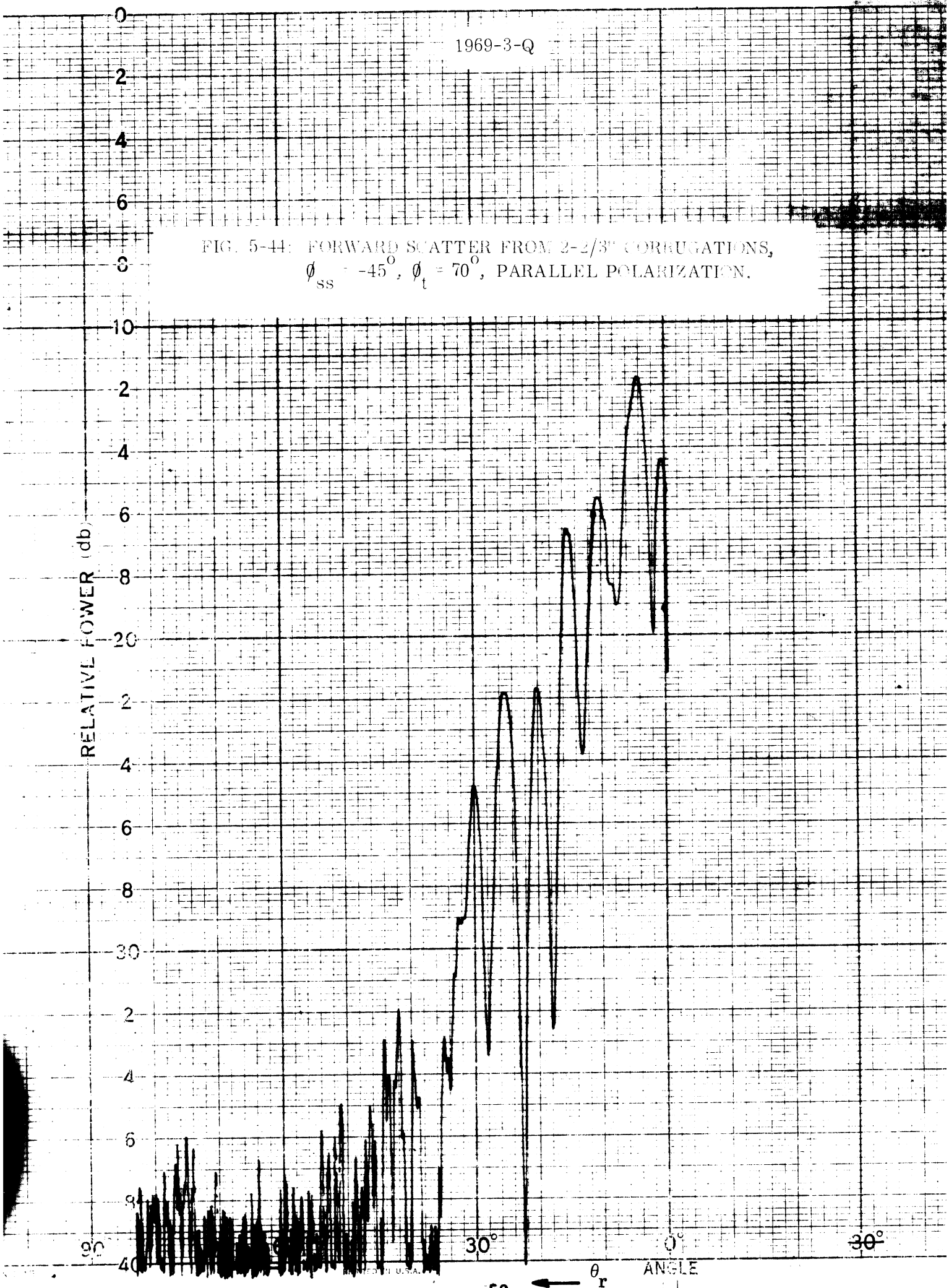

FIG. 5-44: FORWARD SCATTER FROM 2-2/3" CORRUGATIONS, $\phi_{ss} = -45^{\circ}$, $\phi_t = 70^{\circ}$, PARALLEL POLARIZATION.

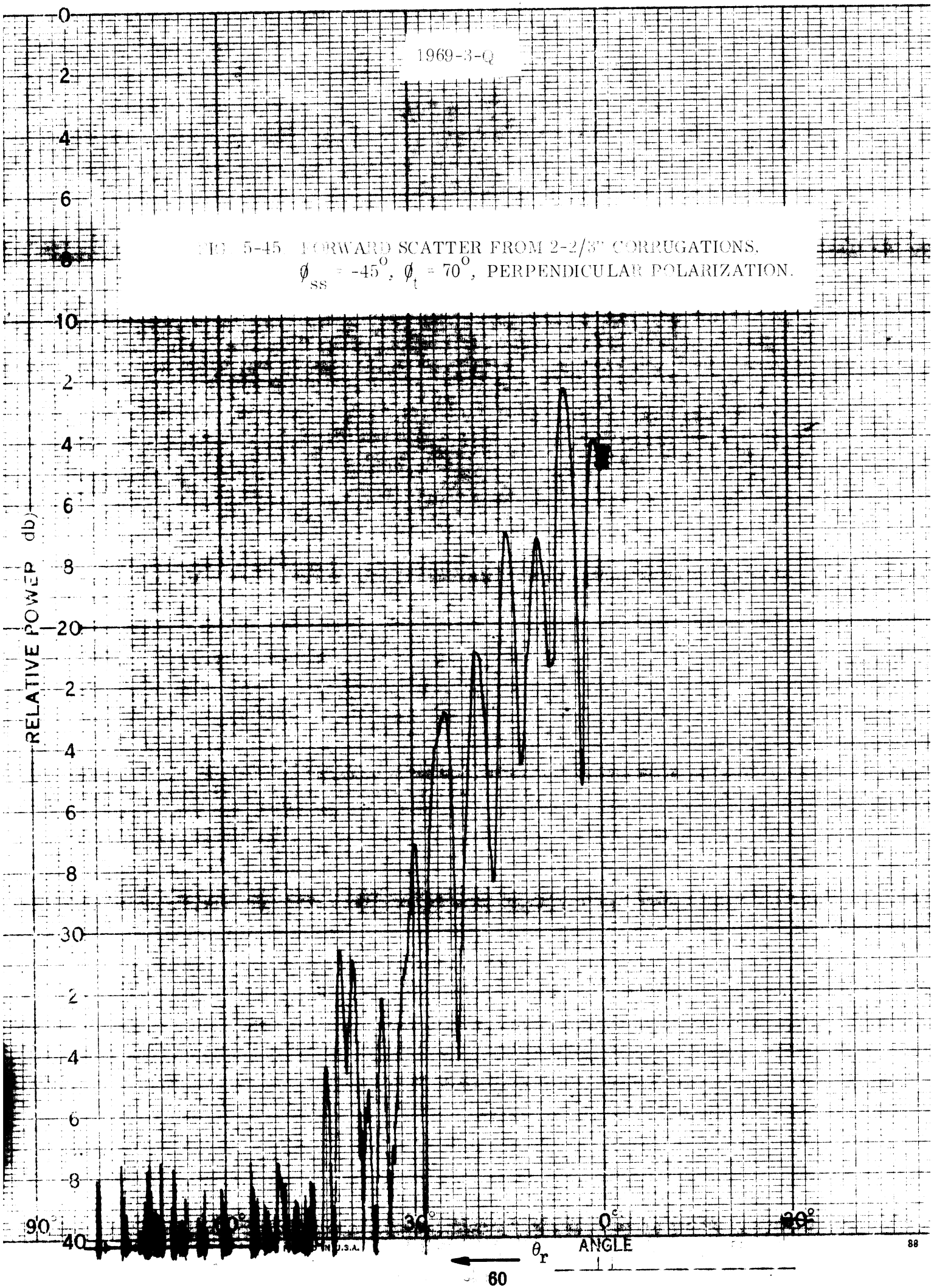
1969-3-Q
FIG. 5-45. FORWARD SCATTER FROM 2-2/3" CORRUGATIONS.
$\phi_{ss} = -45^{o}$, $\phi_{t} = 70^{o}$, PERPENDICULAR POLARIZATION.
RELATIVE POWER (db)
0
2
4
6
8
10
2
4
6
8
20
2
4
6
8
30
2
4
6
8
40
90°
60°
30°
0°
30°
θ_r
ANGLE
88

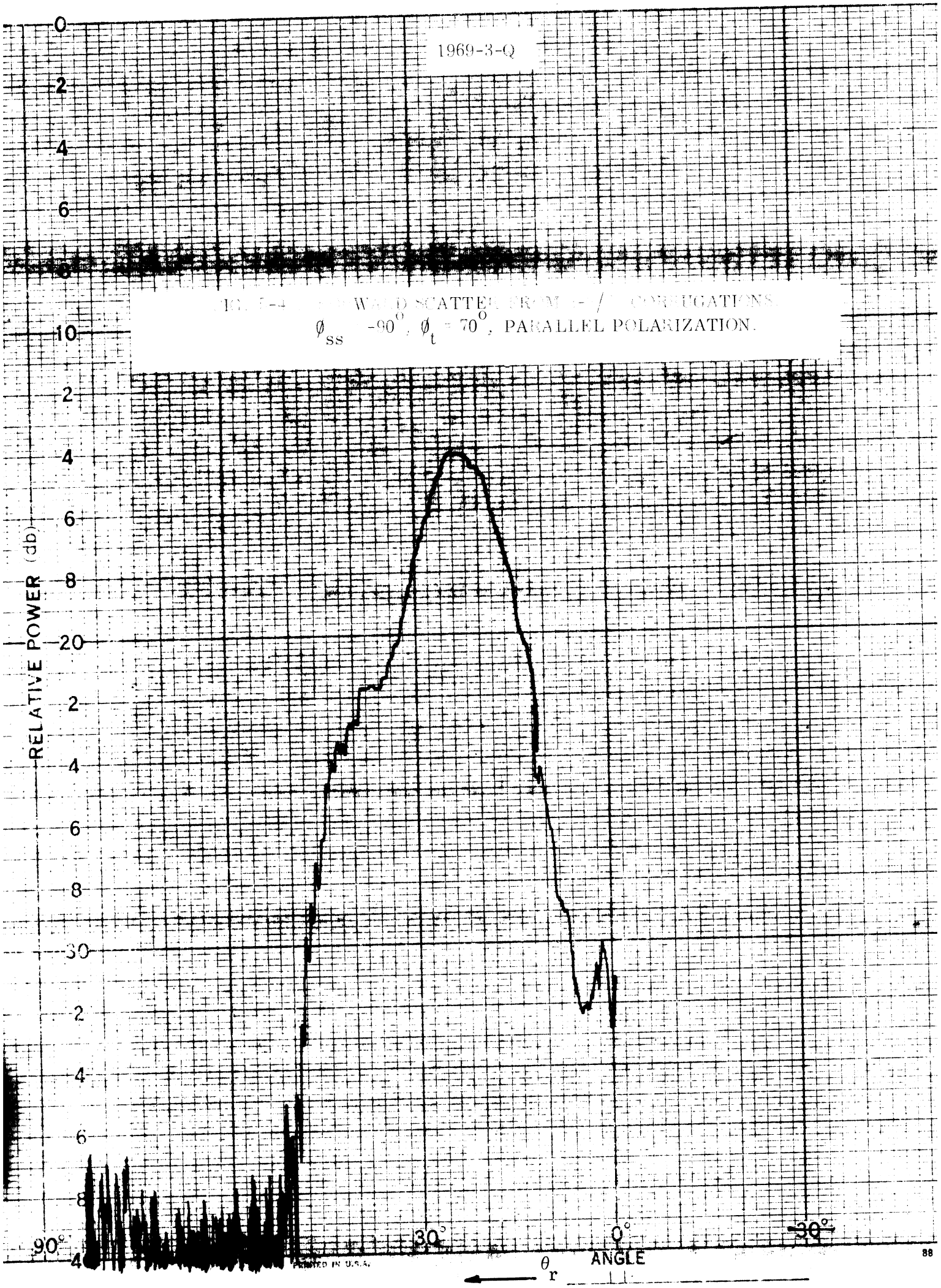

FIG. 5-4 [illegible] WARD SCATTER FROM [illegible] CORRUGATIONS.
$\phi_{ss} = -90^{\circ}$, $\phi_t = 70^{\circ}$, PARALLEL POLARIZATION.

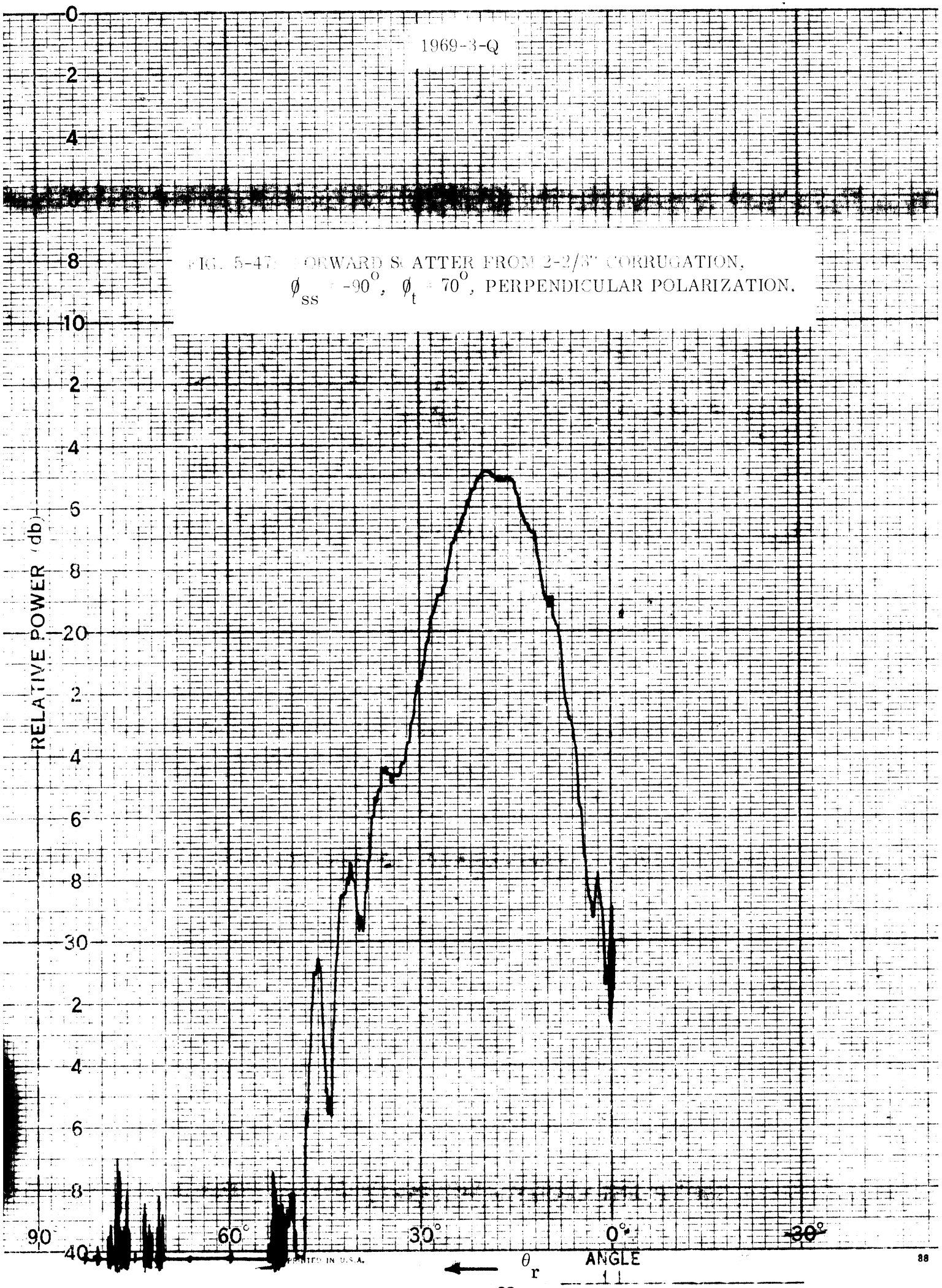

FIG. 5-47 FORWARD SCATTER FROM 2-2/3" CORRUGATION, $\phi_{ss} = -90^{\circ}$, $\phi_t = 70^{\circ}$, PERPENDICULAR POLARIZATION.

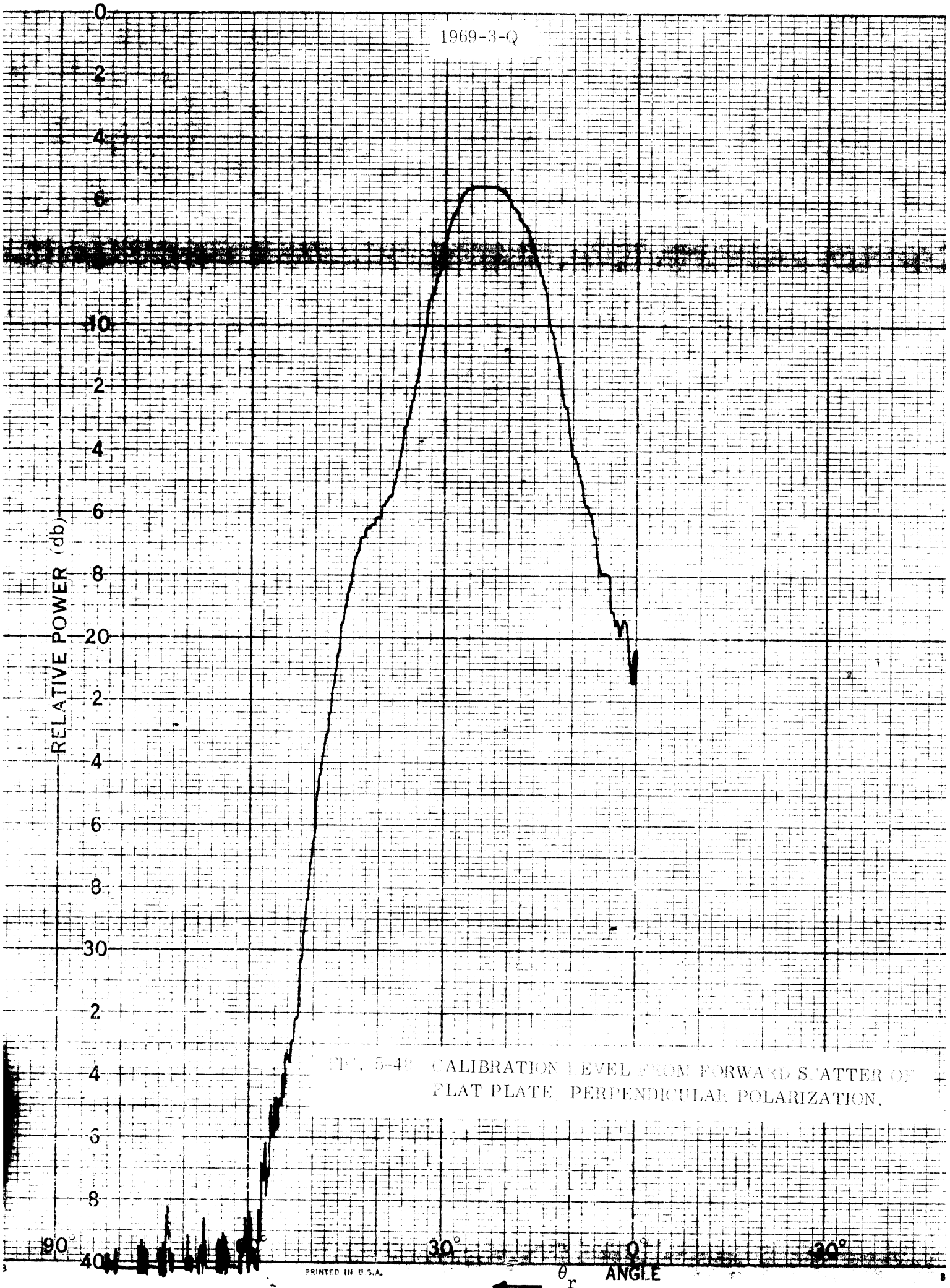

FIG. 5-42 CALIBRATION LEVEL FROM FORWARD SCATTER OF FLAT PLATE PERPENDICULAR POLARIZATION.

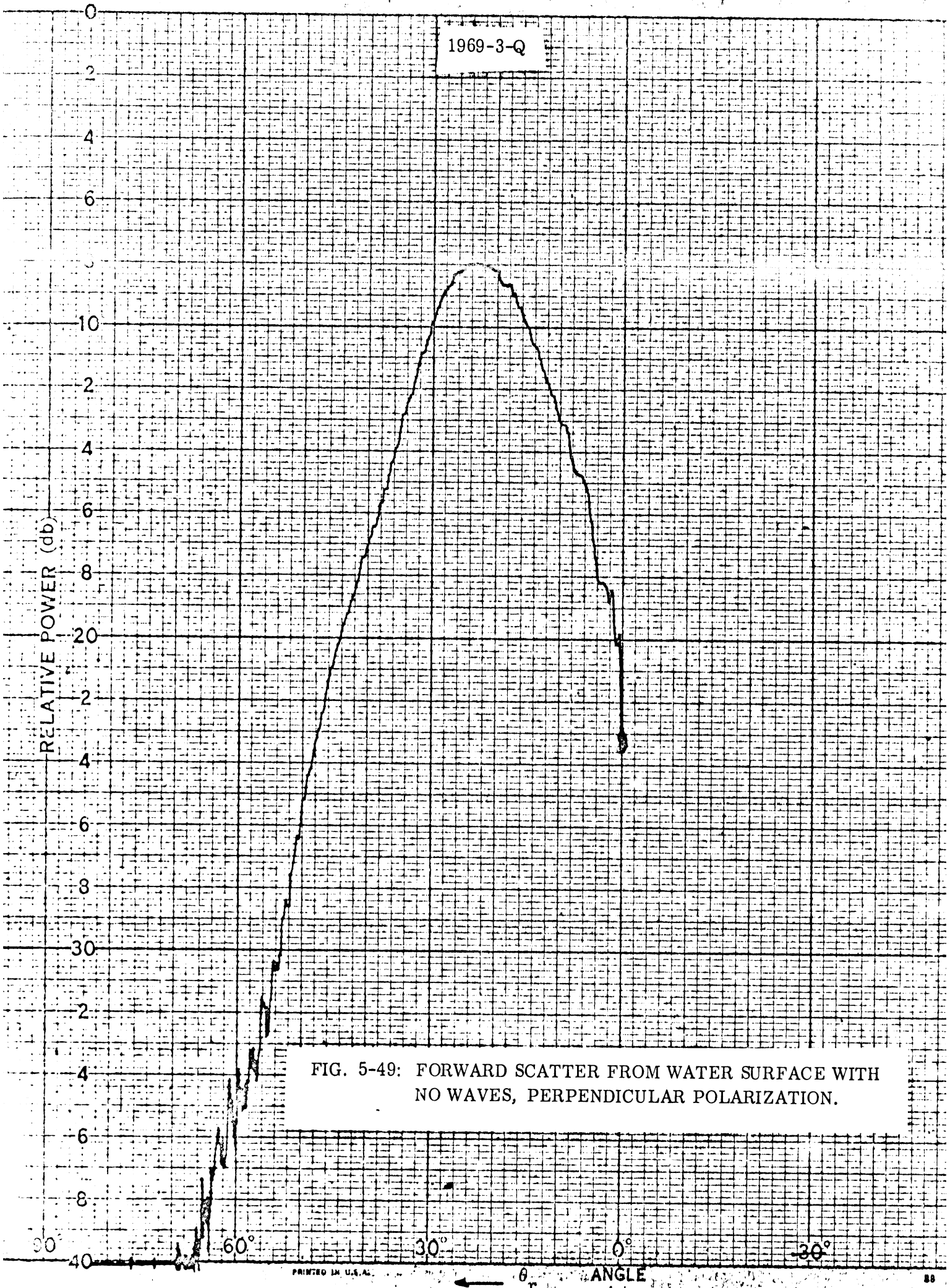

FIG. 5-49: FORWARD SCATTER FROM WATER SURFACE WITH NO WAVES, PERPENDICULAR POLARIZATION.

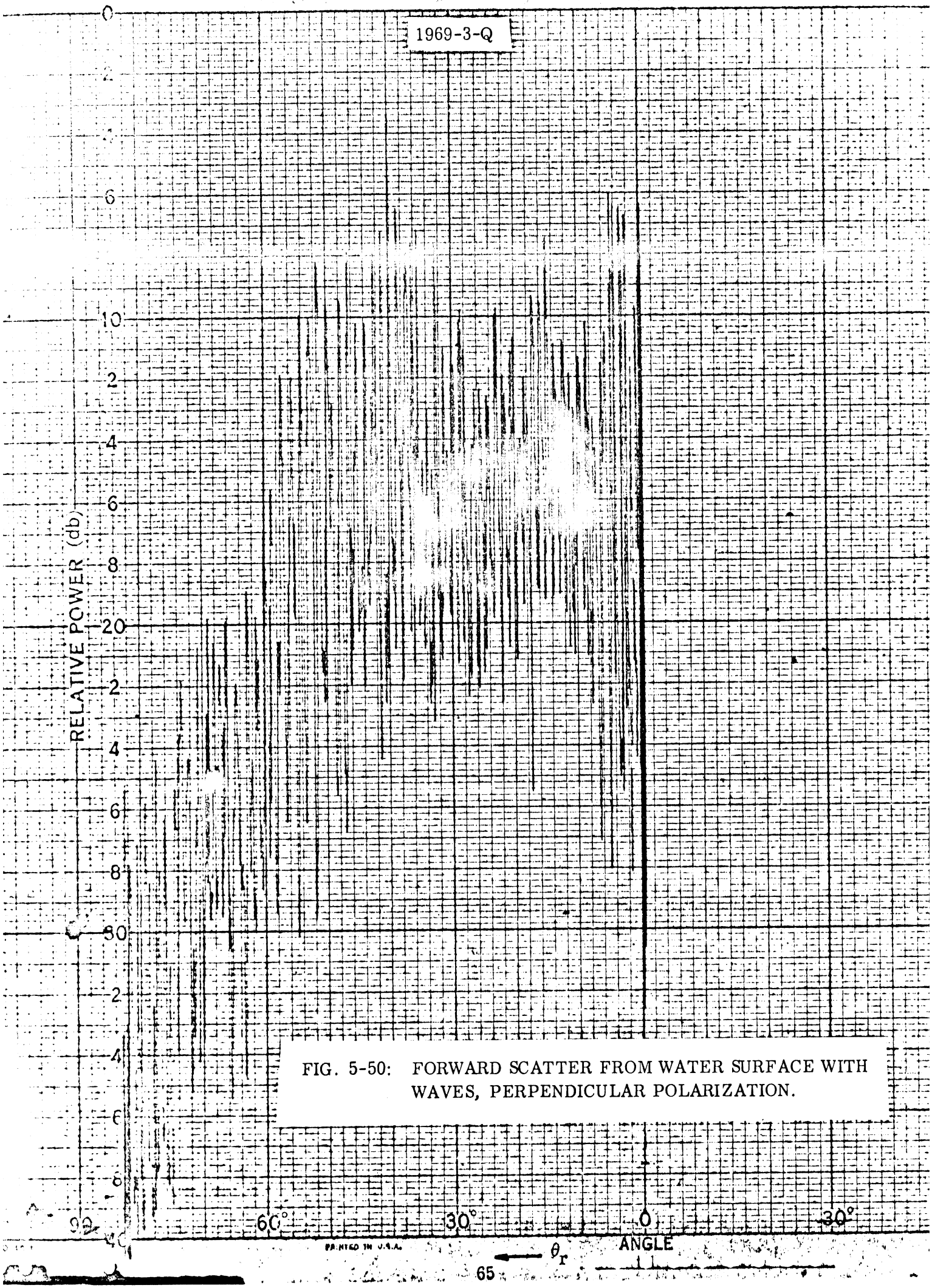

FIG. 5-50: FORWARD SCATTER FROM WATER SURFACE WITH WAVES, PERPENDICULAR POLARIZATION.

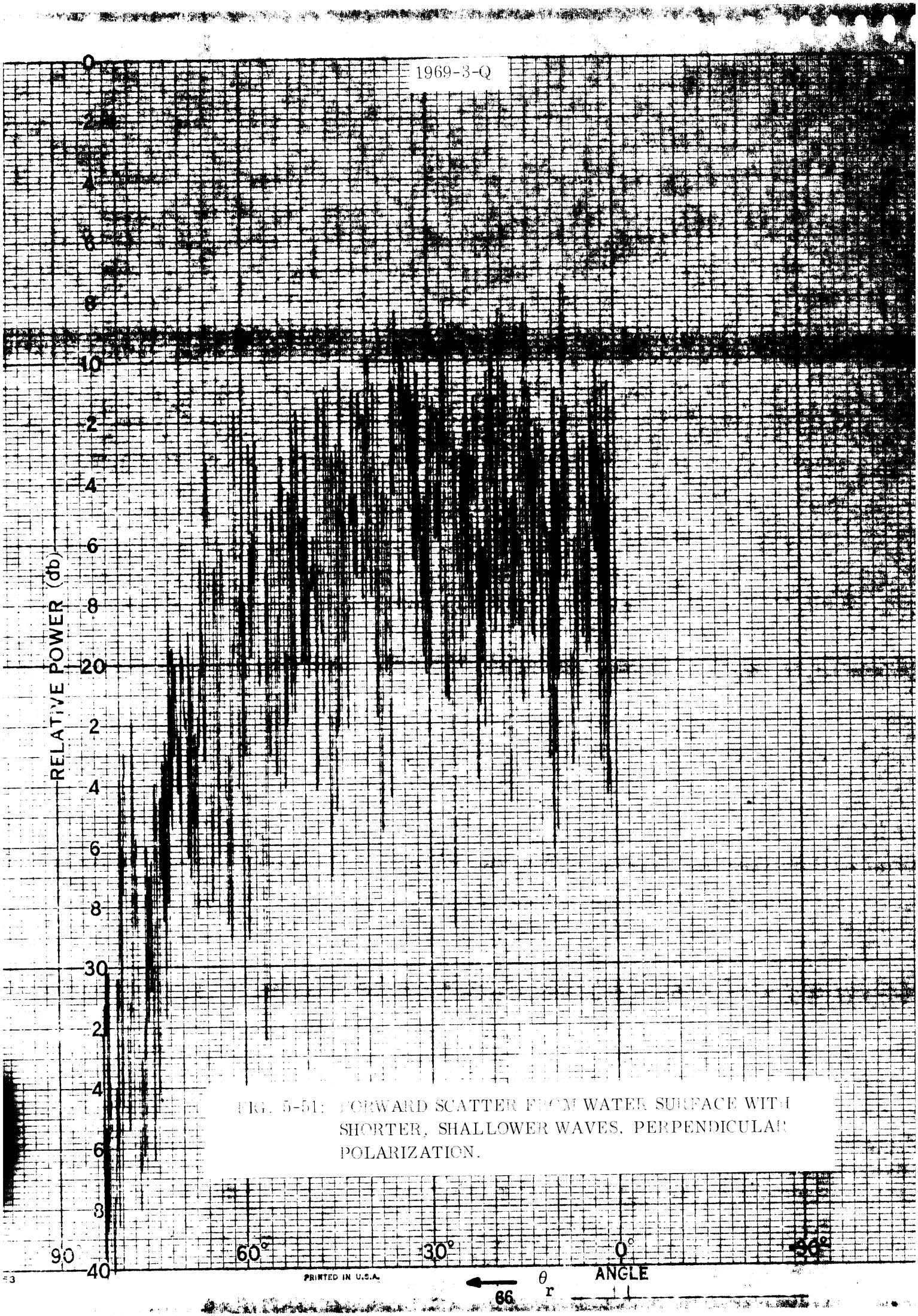

FIG. 5-51: FORWARD SCATTER FROM WATER SURFACE WITH SHORTER, SHALLOWER WAVES, PERPENDICULAR POLARIZATION.

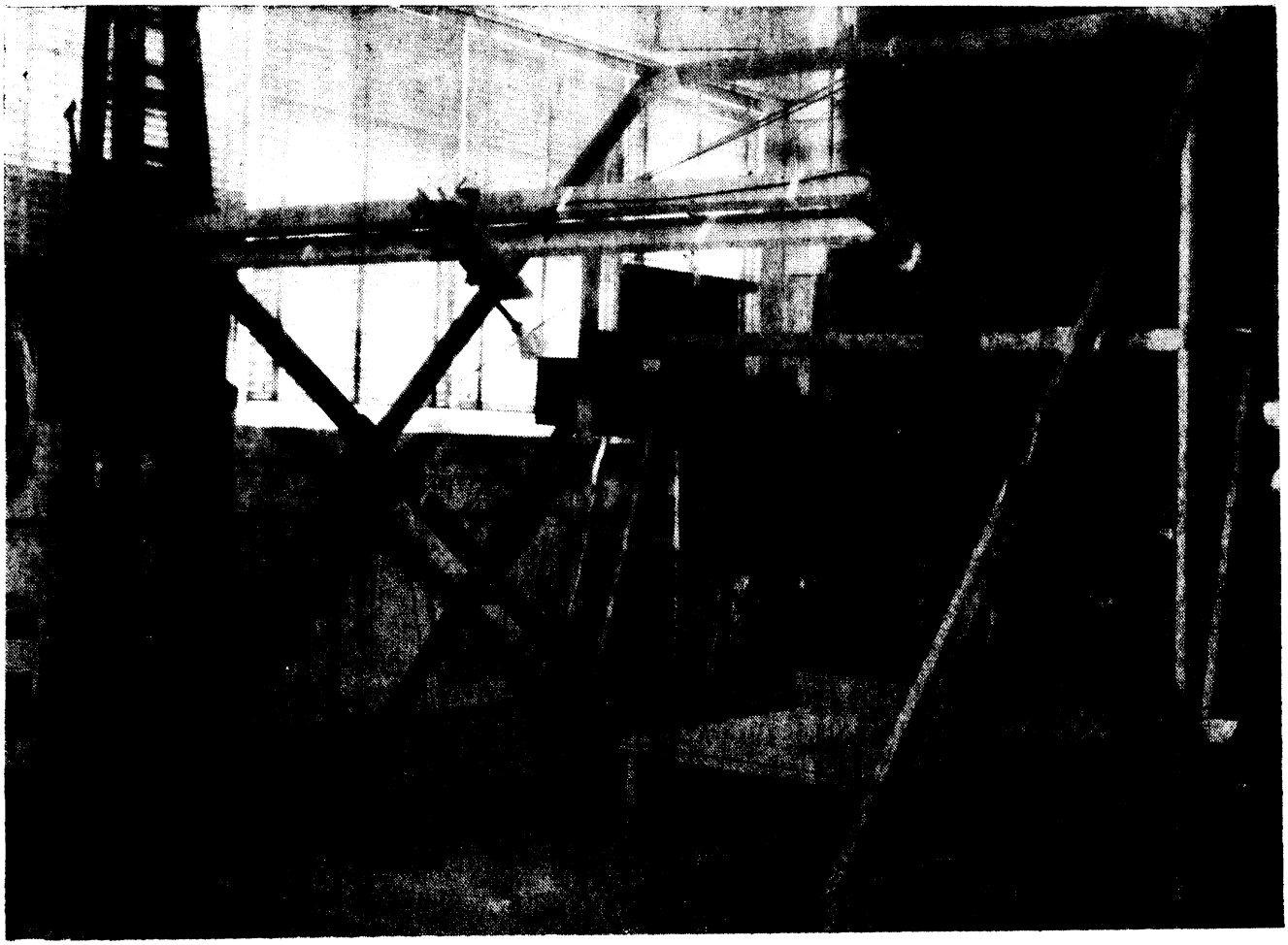

FIG. 5-52a) FORWARD SCATTER TEST STRUCTURE WITH ELONGATED TANK.

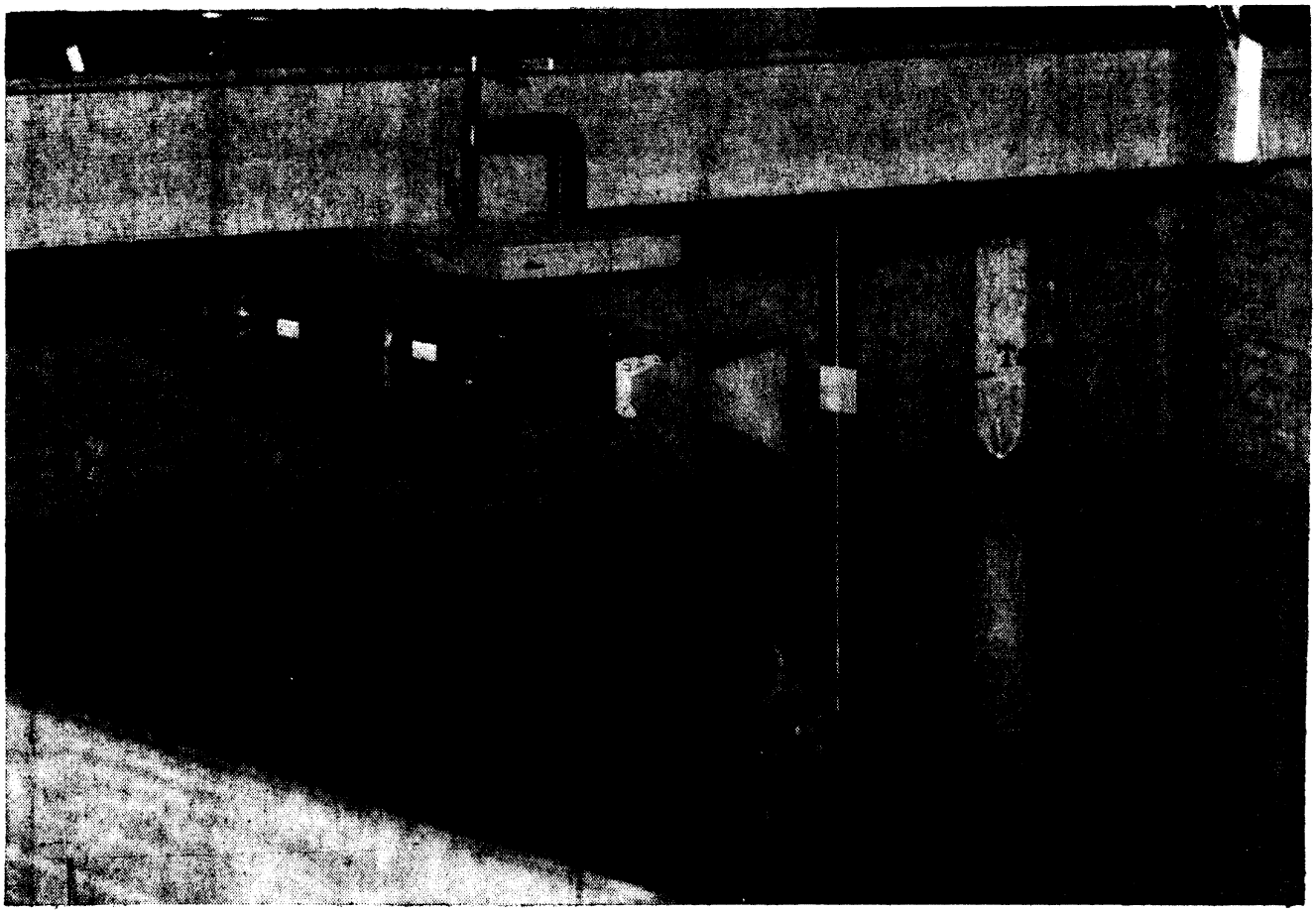

FIG. 5-52b) HORN POSITIONED IN TANK, WATER LEVEL AT BOTTOM OF TAPE.

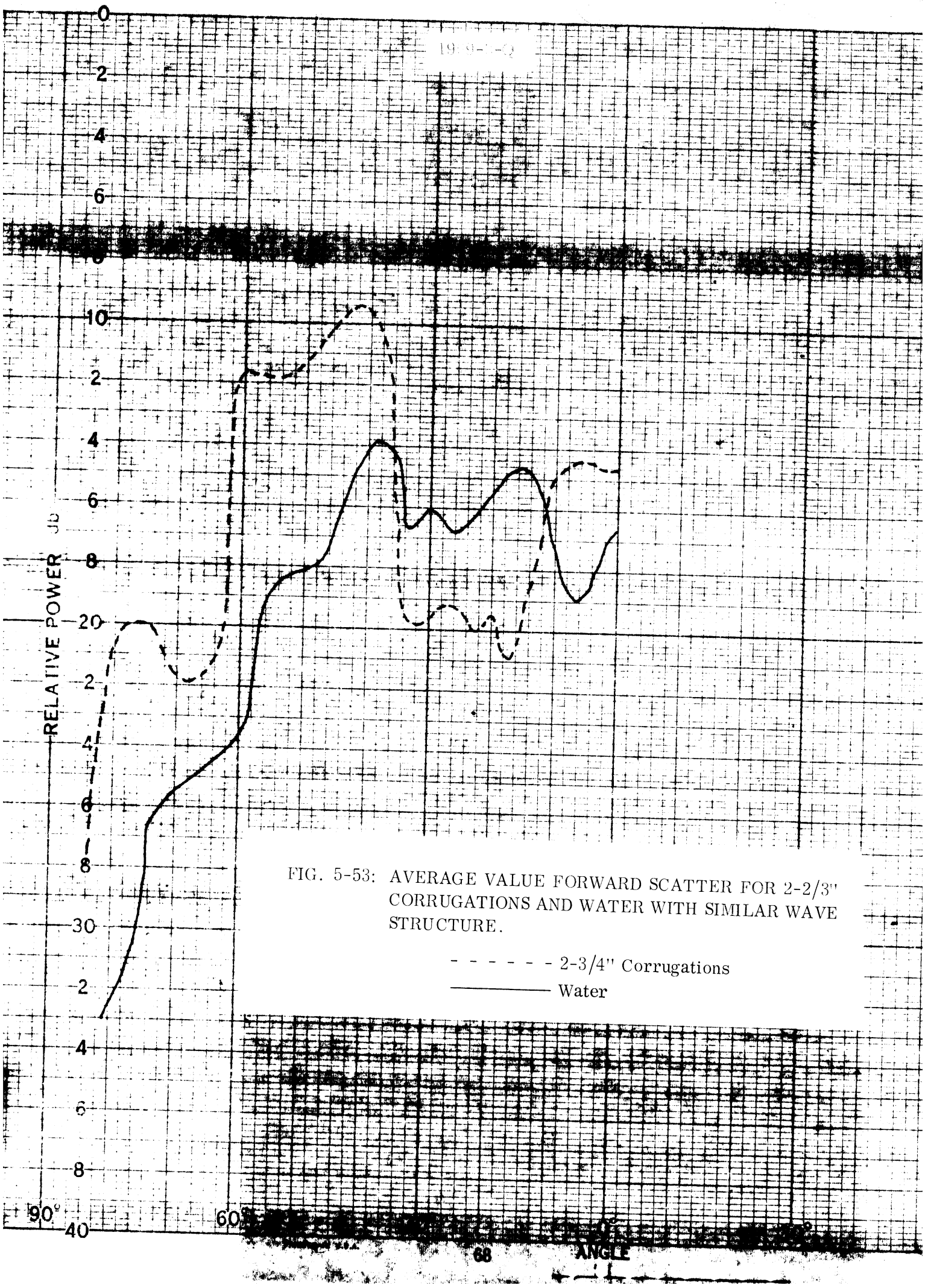

FIG. 5-53: AVERAGE VALUE FORWARD SCATTER FOR 2-2/3" CORRUGATIONS AND WATER WITH SIMILAR WAVE STRUCTURE.

- - - - - - 2-3/4" Corrugations

———— Water

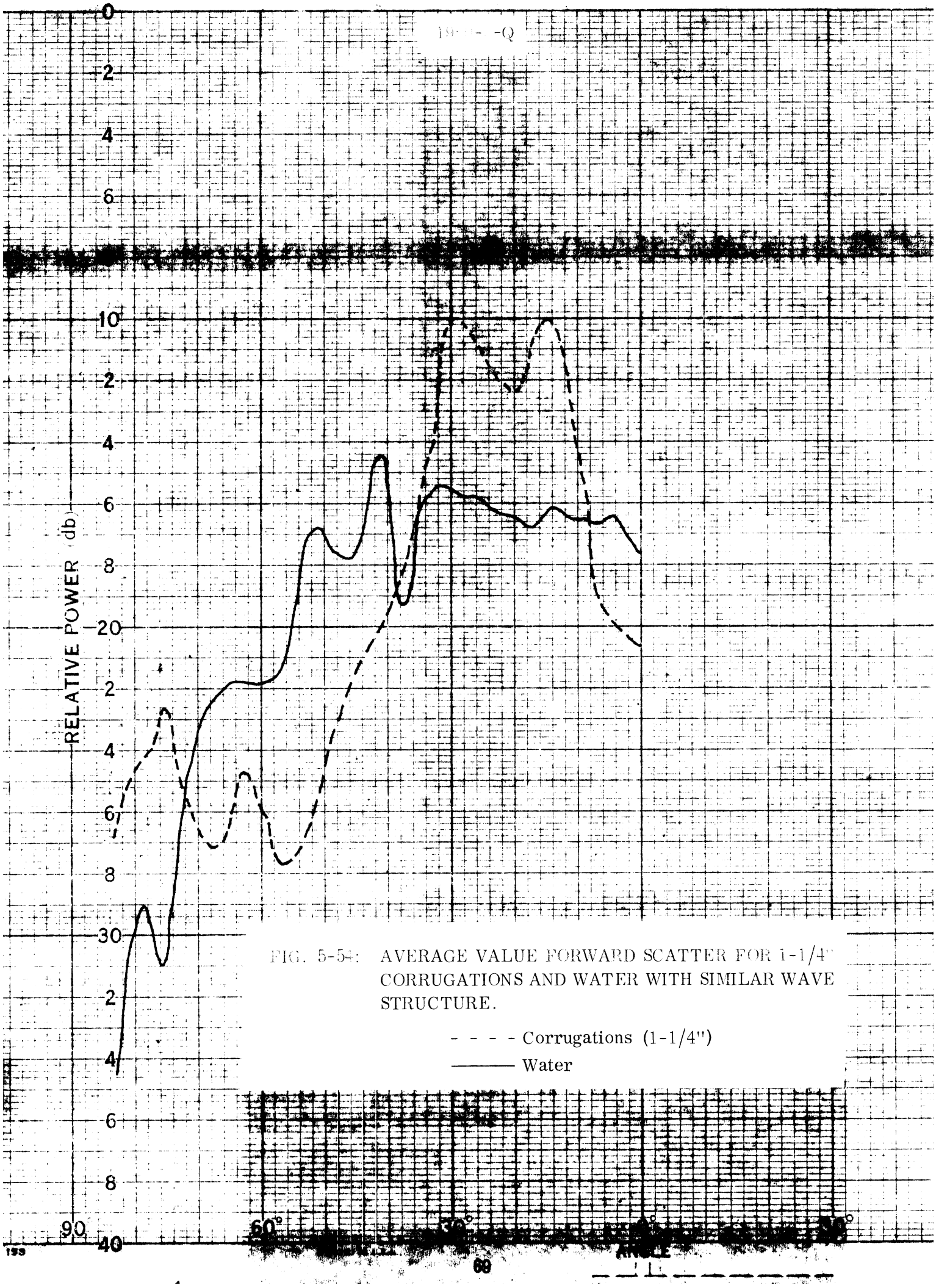

FIG. 5-54: AVERAGE VALUE FORWARD SCATTER FOR 1-1/4" CORRUGATIONS AND WATER WITH SIMILAR WAVE STRUCTURE.

- - - - Corrugations (1-1/4")

——— Water

VI

POWER RECEIVED CALCULATIONS (Tactical Situation)

6.1 Introduction

Employing the test structure discussed in Chapter IV, forward scattering patterns have been collected for several different surface configurations. Surface configurations considered have been a flat metallic plate, two corrugated metallic surfaces, and a wavy water surface. Data collected has shown that relatively strong signals may be scattered near the horizon from a ripply sea surface. Because of the large signal levels that may be present near the horizon, some elementary calculations have been made to determine probable signal levels that may be available at the aperture of a distant receiving antenna.

To make these calculations, use has been made of the Friis transmission formula (Kraus, 1950) slightly re-arranged from its normal form. The modified form of the Friis transmission formula is,

$$(P_r - G_r) = P_t + G_t + L_p + L_s \qquad (6.1)$$

where all units are expressed in dB or dBm. P_r and P_t are the power received and power transmitted in dB above a milliwatt (dBm). G_t and G_r are respectively the gains of the transmitting and receiving antennas and L_p and L_s are respectively the path and scatter losses associated with the RF energy. L_p is obtained from the expression $L_p = 20 \log (\lambda / 4\pi R)$. Data for L_s is obtained from the forward scattering pattern data that has been collected employing the test setup discussed in Chapter IV. The geometry for this problem is shown in Fig. 6-1. Employing the above geometry, the path loss (L_p) for the forward scattered energy is obtained assuming $R = H_r + H_t$ from Fig. 6-1. When determining the path loss for the side lobe calculations, the straight line distance (R_{sl}) between the transmitting and receiving site is used for R of the path loss expression.

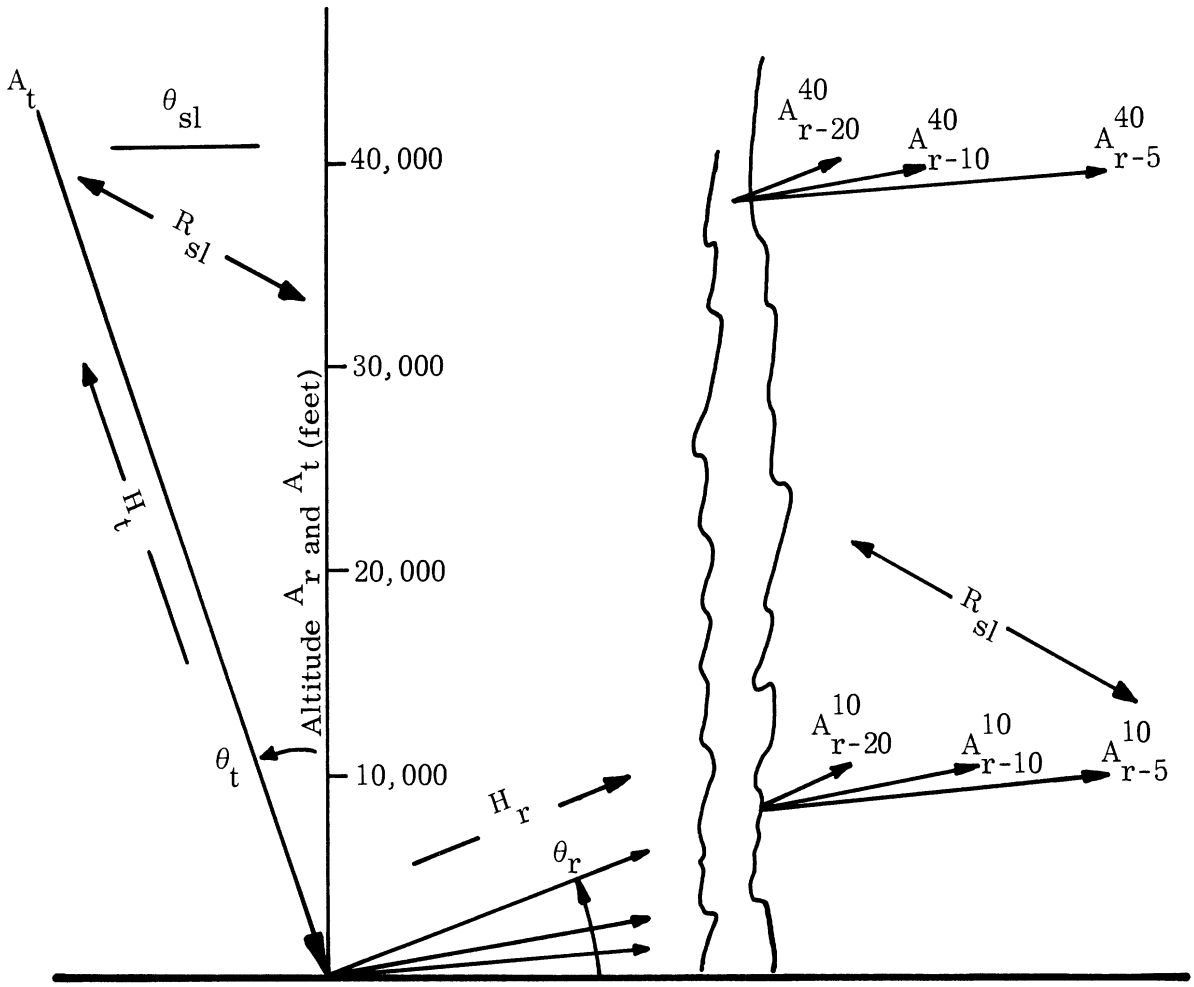

FIG. 6-1: DOPPLER SYSTEM GEOMETRY.

6.2 Forward Scattering Calculations

For the purposes of the following calculations, six conditions are considered. For all six conditions, it is assumed that the transmitter is located at an altitude of 40,000 feet above the reflecting surface and at an angle $\theta_t = 20^o$. The six conditions are associated with the receiving site. Three conditions assume the receiving site is located at an altitude of 10,000 feet having θ_r's with respect to the scattering surfaces of 5^o, 10^o, and 20^o. The last three conditions assume that the receiving site is located at an altitude of 40,000 feet and again having θ_r's of 5^o, 10^o, and 20^o, (see Fig. 6-1).

The nomenclature to be used is as follows: $A^{40}_{r,\ 20}$. The superscript 40 denotes the altitude is 40,000 feet, r denotes the receiving site, and 20 denotes that θ_r is equal to 20^o, and A denotes altitude.

Employing the geometry of Fig. 6-1, the data of Table 6-1 has been compiled assuming that the transmitting frequency is 13 GHz. From Table 6-1, one may obtain the path loss (L_p) associated with energy transmitted via the scattering path H_r, H_t.

TABLE 6-1

θ_r^o	$H_t^{10} + H_r^{10}$ (miles)	L_p^{10} (dB)	$H_t^{40} + H_r^{40}$ (miles)	L_p^{40} (dB)
20	13.2	141	29.9	148
10	18.6	144	51.4	153
5	29.4	148	94.6	158

Relative Path Loss versus θ_r (Forward Scatter)

To obtain the scattering loss (L_s), experimental data for wavy water was used (Fig. 6-2). On the data of Fig. 6-2, the scattering coefficient associated with a flat metallic plate has been noted and serves as the 100 per cent reflection

coefficient reference. It is assumed that there are no losses in the plate and the reflection is specular. Figure 6-2 serves as a calibration curve and the scattering loss may be read directly from it. Employing this curve the scattering loss associated with the ripply water for angles of 70^{o}, 80^{o}, and 85^{o}, corresponding to θ_r's of 20^{o}, 10^{o}, and 5^{o} respectively, have been obtained and are shown in Table 6-2.

TABLE 6-2

θ_r^{o}	L_s (dB)
20	-14
10	-18
5	-25

Forward Scatter Loss versus θ_r

Employing equation (6. 1) and the above data, one may calculate $(P_r - G_r)$. Example 1: Assume that the power transmitted (P_t) is 10 watts (+40dBm); gain, G_t of the transmitting antenna, is 20dB with respect to an isotrope; L_p, the path loss is -140dB and L_s, the scattering loss is -20dB, $(P_r - G_r)$ is then -100dBm. Employing the more exact data of Table 6-1 and 6-2 $(P_r - G_r)$ associated with each of the θ_r's may be obtained as noted in Table 6-3 for A_r = 10, 000 and 40, 000 feet.

TABLE 6-3

θ_r^{o}	$P_r^{10} - G_r^{10}$ (dBm)	$P_r^{40} - G_r^{40}$ (dBm)
20	-95	-103
10	-102	-111
5	-113	-124

Received Signal Level versus θ_r (Forward Scatter)

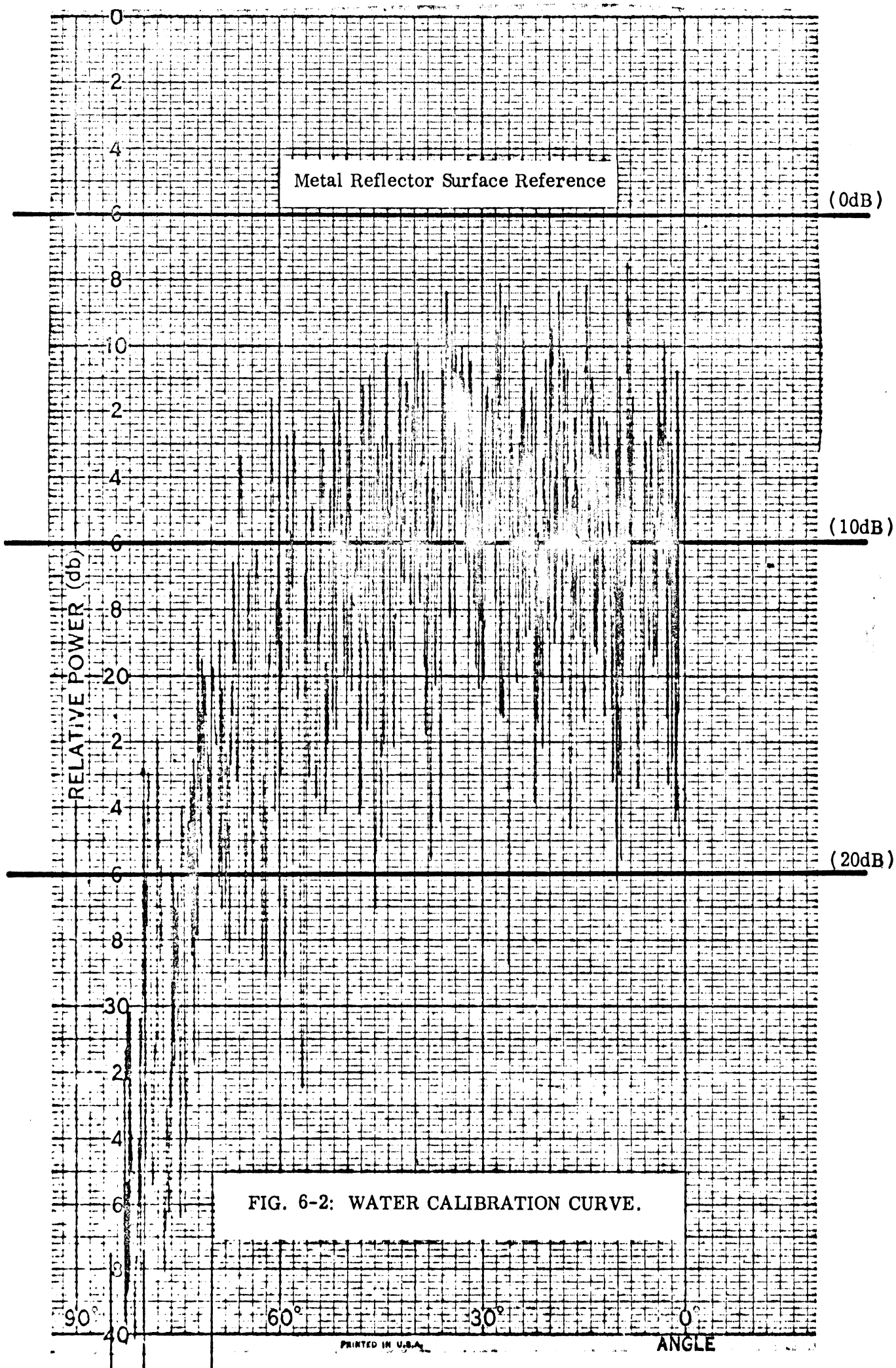

FIG. 6-2: WATER CALIBRATION CURVE.

6.3 Side Lobe Calculation

Consideration was next given to the power level that may be available at the receiving site as a result of energy radiated from the side lobe of the transmitting antenna.

Again, employing the geometry of Fig. 6-1, the range from the transmitting antenna to the receiving antenna was calculated assuming the receiving antenna was located at any of the six conditions noted previously. The range between the transmitting and receiving antennas is denoted as R_{sl} and the data for the above condition is listed in Table 6-4 along with the path loss (L_p).

TABLE 6-4

$\theta_r^{o}\delta$	R_{sl}^{10} (miles)	L_p^{10} (dB)	R_{sl}^{40} (miles)	L_p^{40} (dB)
20	9.77	-139	23.58	-146
10	14.65	-142	45.83	-152
5	25.13	-147	89.89	-158

Relative Path Loss versus θ_r (Side Lobes)

θ_{sl}, the depression angle of the side lobe from which radiation may be transmitted, has been calculated and is shown in Table 6-5 for those cases where the receiving antenna is located at an altitude of 10,000 feet. The gain (G_t) associated with the transmitting antenna for this particular depression angle is also given in Table 6-5 as dB above an isotropic source.

TABLE 6-5

θ_r^{o}	θ_{sl}	GPL G_t (dB)	Ryan G_t (dB)
20	30^{o}	-1	+8
10	21^{o}	-3	+4
5	13^{o}	-7	-3

Transmitter Gain for Side Lobes

To obtain G_t it has been assumed that the GPL antenna has a maximum gain of 20dB with respect to an isotropic source, and the Ryan antenna has a gain of 30dB with respect to an isotropic source. Further, the G_t data has been obtained employing Figs. 6-3 and 6-4 for the GPL and Ryan antennas respectively. On these figures, the level that was the largest for the three depression angles has been circled. It is recognized that there are many other points in each of these graphs where the level is considerably less than that shown. However, for the purposes of these calculations a worse case condition is being employed, and it is to be understood that it is not representative of all situations that the system may encounter.

Again, employing equation (6.1) and setting $L_s = 0$ since there is no scattering loss, the following example is presented. Example 2: $P_t = 40$dB (10 watts), G_t is 0dB, and L_p is -140dB. Employing these assumptions $(P_r - G_r)_{sl}$ is equal to -100dBm. This suggests that the power received at the receiving antenna is in the neighborhood of results for Example 1 for the forward scattering data. More exact side lobe calculations for $(P_r - G_r)_{sl}$ is presented in Table 6-6 for both the Ryan and GPL system, assuming the receiving antenna is located at an altitude of 10,000 feet. For this data we have assumed that P_t for the GPL system is 40dBm (10 watts) and for the Ryan system it is 30dBm (1 watt).

TABLE 6-6

θ_r^o	GPL $(P_r - G_r)^{10}$	Ryan $(P_r - G_r)^{10}$
20	-100dBm	-101dB
10	-105dBm	-108
5	-113dBm	-120

Received Signal Level θ_s (Side Lobes)

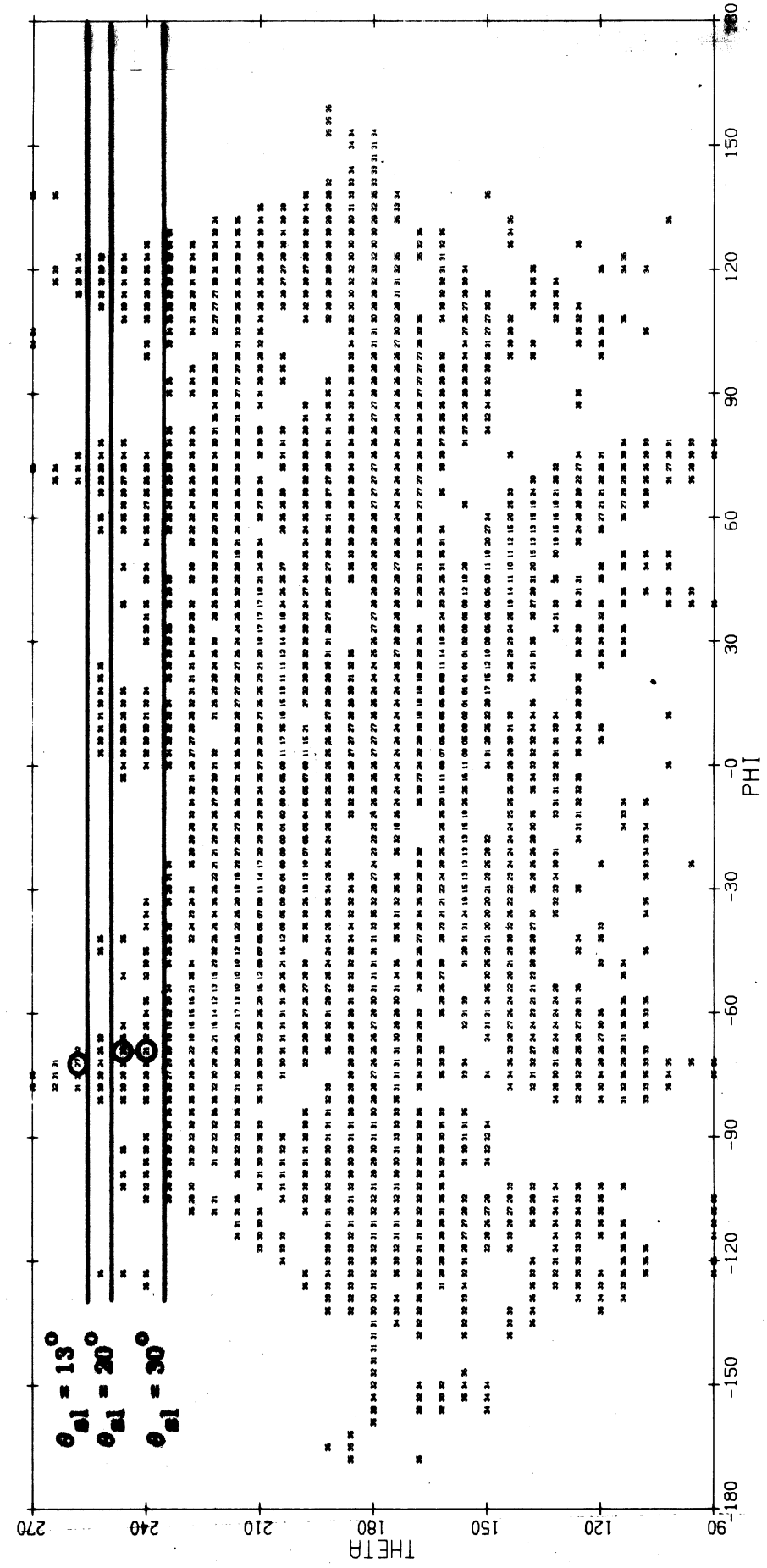

FIG. 6-3: GPL ANTENNA CONTOUR PLOT.

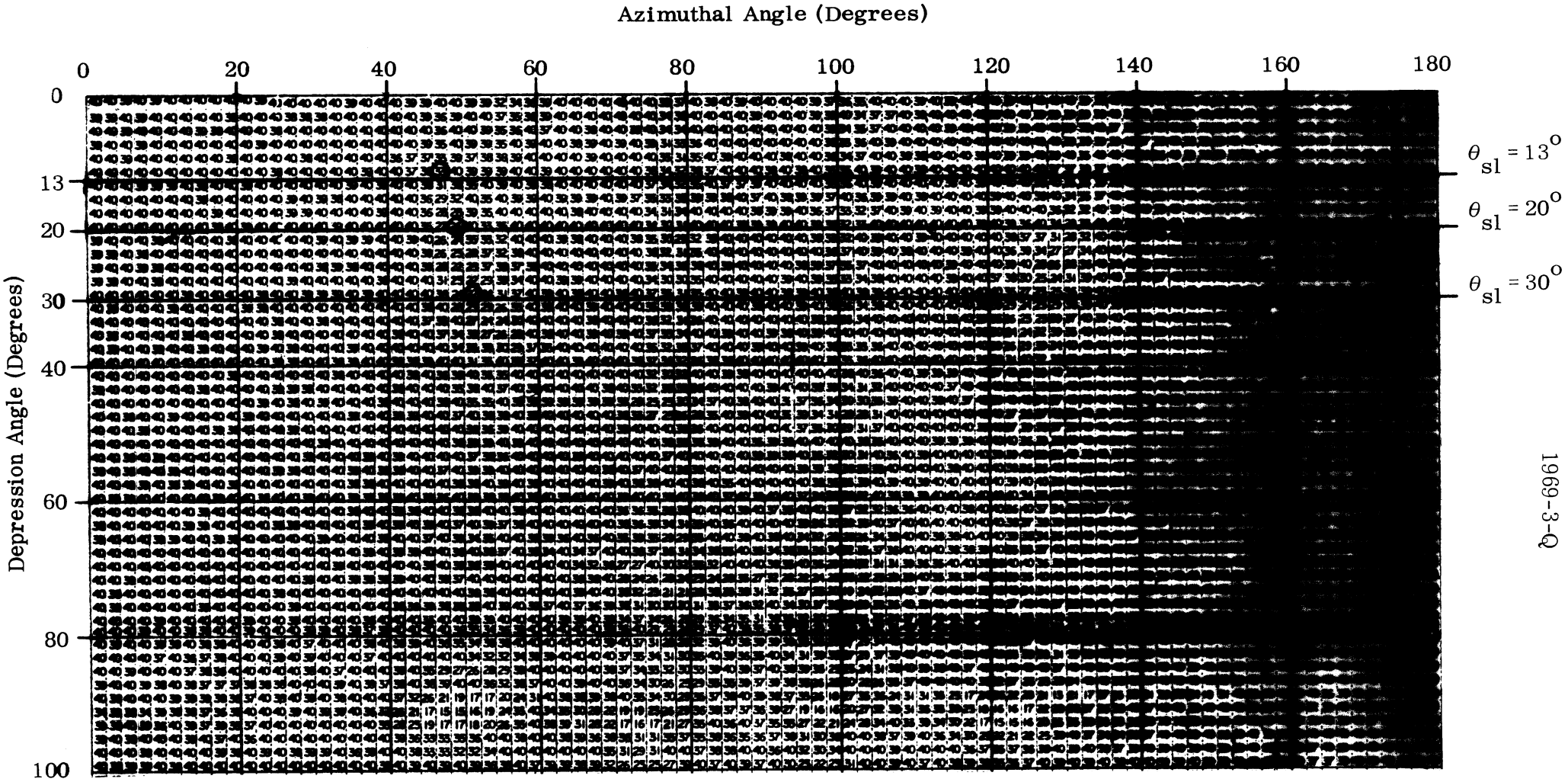

FIG. 6-4: RYAN 533 ANTENNA CONTOUR PLOT.

For the case when the receiving antenna and transmitting antennas are at the same altitude (40, 000 feet) it has been assumed that the side lobe level is 40dB below the pattern maximum, such that the relative gain (G_t) of the side lobe for the GPL antenna would be -20dB and for the Ryan -10dB.

6.4 Nomographs

The data obtained employing the above method has been further summarized in the two nomographs shown in Figs. 6-5 and 6-6. These nomographs although simple in nature, give a rather broad picture of the relative signal level that may be received at a distant point by the received antenna assumed to be located at an altitude of either 10, 000 feet or 40, 000 feet and whose θ_r angles are either 20^o, 10^o, or 5^o. Further, it is assumed that the transmitting antenna is located at 40, 000 feet and has a θ_t of 20^o. From these nomographs, one may assume various transmitter power levels (P_t), and transmitting antenna gains (G_t) to determine the relative signal level available at the aperture of the receiving antenna ($P_r - G_r$) in dBm. An example has been diagrammed in Fig. 6-5. Here it is assumed that the power available from the transmitter (P_t) plus the gain of the transmitting antenna (G_r) is 60dBm and the receiving antenna is at 10, 000 feet at a θ_r of 20^o. To determine the received signal level ($P_r - G_r$) from the forward scattered data, one simply draws a line to the right until it intersects the solid curve $\theta_r = 20^o$. Then dropping straight down from this point of intersect, one may read the signal level available at the aperture of the receiving antenna ($P_r - G_r$) as -95dBm. A similar extraction of the signal level available at the same receiving antenna may be made for the side lobe by assuming the data is from a side lobe and in this case one must determine ($\theta_t + G_t$) which is typically 30dBm for the GPL antenna. Again tracing a line to the right from ($\theta_t + G_t$) = 30dB to the $\theta_r = 20^o$ (dashed curve for the side lobe data) and then dropping straight down, a signal level of -109 dBm is obtained. For this example the signal level ($P_r - G_r$) available at the aperture of the receiving antenna would

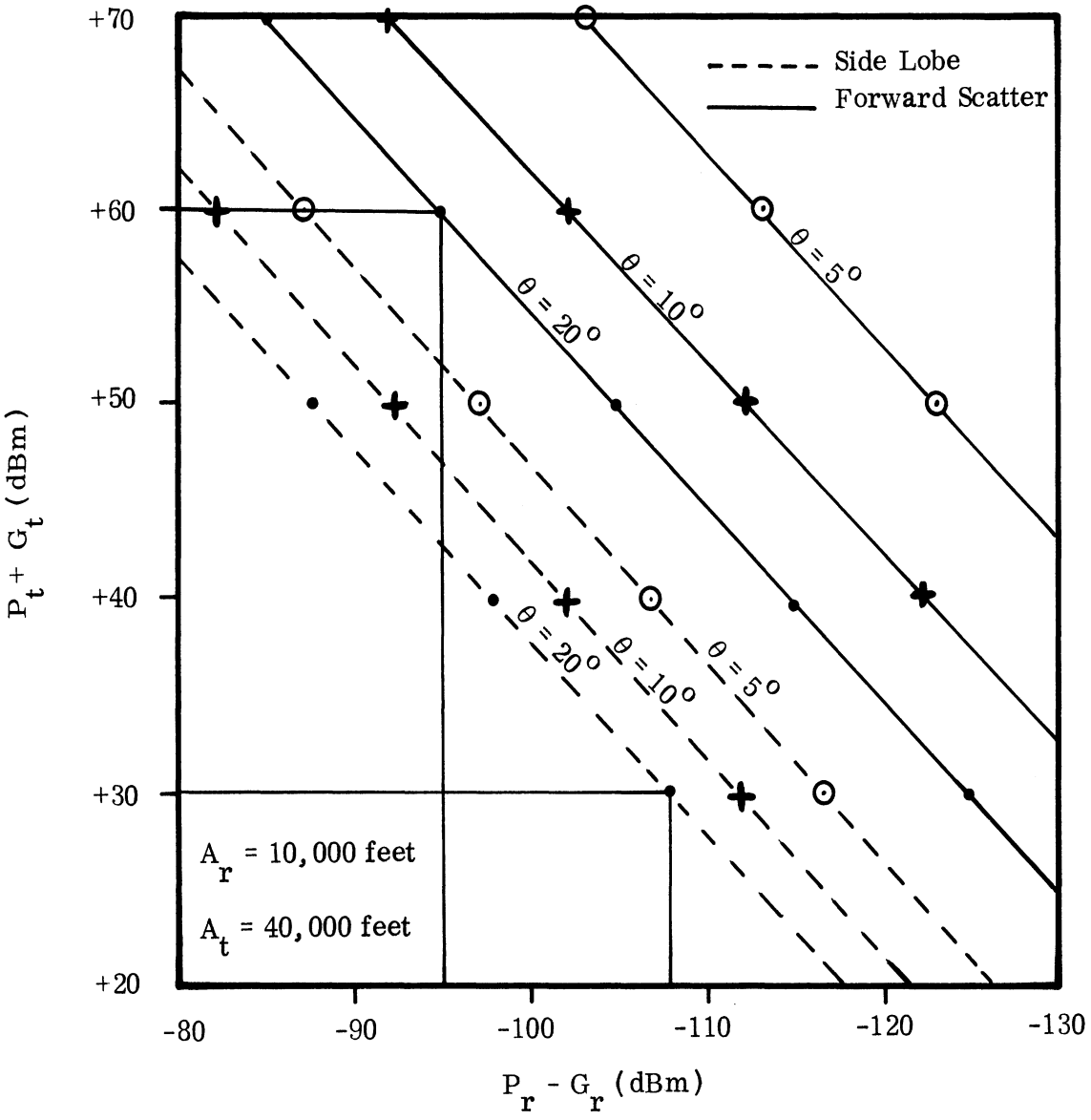

FIG. 6-5: POWER INTENSITY FROM FORWARD SCATTERING AND DOPPLER SIDELOBES (A_r = 10,000 feet; A_t = 40,000 feet).

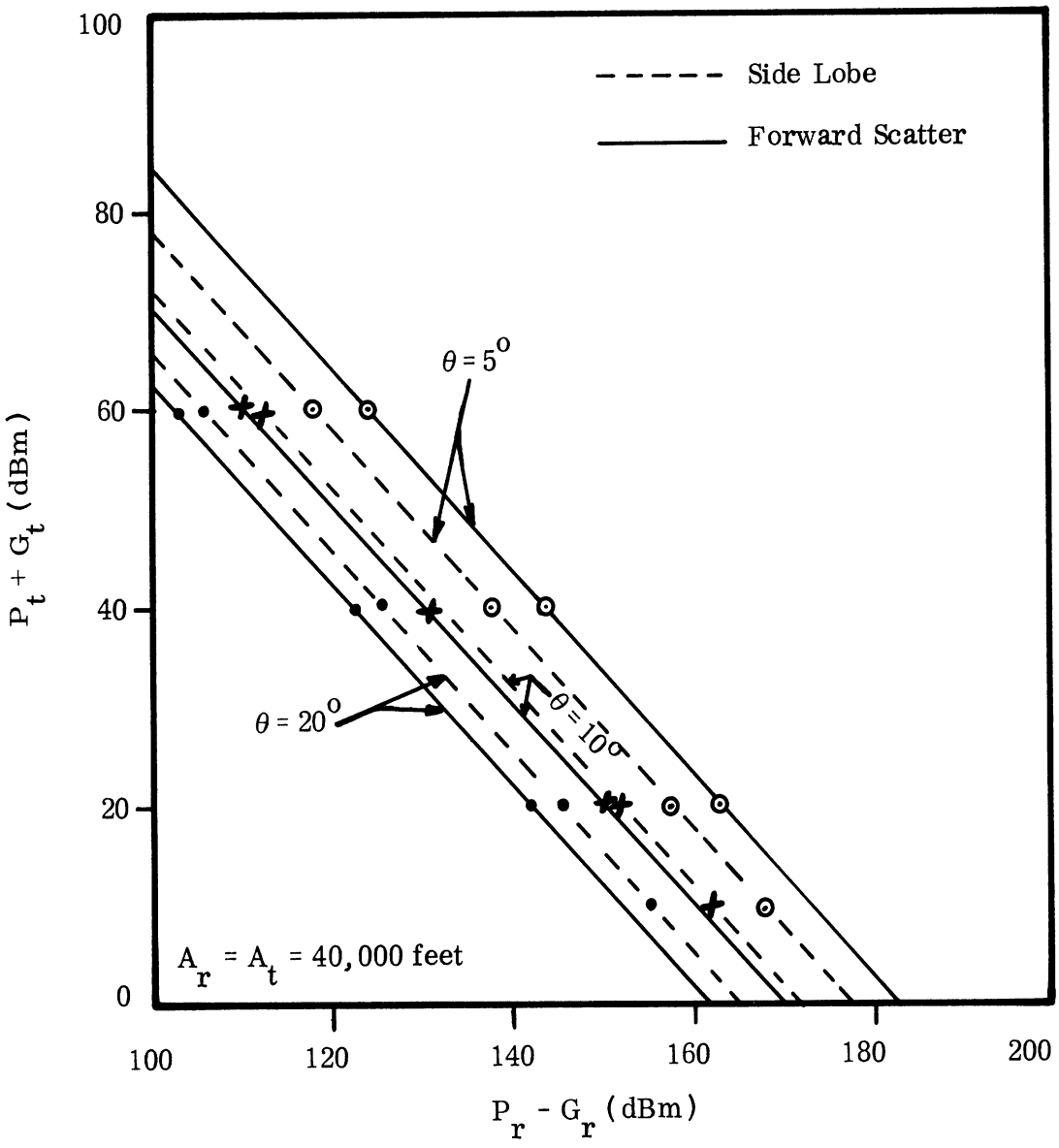

FIG. 6-6: POWER INTENSITY FROM FORWARD SCATTERING AND DOPPLER SIDELOBES ($A_r = A_t = 40,000$ feet).

be strongest coming from the forward scatter and weakest from the side lobes. A similar nomograph has been prepared for the case where $A_r = A_t = 40,000$ feet (Fig. 6-6).

6.5 Conclusions and Recommendations

It is to be noted that the data presented in this chapter is for six cases: two receiving heights, three relative receiving angles of θ_r, and one transmitter height. It is to be recognized that there are a vast number of conditions that could exist and it would be extremely time consuming to carry out many of the calculations employing the experimental data that has been employed for the above example. Therefore, it is important to continue with the present theoretical program to generate, theoretically, the forward scattering patterns. These scattering patterns may then be employed in conjunction with the theoretical or experimental three-dimensional antenna pattern data to determine the signal levels available at receiving aperture antennas for the desired conditions.

VII

FORWARD SCATTERING FLY-BY TESTS

During recent months the Radiation Laboratory has been conducting a laboratory investigation to gain increased knowledge of the probable level of energy that may be scattered in the forward direction from a Doppler-Navigation system, typical of those used on board Naval aircraft. Initial results of this study have suggested that an appreciable amount of rf energy may be scattered in the forward direction. Judging from these results it seems desirable to measure the level of the forward scatter signal employing an aircraft and a typical real-world geometry.

For the planned fly-by tests, use would be made of a Navy aircraft employing a GPL-153 Doppler Navigation system. It is anticipated the Doppler system will be operated in its normal mode, i.e., employing the stabilized antenna platform and beam switching. For these tests interest is primarily centered about energy scattered in the forward direction from a water surface. To provide for this it has been recommended that use be made of one of the Great Lakes (Lakes St. Clair or Erie) in the vicinity of Ann Arbor.

To aid in establishing requirements for these tests, a few calculations have been performed assuming the following:

P_t = 40dBm (10 watts)

G_t = 20dB

G_r = 25dB (circularly polarized receiving horn)

P_r = -70dBm (receiver sensitivity)

L_p = path loss dependent on range (see text)

L_s = -25dB

Before discussing the above, let us first determine the geometry of the test setup. Referring to Fig. 7-1, the location of the specular reflection point (x coordinate) has been established for nine receiving site locations, i.e., y = 50, 100, and 200 feet and $\theta_r = 5^o$, 10^o, and 20^o, as shown in Table 7-1.

TABLE 7-1

Horizontal Distance From Receiver To Specular Reflection Point (x)

θ_r^o	y = 50'	y = 100'	y = 200'
5	575'	1150'	2298'
10	284'	568'	1136'
20	137'	275'	550'

To minimize the possibility of having the receiving antenna illuminate the shore area of the lake, an antenna having half-power beamwidths of approximately 7^o is to be employed (G_r = 25dB circularly polarized). Again referring to Fig. 7-1 (assuming y = 200' and $\theta_r = 10^o$) the lower half power ray of the receiving antenna will intercept the water surface approximately 834 feet from the receiving site and the upper half power ray will intercept the water at 1754 feet. Therefore, the patch of water illuminated by the receiving antenna for these conditions would be approximately 120 feet wide by 920 feet long. As will be shown later, it is desirable for the receiving antenna to provide as much gain as possible to ensure some probability that a signal will be received at the receiving site. Therefore, it is anticipated that the aircraft will have to make several passes over the specular point to ensure that a signal will be received because of the narrow width of the specular area illuminated by the receiving antenna. To be sure that the transmitting antenna (AN-153)

illuminates a wide enough swath on the water surface, it will be desirable for the aircraft first to be flown at an altitude of 10,000 feet. Assuming the aircraft is flown at 10,000 feet at the rate of 180 mph and that the half power beamwidth of the AN-153 antenna along the track of the aircraft is 6^{o}, it may be shown that data may be collected for approximately 12 seconds provided adequate signal is available to the receiver.

To determine the signal available to the receiver use will be made of the Friis transmission formula in the following form:

$$P_r - G_r = P_t + G_t + L_p + L_s$$

All of the necessary data for this expression has been noted above with the exception of L_p where $L_p = 20 \log (\lambda / 4\pi R)$. Assuming $\lambda = .074$ feet, $A_t = 10,000$ feet, $\theta_t = 20^{o}$, $y = 200$ feet, and $\theta_r = 10^{o}$, L_p may be shown to be approximately -125dB. Substituting the appropriate values in the Friis expression, it may be shown the power available to the receiver (P_r) for the above condition (A_t, θ_t, y and θ_r) is in the neighborhood of -60dBm which is 10dB above the noise level of the receiver.

7.1 Conclusion

For the purposes of the fly-by tests to measure the forward scatter associated with the AN-153 Doppler system, the receiving and transmitting sites would possess the following characteristics:

1) y = 100' - 200' and be within 100' of the water,
2) $\theta_r = 5^{o}$, 10^{o}, and 20^{o} with emphasis on 10^{o},
3) P_r = -70dBm as a worse case condition,
4) G_r = 25dB circularly polarized minimum,
5) A_t = 10,000 feet typical lower altitudes will be considered,
6) $\theta_t = 20^{o}$ or depression angle of AN-153
7) P_t = 10 watts (10dBm) or power available from AN-153
8) G_t = 20dB.

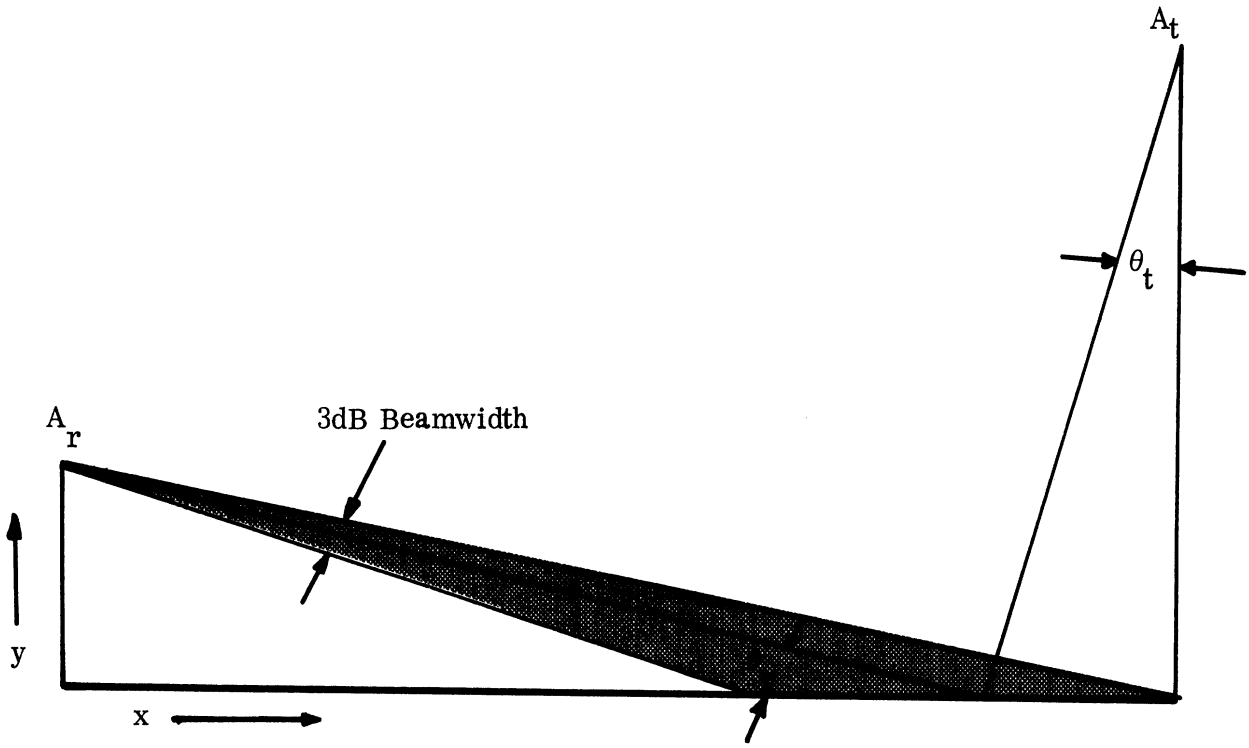

FIG. 7-1: GEOMETRY FOR FLY-BY TESTS.

VIII

SUMMARY

In this report we have described an experimental arrangement for making forward scatter measurements to simulate the Doppler Navigational radar geometry, frequency and polarization. After appropriate calibration measurements, data were collected for two different corrugated surfaces and for wavy water surfaces for incidence angles of 20^{o} and for angles of reflection extending from 0^{o} to about 85^{o}.

With the transmitted energy parallel to the plane of incidence the scattering effects introduced by the corrugated or wavy surfaces are much more pronounced than with perpendicular polarization. This is characterized by a greater oscillation from maximum to null in the scattering patterns and by having more energy scattered forward near the horizon. This latter effect was one of the important findings of the investigation since the level of the energy scattered in regions between 5^{o} and 20^{o} above the horizon was, for some aspects, within 15dB of the 100 per cent reflection level. (The peaks ranged from -15dB to -25dB). This is believed to be more critical since the energy exists over rather wide angular extent as compared to the side lobe or direct beam radiation.

Tests were made of a second frequency (15 GHz in lieu of 13 GHz) to determine whether or not the above effect was resonant and closely coupled with the wave structure of the corrugations. No resonant effects were found.

Measurements were made to determine the cross polarized response from the corrugated surfaces. The cross polarized response was negligible except for the case when the corrugations were at an angle of 45^{o} or so with respect to the plane of incidence. With the latter arrangement, the cross polarized response was, for some aspects, within 9dB of the direct return.

With the exception of one test, all measurements were made with the plane of incidence and the plane of observation being the same. The results obtained when

the plane of incidence was rotated about 20^{o} from the plane of observation showed little variation when compared to the more standard arrangement except that the level of the scattered energy was lower.

Calculations were made to determine energy levels at possible receiver sites of interest as a result of forward scattering from the water surface and as direct radiation from the transmitter antenna side lobes. The signal level from the two paths are comparable although the scattered signal tends to be higher.

A proposed fly-by test was described and expected signal levels were calculated for the scatter geometry. The level is such that the signals should be detectable for limited ranges with the system to be used.

Work has continued on the theoretical aspects of the investigation along the lines described in the previous report. Progress has been made in developing a suitable computer program. Preliminary results based on a physical optics method and with slide-rule calculations are indicating satisfactory agreement with the experimental results.

REFERENCES

Beckmann, P., and A. Spizzichino, The Scattering of Electromagnetic Waves from Rough Surfaces, Volume 4, pp. 10-16, The MacMillan Company, New York, (1963).

Kraus, J.D. Antennas, McGraw-Hill Book Company, New York, Chapter 3, p. 54-56 (1950).

Silver, Samuel, Microwave Antenna Theory and Design, MIT Radiation Laboratory Series, pp. 198-199, McGraw-Hill Book Co., Inc. (1949).

Von Hippel, A.R., Dielectric Materials and Applications, The Technology Press of M.I.T., John Wiley and Sons, Inc. New York, p. 12, 294 (1954).

Security Classification

DOCUMENT CONTROL DATA - R & D

(Security classification of title, body of abstract and indexing annotation must be entered when the overall report is classified)

1. ORIGINATING ACTIVITY (Corporate author) The University of Michigan Radiation Laboratory, Dept. of Electrical Engineering, 201 Catherine Street, Ann Arbor, Michigan 48108	2a. REPORT SECURITY CLASSIFICATION UNCLASSIFIED 2b. GROUP

3. REPORT TITLE

DOPPLER RADIATION STUDY

4. DESCRIPTIVE NOTES (Type of report and inclusive dates)

Interim Report No. 3 (1 January - 1 April 1969)

5. AUTHOR(S) (First name, middle initial, last name)

Chiao-Min Chu, Joseph E. Ferris, and Wiley E. Zimmerman

6. REPORT DATE	7a. TOTAL NO. OF PAGES	7b. NO. OF REFS
May 1969	89	4

8a. CONTRACT OR GRANT NO.	9a. ORIGINATOR'S REPORT NUMBER(S)
N62269-68-C-0715 b. PROJECT NO.	1969-3-Q
c.	9b. OTHER REPORT NO(S) (Any other numbers that may be assigned this report)
d.	

10. DISTRIBUTION STATEMENT

11. SUPPLEMENTARY NOTES	12. SPONSORING MILITARY ACTIVITY
	U.S. Naval Air Development Center Johnsville, Warminster, Pa. 18974

13. ABSTRACT

This report presents a collection of experimental acquired bistatic scattering data. Results have been collected for flat and corrugated metallic surfaces and calm and agitated tap water surfaces. Most of the data is for a frequency of 13.0 GHz with some data at 15.0 GHz. A description of the test setup used is presented. Based on these results elementary calculations were made for a tactical situation and the results are reported. A description of the proposed fly-by test is presented.

DD FORM 1 NOV 68 1473

UNCLASSIFIED

Security Classification

14 KEY WORDS	LINK A		LINK B		LINK C	
	ROLE	WT	ROLE	WT	ROLE	WT
Doppler Radar						
Radiation Characteristics						
Specular Scatter						
Back Scatter						
Diffuse Scatter						
Bistatic Scatter						
Sea Scatter						
Terrain Scatter						